5-2006

Comparative TMJ imaging accuracy using iCAT cone beam computerized tomography.

Oana Bida Honey
University of Louisville

Follow this and additional works at: https://ir.library.louisville.edu/etd

COMPARATIVE TMJ IMAGING ACCURACY USING iCAT CONE BEAM
COMPUTERIZED TOMOGRAPHY

By

Oana Bida Honey
Hon. B.S., University of Toronto, 2002
D.M.D., University of Louisville, 2006

A Thesis
Submitted to the Faculty of the
Graduate School of the University of Louisville
in Partial Fulfillment of the Requirements
for the Degree of

Masters of Science in Oral Biology

Department of Orthodontics and Pediatric Dentistry
University of Louisville
Louisville, KY

May 2006

COMPARATIVE TMJ IMAGING ACCURACY USING iCAT CONE BEAM
COMPUTERIZED TOMOGRAPHY

By

Oana Bida Honey
Hon.B.S., University of Toronto, 2002
D.M.D., University of Louisville, 2006

A Thesis Approved on

March 31, 2006

by the following Thesis Committee:

_____
Thesis Director

_____

_____

_____

DEDICATION

This thesis is dedicated to my parents,

Adriana and Mike Bida, and my husband, David, who always give me

unconditional love and support in all of my endeavors.

ACKNOWLEDGEMENTS

ABSTRACT

COMPARATIVE TMJ IMAGING ACCURACY USING iCAT CONE BEAM
COMPUTERIZED TOMOGRAPHY

Oana Bida Honey, Hon.B.S.

March 31, 2006

A blinded observational cross-sectional *in vitro* study was conducted to compare
the diagnostic accuracy of observers viewing images made using cone beam
computerized tomography (CBCT), panoramic radiography and linear tomography.

The sample consisted of 37 TMJ articulations from 30 human skulls
demonstrating either normal condylar morphology (n=19) or erosion of the lateral pole
(n=18). The articulations were imaged using corrected angle linear `tomography,` normal
and TMJ specific panoramic radiography and CBCT. Images and 10 re-reads were
presented to 10 observers. Multiple CBCT multi-planar images were presented both
statically and interactively. Intra-observer reliability was determined by weighted kappa
(K_w) and diagnostic accuracy by the fitted area under the ROC curve (A_z). Means were
compared using ANOVA (p≤.05).

Our results show CBCT images provide superior reliability and greater accuracy
than corrected angle linear tomography and TMJ panoramic projections in the detection
of condylar cortical erosion.

TABLE OF CONTENTS

CHAPTER

LIST OF FIGURES

INTRODUCTION

In the initial assessment of the orthodontic patient, imaging is an important diagnostic adjunct in the assessment of the temporomandibular joint (TMJ) condition prior to fixed appliance therapy. Of the various conditions that affect the TMJ, those of greatest concern are congenital and developmental disturbances, degenerative and rheumatoid arthritis, and derangements of the intra-articular disc. These conditions are of concern because they can produce skeletal deformities and malocclusions or may cause pain and dysfunction. Panoramic, transcranial and tomographic radiography are the most commonly used imaging modalities in the assessment of TMJ morphology because of their availability, relative ease of use and radiation/cost efficiency. Unfortunately, many investigators have used the panoramic radiograph to assess changes in the condyle with regard to the effects of functional appliances and orthodontics. However, the inherent anatomic diversity of the TMJ articulation (eg., the condyle) compounded by various factors that influence two dimensional image presentation, (eg., anatomic superimposition, beam projection angle and patient positional changes) may invalidate the results from previous reports.

While computed tomography (CT) provides optimal imaging of the osseous components of the TMJ, scanners are large and expensive systems designed for full-body imaging and are not readily available. Recently, cone beam computed tomography

(CBCT) or volumetric CT devices have been developed specifically for the maxillofacial region. This modality is capable of providing sub-millimeter spatial resolution images of high diagnostic quality of the TMJ with markedly shorter scanning times (20-70 sec) and radiation dose up to twenty times lower compared with conventional CT scans.

The availability of fast scan CBCT now provides an alternate imaging modality capable of providing a three-dimensional (3D) representation of the TMJ with minimal distortion using multi-planar reformatted (MPR) images. The aim of this study was: 1) to investigate the possibility of producing images suitable for TMJ analysis from CBCT scan data, and 2) to compare the reliability and accuracy of measurements derived from this analysis as well as conventional cephalograms with anatomic truth.

TMJ Imaging

In order to formulate a diagnosis, the need for imaging in the oral and maxillofacial region is based on the clinician's information requirement supplemental to that already obtained from clinical examination. The value of specific diagnostic imaging modalities may be assessed as to how observations from images change our diagnosis and subsequent treatment or, in broader terms, how they alter our perception of the dynamics of a disease process.

The goals of TMJ imaging are fourfold: 1) To provide a clear visualization of the morphologic and surface features of the osseous and soft tissue components of the TMJ articulation and provide an assessment of the relationship between the temporal (glenoid fossa) and mandibular components (condyle) including the mandibular condyle, glenoid fossa and articular eminence, articular disk and attachments 2) Confirm the extent of the disease 3) Stage the progression of the disease and 4) Evaluate the effects of treatment.

Fulfillment of these goals requires a modality that is precise enough to identify changes over time. Unfortunately not one modality provides affordable hard tissue and soft tissue delineation. Therefore, TMJ imaging will always necessitate a selection process based on provisional diagnosis and the structure(s) to be visualized.

TMJ Imaging Strategies

A number of strategies have been proposed for the use of imaging in TMJ assessment, either by individual authors, often based on the results of their specific research, or by organizations within dentistry. Other terms for the recommendation of particular imaging modality to a patient's presentation have been referred to as image guidelines, protocols, decision algorithms, decision tree analysis or patient selection criteria. Most have been developed for the assessment of patients with a collection of conditions known as temporomandibular disorders; however, the absence of clear and accepted guidelines for diagnosis means that many patients and practitioners may attempt therapy with new, inappropriate or inadequately tested approaches.

As with most musculoskeletal conditions, the diagnosis of TMD is based upon an evaluation of the patient's history and clinical examination, supplemented, when appropriate, by TMJ imaging. Unfortunately, the guidelines for TMJ imaging are conflicting. According to Mohl, TMJ imaging, when indicated, is useful in the detection of pathology within the joint, provided that validated criteria are applied to an analysis of the image. However, the assessment of condylar position as a diagnostic criterion for TMD has very poor reliability and validity.

Conversely, Dixon stated that the present knowledge levels of TMD preclude the use of TMJ imaging, in the absence of definite signs and symptoms, to predict the

potential that a disorder will surface in the future. Further, since even less valid information on how treatments (eg., orthodontic treatment, splints) might interact with the potential for disease exacerbation, imaging should be reserved for experimental protocols only. Based on the high unexpected incidence of radiographic changes in the temporomandibular joints of asymptomatic patients, most do not receive any type of TMJ imaging assessment.

Rao indicated that magnetic resonance imaging (MRI) has become the primary modality for the assessment of the temporomandibular joint, as temporomandibular joint (TMJ) internal derangement is fairly prevalent in patients presenting with facial pain. He also developed an algorithm to facilitate a systematic interpretation of the TMJ imaging study.

Gynther and Tronje proposed that patients with generalized osteoarthritis and signs and symptoms of TMJ involvement demonstrate distinct radiographic characteristics with regard to the TMJ. Twenty patients with generalized osteoarthritis (20 joints) and 21 patients with rheumatoid arthritis (21 joints) were evaluated using corrected sagittal tomography (hard tissue changes, joint space, and condylar position), frontal tomography (hard tissue changes), and individualized oblique lateral transcranial projections (condylar translation). Sixteen (80%) joints in the group of patients with generalized osteoarthritis and 15 (71%) joints in the group with rheumatoid arthritis revealed structural changes, with the condyle being the predominant location. No radiographic criterion was pathognomonic for generalized osteoarthritis or rheumatoid arthritis; however, osteophytes, flattening of the condyle, or a reduced joint space was observed more often in joints with generalized osteoarthritis. Erosions in the condyle

were more common in joints with rheumatoid arthritis. The radiographic findings in patients with generalized osteoarthritis were more similar to those seen in patients who had the common form of TMJ osteoarthritis than to those in patients with rheumatoid arthritis.

With regard to TMD, Larheim stated that MRI has surpassed arthrography and computed tomography for the evaluation of most patients with internal derangement caused by disk displacement, pathologic entities characterized by chronic inflammation (eg., rheumatoid arthritis), and other infrequent conditions (eg., tumors). In fact, for patients who have various forms of disk displacements with or without accompanying bone abnormalities, oblique sagittal and coronal magnetic resonance imaging provide a diagnostic accuracy of at least 90%. Additionally, alterations in the condylar marrow may be detected. T2-weighted MRI can make a significant diagnostic contribution by demonstrating inflammatory reactions such as joint effusion and marrow edema. In the subgroup of patients with chronic inflammatory diseases, MRI may also demonstrate abnormalities not shown with other imaging modalities. Disk deformation, fragmentation, and destruction may indirectly suggest the presence of synovial proliferation/pannus formation, which in selected cases may be directly depicted with intravenous gadopentetate dimeglumine. However, for a more detailed evaluation of the bone condition and of soft tissue calcifications in joints with inflammatory diseases, tumors, or other disorders, computed tomography is the preferable imaging modality.

Currently, the American Board of Orthodontics (ABO) recommends that the radiographic examination for all patients initiating orthodontic treatment consist of at minimum a lateral cephalogram and a panogram with maxillary and mandibular incisor

periapicals. Atchison et al., evaluated criteria specified for the radiographs, their impact, and relevant information in the literature and developed an algorithm or set of decision rules to determine which pre treatment radiographs were indicated. When tested on the six test cases, adherence to the algorithm resulted in a 36% reduction in the total number of radiographs.

Luke *et al,* surveyed 8 orthodontic residents to evaluate the selection criteria and effect on treatment planning used for ordering a corrected lateral tomogram (LT) of the temporomandibular joint (TMJ) and a posteroanterior cephalogram (PAC) for the diagnosis of 144 orthodontic patients. A LT was ordered for twenty-eight (19%) of the patients. The most common reasons cited for requesting the LTs were TMJ clicking (67%) and pain (33%). The residents also perceived a need to order the LT for medico-legal protection in 85% of these cases. The LT tended not to have an impact on treatment planning.

Importance of TMJ Imaging in Orthodontic Therapy

The TMJ is a diarthroidal articulation between the condyle of the mandible and the squamous portion of the temporal bone. The condyle is elliptically shaped with its long axis oriented medio-laterally; the articular surface of the temporal bone is composed of the concave articular fossa and the convex articular eminence.

Dental orthodontics and orthopedics involves the application of forces via bio-mechanical appliances to the orofacial region to affect bone growth and tooth movement to correct dental and skeletal anomalies. These forces may theoretically influence the development and disease processes within the temporomandibular joint because of

6

transduction effects as proposed by the Moss functional matrix theory. In addition patients may present with craniofacial conditions that result in TMJ anomalies.

Hemifacial microsomia is a congenital condition characterized by a unilateral underdevelopment of the lower half of the face which does not catch up with normal growth. It is sometimes part of a larger syndrome, such as Goldenhar Syndrome. Affected patients frequently have partially formed or absent ears on the affected side, asymmetry, and auditory problems. In most cases, patients have an underdeveloped or hypoplastic condyle. Condylar hyperplasia is also a pathological condition that may result in severe dentofacial deformities. Conversely, it causes a progressive overdevelopment of the mandible, possibly resulting in a significant functional and esthetic deformity. Treatment of both conditions usually involves a team approach by an orthodontist and a maxillofacial surgeon. Accurate imaging of the joint is vital to proper diagnosis and treatment.

While treatment planning orthodontics for a patient with degenerative joint conditions, such as TMJ OA, it is vital to assess the TMJ to determine whether the disease process is active or stabilized. Further, proper imaging allows practitioners to evaluate an asymptomatic TMJ for potential degenerative changes prior to orthodontic treatment. Orthodontic treatment was previously implicated as a cause for temporomandibular joint dysfunction (TMD) in 1987, when a Michigan malpractice trial awarded a patient $850,000 from her orthodontist, because she developed TMD after her orthodontic treatment was completed. This outcome, along with several others similar in nature, resulted in a rapid increase in the number and quality of clinical studies evaluating the relationship between TMD and orthodontic treatment. From these studies, no concrete

evidence correlating temporomandibular dysfunction with orthodontic treatment was found. Currently, orthodontic treatment is not believed to cause TMD, but studies using more accurate imaging techniques are necessary to determine the true relationship or lack thereof.

The effect of functional appliances (used in orthodontic treatment) in patients with chronic arthritis affecting the TMJ, however, is still somewhat controversial. Class II malocclusion has been associated with anterior disk displacement; functional appliances are a common treatment modality for such patients who are affected skeletally and have growth remaining. Interestingly, Pancherz and Ruf documented positive effects after orthodontic treatment with the Herbst appliance, which resulted in disk retrusion, but this effect was later found to be only temporary. Further, Kitai and Kreiborg found that functional appliance treatment in patients with chronic arthritis affecting the TMJ resulted in bone apposition at the superior and posterior surface of the condyle as well as at the roof of the glenoid fossa. They found that the masticatory muscles remained stable relative to the anterior cranial base and did not follow the forward movement of the condyle. They recommended close monitoring of such patients during orthodontic treatment. However, functional appliance use has been cautioned against in children with chronic arthritis with TMJ involvement, as it may stimulate increased bone turnover in the joint area leading to a net loss of skeletal tissue at the condyle instead of a net gain.

TMJ Imaging Modalities

The efficacy and utility of a variety of differing imaging strategies has recently been reviewed with regard to TMJ imaging. These include plain film radiography (specifically transcranial, transorbital, transpharyngeal TMJ radiography, and the

Townes/submentovertex views), panoramic and tomographic radiography and advanced imaging modalities.

By far, the panoramic radiograph is the most commonly used imaging modality for TMJ assessment. The TMJ presents as a distorted image on the panoramic radiograph due to the collimated beam projection angulation. Horizontally, the beam is directed anteriorly through one side of the patient, projecting the contralateral side at a fixed angle (approximately 30 degrees depending on the panoramic machine used) (Figure 1).
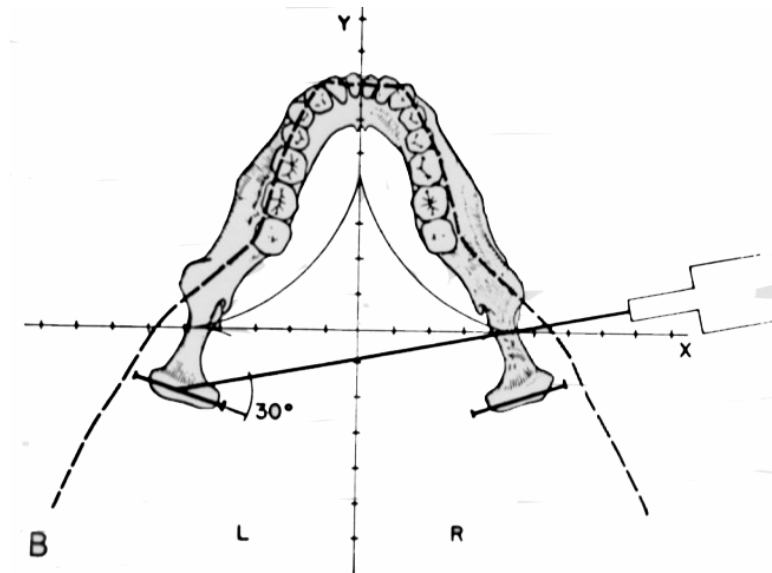
Figure 1. Schematic illustration of the panoramic horizontal beam projection angulation with respect to condylar angle. See text for further explanation.

This results in the medial portion of the condyle appearing as the posterior surface of the image, and the lateral surface appearing as the medial image. Vertically, the beam is projected upward toward the contralateral TMJ at an angle of approximately 7-10

9

degrees. This results in the medial surfaces being projected higher than the lateral surfaces. Therefore, this geometric arrangement results in the panoramic radiograph depicting the lateral and medial third of the condylar head with TMJ appearance varying with the machine used. Ruf and Pancherz investigated the accuracy of panoramic radiography (Orthopantomogram 5, Siemnes, Bernsheim, Germany) in reproducing the temporomandibular joint area on a dry skull with variations in skull position (ideal compared to posterior and anterior inclinations up to 40°, Lateral tilt and twist up to 40° and combinations thereof). They found that the radiographic image of the TMJ did not correspond to the anatomic condylar/fossa components or to their actual relationship. In the ideal position, the image of the lateral pole was visualized as the anterior border of the condyle. The posterior pole was visualized correctly as the posterior border of the condylar image. However, they found that the medial pole was superimposed over the center of the condyle near the posterior condylar border and above the posterior pole. To a large extent, changes in skull position affected the radiographic temporomandibular joint image, simulating anterior condylar flattening, osteophytes, narrowing of joint space, and left/right condylar asymmetry. They concluded that panoramic radiography may have questionable reliability for temporomandibular joint diagnostic purposes.

Most orthodontists in clinical practice utilize panoramic radiography to detect TMJ/osseous pathology. In addition, numerous authors have used panoramic imaging to record and evaluate activator treated TMJs in growth and maturing stages, patients treated for intracapsular fractures, the effect of Herbst appliance therapy, and the effect of distraction osteogenesis. The well-documented limitations of panoramic radiography in TMJ assessment must call into question the validity of the selection of this modality in

10

any situation other than gross morphologic assessment. This is especially a concern now that advanced imaging modalities, such as cone beam computed tomography (CBCT), are increasingly available.

Advanced Imaging Modalities

Advanced technologies are those that acquire images using a digital receptor and that provide the possibility of multiple planar reformatting (MPR). In these modalities, multiple images become truly inter-relational in that direct comparisons in multiple planes can be made. Advanced technologies that are available to image the TMJ include computerized tomography (CT), magnetic resonance imaging (MRI), and nuclear medicine. While MRI is the primary modality for the assessment of TMJ conditions involving the soft tissue, especially the intra-articular disc, computed tomography (CT) provides optimal imaging of the osseous components of the TMJ and will be discussed in further detail.

The basis of advanced imaging is the recording of transmitted, attenuated x-rays of an object by a digital receptor to produce a digital image. Digital images are composed of pixels, or picture elements, arranged in a 2-dimensional rectangular grid. Each pixel has a specific size, color, intensity value, and location within an image and is the smallest element of the digitized image. In general, radiographic images use gray color with an intensity value between 8 bits (256 shades of gray) and 12 bits (4096 shades of gray). The number of pixels per given length of an image (pixels/mm), the number of gray levels per pixel (bits), and the management of the gray levels determine image resolution or the degree of sharpness of the image. A voxel is a three-dimensional stack of

bitmapped images, (each voxel having a height, width, and thickness) and is the smallest element of a three-dimensional image.

Computed Tomography

In addition to utilizing images that are digital, technological advancements now allow dentistry to create images of the maxillofacial region in 3-dimensions. The first three dimensional imaging technique used in dentistry was computerized tomography (CT). CT units can be divided into two groups based on the acquisition x-ray geometry: fan beam and cone beam (Fig 2). Essentially, the latter method for capturing an image differs from the traditional CT in that it does so by cone beam volumetric tomography. A three-dimensional x-ray beam passes through the object volume investigated. Simultaneously, the beam hits a two-dimensional extended detector and forms a true volumetric acquisition in a single scan (Figure 4).
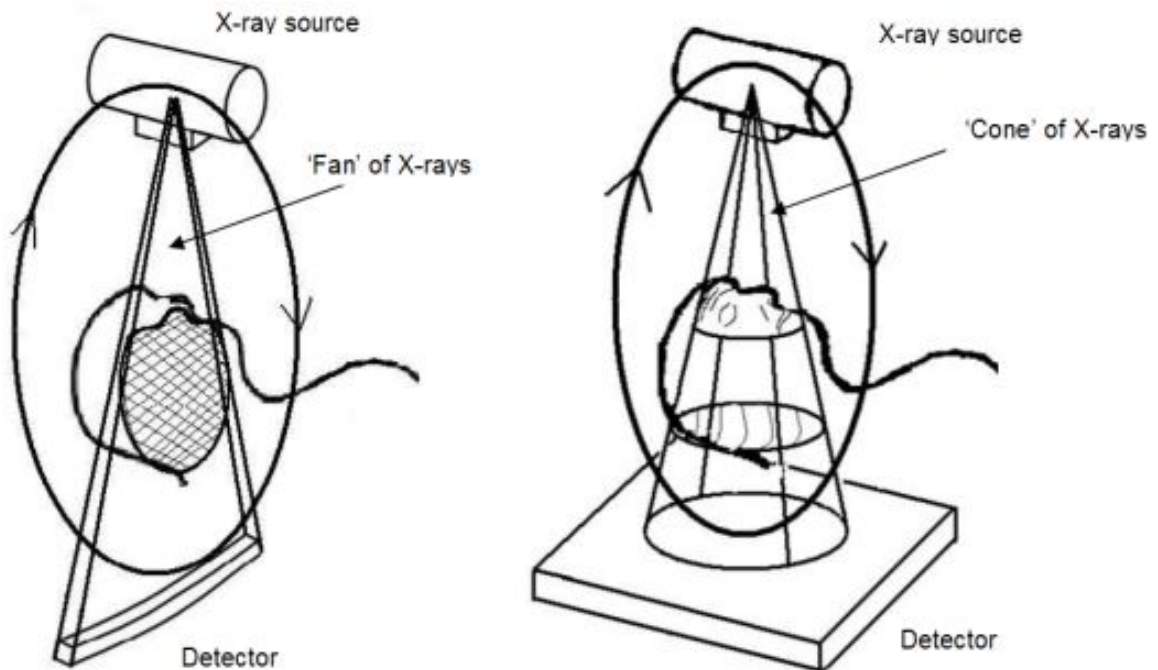
a.   b.

Figure 2. X-ray beam projection scheme comparing conventional or "fan beam"

CT (a.) and cone beam CT (b.) geometry (Images courtesy Predag. Sukovic, Xoran

Technologies, Ann Arbor, MI USA)

Fan beam acquisition

CT scanners consist of an X-ray source and detector mounted on a rotating gantry (Fig. 2a). During one rotation of the gantry, the detector detects the flux (I_0) of x-rays that have passed through the patient. These integrals constitute so-called "raw data" that are then fed into an image reconstruction method that generates cross-sectional images whose pixel values correspond to linear attenuation coefficients. Such machines acquired image data through a thin, broad, fan shaped x-ray beam which was transmitted through the patient. In first generation scanners, both the detector and source rotated one degree - a design known as the "translate-rotate" or "pencil-beam" scanner. Second generation or "hybrid" machines, introduced in 1975, used more than one detector and used small fan-beam, as opposed to pencil-beam, scanning. Like the first generation of CT scanners, these scanners also used a translate-rotate design, however image quality was poor due to patient motion artifacts caused by the significant amount of time required to take the scan.

Third generation CT scanners appeared in 1976 and are the systems most widely used today. These scanners use a large, arc-shaped detector that acquires an entire projection without the need for translation. This rotate-only design, frequently referred to

as "fan-beam", utilizes the power of the X-ray tube much more efficiently than the previous generations. Fourth generation scanners shortly followed third generation scanners, replacing the arc-shaped detector with an entire circle of detectors. In this design, the X-ray tube rotates around the patient, while the detector stays stationary. Since these fourth generation scanners tend to be more expensive and suffer from higher levels of Compton scatter artifacts, most of the commercially available CT scanners today are third generation. Recent advances in CT include multirow detectors and spiral scanning. Multirow scanning allows for the acquisition of several cross-sectional slices at the same time, reducing scanning times. Today's state-of-the-art scanners have 64 rows of detectors. Spiral (helical) scanning incorporates a moving table with the rotating X-ray tube, with the net effect that the X-ray tube describes a helical path around the patient.

Cone Beam Acquisition

Cone-beam CT scanners utilize a two dimensional detector (Fig. 2b), which allows for a single rotation of the gantry to generate a scan of the entire region of interest, as compared to conventional CT scanners whose multiple "slices" must be stacked to obtain a complete image. In comparison with conventional fan-beam or spiral-scan geometries, cone-beam geometry has higher efficiency in X-ray use, inherent quickness in volumetric data acquisition, and potential for reducing the cost of CT. Conventional fan-beam scans are obtained by illuminating an object with a narrow, fan-shaped, beam of X-rays. The X-ray beam generated by the tube is focused to a fan-shaped beam by rejecting the photons outside the fan, resulting in a highly inefficient use of the X-ray photons. Further, the fan-beam approach requires reconstructing the object slice-by-slice and then stacking the slices to obtain a 3D representation of the object. Each individual

slice requires a separate scan and separate 2D reconstruction. The cone beam technique, on the other hand, requires only a single scan to capture the entire object with a cone of X-rays. Thus, the time required to acquire a single cone-beam projection is the same as that required by a single fan-beam projection. However, since it takes several fan beam scans to complete the imaging of a single object, the acquisition time for the fan beam tends to be much longer than with the cone beam. Although it may be possible to reduce the acquisition time of the fan beam method by using a higher power X-ray tube, this increases the cost and size of the scanner as well as the electric power consumption, thus making the design unsuitable for a compact scanner.

A number of groups have worked on developing task-specific CBCT scanners over the past two decades. Computed tomography angiography (CTA), in particular, has been an active area of investigation due to its lenient requirements for contrast resolution and strict requirements on spatial resolution - a natural fit for CBCT. The first CBCT scanner ever to be built was built for angiography among other tasks at Mayo in 1982.

Fahrig et al. developed a CBCT system based on an image intensifier and C-arm for use in angiography. Wiesent also developed a C-arm plus image intensifier system for interventional angiography. Saint-Felix et al. developed a CTA CBCT system based on the gantry of a conventional CT scanner which reconstructs vasculature from a set of digitally subtracted angiography (DSA) images. Ning et al. developed a CBCT angiography imager based on GE 8800 CT scanner with an image intensifier - CCD chain and later with a flat-panel detector. Schueler et al. have developed a CBCT CTA scanner based on a biplanar C-arm system. Kawata et al. also developed a CBCT CTA system.

Jaffray and Siewerdsen developed a CBCT system for radiotherapy guidance based on an amorphous silicon (a-Si:H) flat-panel detector. Cho et al. also developed a CBCT system for radiotherapy applications. Efforts are also now being made towards dedicated CBCT-based imaging systems for mammography.

Although CBCT equipment has existed for over two decades, only recently has it become possible to develop clinical systems that are both inexpensive and small enough to be used in operating room, medical offices, emergency rooms, and intensive care. Four technological and application-specific factors have converged to make this possible. First, compact and high-quality flat-panel detector arrays were developed. Second, the computer power necessary for cone-beam image reconstruction has become widely available and is relatively inexpensive. Third, x-ray tubes necessary for cone-beam scanning are orders-of-magnitude less expensive than those required for conventional CT. Fourth, by focusing on head/neck scanning only, one can eliminate the need for sub-second gantry rotation speeds that are needed for cardiac and thoracic imaging. This significantly reduces the complexity and cost of the gantry.

CBCT in Oral and Maxillofacial Imaging

The first commercial CBCT system for dento-maxillofacial imaging was the NewTom-9000 (Quantitative Radiology, Verona, Italy)[26] which was approved by the Food and Drug Administration in April 2001. Since then several commercial systems are now available. (Fig 3)

a.
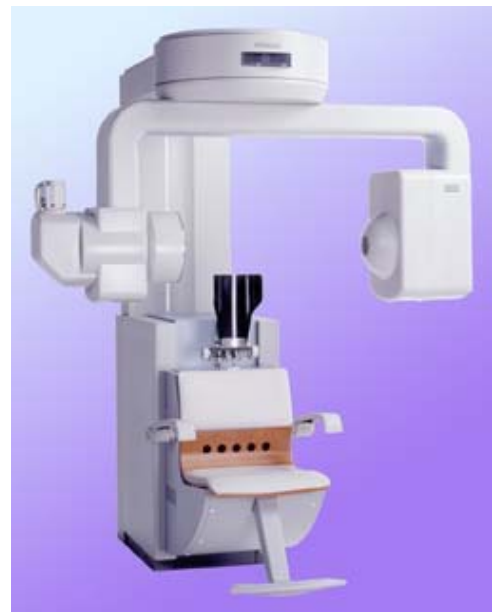
b.

c.   d.

Figure 3: Currently commercially available CBCT units for dento-maxillofacial radiology. a. Newtom 9000G (Quantitative Radiology, Verona, Italy) b. CB MercuRay® (Hitachi, Medical Corp., Kashiwa-shi, Chiba-ken, Japan) c. 3D Accuitomo – XYZ Slice View Tomograph, (J. Morita Mfg. Corp., Kyoto, Japan) d. iCAT / DentoCat / MiniCAT (Xoran Technologies, Ann Arbor MI, USA/Imaging Sciences International, Hatfield, PA)

CBCT units can be divided into two groups based on the acquisition hardware configuration: Image intensifier tube/charge coupled device (IIT/CCD) combination or flat panel imager (FPI).

1) Image intensifier tube coupled with charge coupled device (IIT/CCD). All currently available CBCT units with dento-maxillofacial application have this configuration except one - the i-CAT. The IIT/CCD configuration comprises an x-ray image intensifier tube coupled to a charge coupled device via a fiber

optic coupling. A typical intensifier is a cylindrical shaped device containing a number of components housed in a vacuum. It has three key elements (Fig 4.).

a. X-rays emerging from the patient enter the device at the input window and strike the input phosphor. The input phosphor is made from CsI, doped with Na, which is deposited on an aluminium substrate. The CsI:Na is grown in a structure of monocrystalline needles, each about 0.005 mm in diameter and up to 0.5 mm long. The input phosphor scintillates and light photons strike the flat, circular photocathode formed from various semiconductor materials within which photon energy is converted to electrons.

b. These electrons are accelerated by virtue of a high-voltage differential acting across it and focussed by the electron optics onto the output window.

c. On the output window is deposited the output phosphor, made from ZnCdS: Ag that produces light providing an image of the x-ray pattern that emerged from the patient which has a substantially greater intensity than when an intensifying screen is used on its own. This light can then be captured by a charge coupled device via a fiber optic coupling.
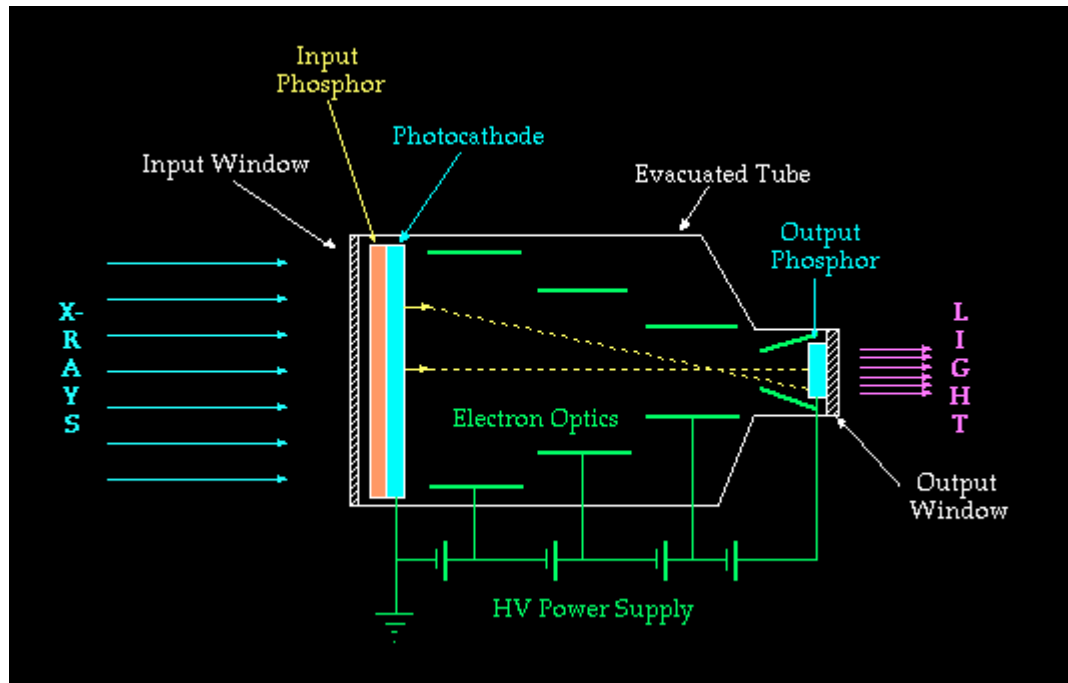
Figure 4. Image intensifier tube.

2) Flat panel imager (FPI). The iCAT is currently the only dento-maxillofacial CBCT unit that uses a FPI technology.   This imaging system consists of detection of x-rays using a "indirect" detector based on a large area solid state sensor panel coupled to an x-ray scintillator layer - essentially the same underlying technology that is used to construct flat-panel computer monitors and large-area document imagers.

   The purpose of the sensor panel is to accumulate electrical charge generated by the absorption of x-rays from a scintillator and to provide it row by row during scanning to the charge amplifiers. In panels used with a scintillator, the charge storage device is a photodiode. The switch used to permit the charge to flow out can be a single diode, a diode pair or a thin-film transistor. All possible combinations of these storage devices can be made to

work but each has a specific set of advantages and disadvantages. The switch used in the iCAT is a commercially available photodiode/hydrogenated amorphous silicon (aSi:H) TFT combination (Varian Medical Systems, Inc., Palo Alto, CA, USA) because of its simplicity of use, commercial availability and flexibility of design. The characteristics of aSi:H based flat panel detector arrays provide a greater dynamic range and greater performance than the II/CCD technology of other CBCT units. Of particular note, image intensifiers create geometric distortions that must be addressed when processing the data later in the software, while flat-panel detectors do not suffer from this problem. This could potentially reduce the measurement accuracy of CBCT units employing this configuration.

A scintillator is a compound that absorbs x-rays and converts the energy to visible light. A good scintillator yields many light photons for each incoming x-ray photon; 20 to 50 visible photons out per 1kV of incoming x-ray energy are typical. Scintillators usually consist of a high-atomic number material, which has high x-ray absorption, and a low-concentration activator that provides direct band transitions to facilitate visible photon emission. Scintillators may be granular like phosphors or crystalline like cesium iodide (Figure 5). The most common scintillators are granular and consist of gadolinium and lanthanum oxysulfides doped with terbium. Various grain sizes and chemical mixtures are used to produce a variety of resolution and brightness varieties. In use, these are mixed with a glue binder and coated on to plastic sheets. These were designed to be pressed against arrays of

amorphous silicon photodiodes to make electronic x-ray detectors with sensitivity at least as good as that of film. Tens of electron volts are needed to produce each visible photon in a phosphor screen and x-ray absorption is good. Light scatter can be a problem if the layers must be thick to stop higher-energy x-rays. For a better combination of resolution and brightness, cesium iodide (CsI) can be used. CsI has the useful property that it grows as a dense array of fine needles (10 to 20 micrometers in diameter) which produce crystals that act as mini-light collimators. This allows very thick (up to 1 mm) layers to be used with excellent retention of resolution. Because cesium has a high atomic number, it is an excellent x-ray absorber so this material makes very efficient use of the incoming x-rays. About 20-25 electron volts are needed to generate each light photon. When doped with thallium, CsI emits at about 550 nm, just at the peak of the spectral sensitivity of amorphous silicon.

a.   b.
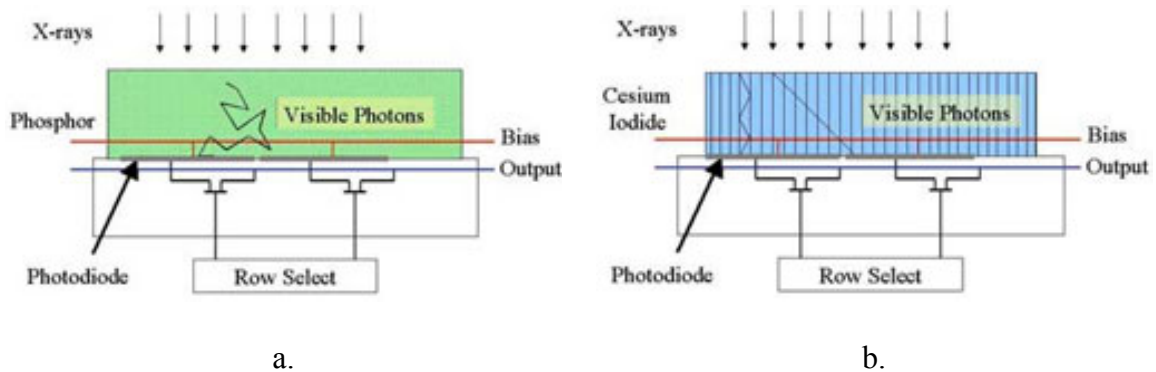
Figure 5: Comparison of FPI with phosphor scintillator (a.) and cesium iodide scintillator (b.) (Images courtesy of Varian Medical Systems, Inc., Palo Alto CA, USA)

The combination of CsI and amorphous silicon has the highest detector quantum efficiency (DQE) of all materials in production today. While the iCAT uses a commercially available (CsI/ASi) FPI (Varian Medical Systems Inc., Palo Alto, CA, USA) the performance of this FPI-based CBCT has not been sufficiently examined yet.

The cone-beamed technique uses a single scan in which the x-ray source and a reciprocating x-ray sensor are attached by a "U-" or C-arm and rotate around the patient's head acquiring multiple projection scan images. The field of view (FOV) or area of interest able to be covered is primarily dependent on the detector size (IIT field and either CCD or a:SiTFT dimensions) and beam projection geometry. While FOV can be varied by the application of zoomed image reconstruction (e.g. MercuRay [Hitachi, Medical Corp., Kashiwa-shi, Chiba-ken, Japan] this is usually done at the loss of image resolution.

Data is obtained from multiple single projection scan images as the x-ray source rotates around the patient's head. The number of projection scans comprising the data set is variable, depending on the system, and is referred to as the frame rate. With a higher the frame rate, more information is available to reconstruct the image: however, the signal-to-noise of individual MPR slices is also higher. The advantage of a higher frame rate is that it reduces metallic artifact, but this is usually accomplished with a longer scan time. A number of units have variable frame rates. For example, the iCAT has a choce of 10 second, 20 second (standard) and 40 second scans.

CBCT Advantages

Because CBCT provides images of high contrasting structures well, it is extremely useful for evaluating osseous structures. Combined with the limitation of FOV, CBCT is therefore well suited towards the imaging of the craniofacial area. Currently, limitations exist in the application of this technology for soft tissue [31, 32], but efforts are being directed towards the development of software algorithms to improve signal-to-noise and optimize available contrast.

The utilization of CBCT technology in clinical practice provides a number of potential advantages compared with conventional CT related to the beam limitation, scan time reduction, and image display. Specifically the advantages of CBCT are as follows:

1) *Variable FOV.* Collimation of the CBCT primary x-ray beam enables limitation of the x-radiation to the area of interest. Therefore, an optimal FOV (field of view) can be selected for each patient based on suspected disease presentation and the region to be imaged. For example, radiographic investigation of the mandible can be performed by selection of an appropriate FOV. This functionality provides additional dose savings by limiting the irradiation field to fit the FOV, with a resultant exposure dose to the patient.

2) *Sub-millimeter resolution.* CBCT units all use mega-pixel solid state devices for x-ray detection providing a minimal voxel resolution of between 0.25mm isotropically, exceeding the highest grade multi-slice CT.

3) *High speed scanning.* Because CBCT acquires all projection images in a single rotation, scan time can be reduced enormously. In the medical CT system, particularly in high resolution, each thin slice thickness can take up to

several tens of seconds. However, various CBCT systems can scan an entire head in 10 seconds or less. While faster scanning times usually mean less number of projections from which to reconstruct the MPR images, motion artifact due to subject movement is reduced. Reconstruction times vary depending on FOV and scanning speed.

4) ***Dramatic dose reduction.*** Preliminary reports indicate that CBCT patient absorbed dose is significantly reduced when compared to conventional CT.[27] The Newtom 9000 system (Quantitative Radiology, Verona, Italy) also has an automatic exposure control device which selects the starting intensity of the x-ray beam, depending on the size of the patient, and modifies the anodic current according to the density of the transversed tissues (maximum value 15mA). This reduces the patient absorbed dose to approximately that of a film-based periapical survey of the dentition[24, 27, 28] or 1-7 times that of a single panoramic image (varying with the panoramic system used) [25, 29]. Depending on bone density, a traditional CT exposes the patient to approximately 6-8 times that amount when evaluating either the maxilla or mandible [25] and 15 times the amount of CBCT exposure when imaging both the maxilla and mandible.[30]

5) ***Voxel isotropy.*** Voxel representation and therefore resolution are dependent on lateral slice thickness, determined principally by the matrix size of the detector and longitudinal slice thickness (body axis), which in conventional CT is determined by slice pitch a function of gantry motion. Therefore, conventional CT data is obtained anisotropically, where axial voxel

dimensions are equal but where coronal dimensions are greater and are determined by slice pitch, usually a 1mm minimum (Fig 6a). Therefore, spatial resolution in the longitudinal slice (body axis direction) is poorer than that of lateral slice. On the other hand, the CBCT uses a 2D detector and the same high resolution is obtained in the longitudinal slice (body axis direction) and lateral slice (transverse direction). This voxel representation is known as Isotropic (Fig 6b). Because of this characteristic, coronal multi-planar reformatting (MPR) of CBCT data has the same resolution as axial data.
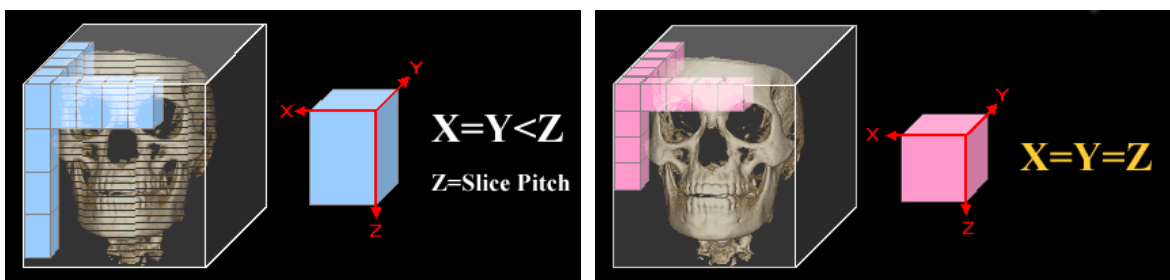
a. Anisotropic Voxel   b. Isotropic Voxel

Figure 6: Comparison of voxel acquisition features on conventional "fan beam" CT (a.)

and "cone beam" CT (b.)

6) ***Real time analysis and manipulation.*** Although conventional CT data is inherently digital, images are supplied to referring clinicians as fixed format, hard copies on film transparencies. CT image algorithms necessary to reformat the data require the computing power of workstations. While such data can be "converted" and imported into proprietary programs for use on personal computers (e.g. Simplant and Simplant CMF: Materialise, Ann Arbor, MI, USA) this process is expensive and requires an intermediary stage that potentially extends the diagnostic phase. Reconstruction of CBCT data is performed natively by a personal computer. In addition, availability of software to the user, not just the radiologist, is available either via direct purchase or innovative "per use" license from the various vendors (e.g. Imaging Sciences International). Further, because the original data is isotropic, it can theoretically be re-orientated such that the patient's anatomic features are re-aligned. At least one manufacturer has incorporated this capability into both their acquisition and viewer software (Imaging Sciences International). Finally, the availability of cursor-driven measurement algorithms provide the clinician with an interactive capability for real-time dimensional assessment.

7) ***Display modes unique to maxillofacial imaging.*** CBCT units reconstruct the projection data to provide as many as 512 coronal, sagittal and axial MPR frames. Common to all standard viewing layouts are usually preset options providing display of coronal, sagittal and axial MPR frames. Basic manipulations include zoom or magnification, window/level, the capability to

add annotation and measurement algorithms. Some proprietary software is capable of advanced imaging processing functions including:

a. Oblique MPR such as linear oblique MRP (useful for TMJ assessment) or curved oblique MPR providing a "panoramic" image.

b. Transaxial/slice MPR such as cross-sectional imaging provides sequential multi-slice images usually orthogonal to the "panoramic" MPR, useful in implant site assessement or lateral oblique MPR which has application in the assessment of the TMJ.

c. Variable slice thickness adjustments for oblique MPR images provide the clinician with the possibility of producing undistorted plain radiograph projection-like images. One example is the creation of a cephalometric plain projection, either sagitally or coronally. This is developed by increasing the slice thickness of a mid sagittal MPR plane to the width of the head (130-150mm) to produce an image composed of the summated voxels, an image which has been referred to as "Ray Sum" (Hitachi Medical Systems). This image can be exported and analyzed using third party proprietary cephalometric analysis software. This functionality may potentially reduce the need for additional radiographic exposure. Oblique MPR images along the curve of the dental arch with slice thickness comparable to the in-focus image layer of panoramic radiographs (25-35mm) can also be individually created to provide a "panoramic" radiograph customized for each patient. However, unlike conventional panoramic radiographs,

these MPR images are undistorted and are free from projection artifacts.

d. Maximum intensity projection (MIP). This is a three dimensional volume rendering technique which is used to visualize high-intensity structures within volumetric data. At each pixel, the highest data value encountered along a corresponding viewing ray is depicted. In combination with oblique MPR and selection of wide slice thickness, this technique is capable of providing 3D surface images. This is particularly useful in cephalometric radiography.

e. Surface and volume rendering algorithms are available with some software which provides three-dimensional reconstruction and presentation of data that can be interactively manipulated.

f. Previously unavailable for viewer use, numerous image enhancement algorithms are now able to optimize image presentation. While the diagnostic efficacy of the application of these algorithms is yet to be studied, preliminary investigations indicate that sharpening and edge filters show the greatest potential in refining anatomic structures for interpretation.

8) *Greatly reduced image artifact.* CT images are inherently prone to artifacts because the image is reconstructed from multiple independent detector measurements. The types of artifact that can occur include streaking, shading, rings, and helical reconstruction. These artifacts originate from either the physical processes involved in the acquisition, patient based artifacts, caused

by such factors as patient movement or the presence of metallic materials in or on the patient, scanner based artifacts, resulting from imperfections in scanner function and helical and multi-slice artifacts, dependent on the image reconstruction method. Many of these artifacts can be reduced by means of special software corrections that use a variety of interpolation techniques to substitute the overrange values in profiles. The projection geometry of CBCT, together with the fast acquisition time, results in a low level of metal artifact in primary and secondary reconstructions.[28, 32] This provides MPR images, particularly orthogonal cross-sectional and oblique panoramic MPR that have a markedly reduced patient based artifacts.

9) ***Variable acquisition modes.*** Many units are capable of variable scanning fields of view (FOV) from large FOV capable of imaging the entire craniofacial complex (currently up to 13.2cm with i-CAT and 19cm with CB MercuRay® to limited FOV for specific diagnostic tasks.

Application of CT to Oral and Maxillofacial Imaging

Conventional CT scanners are large and expensive systems designed for full-body scanning at a high speed to minimize artifacts caused by movement of the heart, lungs, and bowels. Unfortunately, although traditional CT images are useful for diagnosis, there are several limitations/disadvantages to their use in oral and maxillofacial radiology. First, because image data is anisotropic, image dimensions could be off as much as 1.5mm, as the scans take a series of parallel spirals that have small gaps between them. The computer compensates for the small gaps and converts them into specific images by

sophisticated algorithms, but the gaps accumulate into a sizable margin of error. Second, because the scan is not limited to the maxilla and/or mandible, the patient is exposed to significantly more radiation than with a panoramic survey. Third, equipment is costly to purchase and maintain, is large and heavy (requiring a reinforced floor), requires a significant amount of time to produce an image, and produces images with artifacts. Therefore, conventional CT is not well-suited for dedicated dento-maxillofacial imaging, where cost considerations are important, space is often at a premium, and scanning requirements are limited to the head.

The advent of CBCT technology has paved the way for the development of relatively small and inexpensive CT scanners dedicated for use in dento-maxillofacial imaging. Manufacturers' web sites provide numerous examples illustrating the value of CBCT in evaluating the position of impacted teeth, supernumerary teeth, maxillary sinus position (in reference to maxillary molars), mandibular canals, and lingual nerves. Other examples of this modality's uses include implant planning, surgical assessment of pathology, and preoperative/postoperative assessment of craniofacial fractures.[28, 32, 33]

The use of CBCT imaging in orthodontics has particular application in the diagnosis and treatment planning of a multitude of different craniofacial problems that are common in every day orthodontic practice. Specifically CBCT has potential in imaging 1) the effect of condylar trauma (fracture) and structural development during growth, 2) mono-lateral idiopathic hypoplasic / resorption related to symmetrical and asymmetrical development of the bi-maxillary complex during growth, 3) bilateral idiopathic hypoplasic / resorption related to vertical and horizontal development of the

face, 4) the effects of incisor position, mandibular advancement, torque, retraction, position of molars & premolars on the sagittal plane, 5) the effects of intrusion and extrusion on the vertical plane, 6) the effects of pre-maxillary complex, maxillary complex, mandibular symphysis and lower posterior alveolar bone in the transverse plane and, 7) the effects of soft tissue anomalies on growth and development such as airway obstruction (nasal cavity and epi-pharynx), tongue posture and discrepancy between tongue volume and intraoral volume.

Despite anecdotal descriptions of the application of CBCT to orthodontics, the comparative accuracy of this modality in the characterization and assessment of TMJ status has been previously unreported.

CT Imaging Accuracy in the Craniofacial Region

A number of authors have investigated the accuracy of measurements obtained from axial, MPR and 3D reconstructed images of the craniofacial region and, in particular, the TMJ.

Initially, authors investigated the accuracy of linear measurements of transaxial CT images. In 1986, Christiansen *et al.,* 1986) investigated intra- and inter-observer variability and accuracy in the determination of linear and angular TMJ condylar measurements. They used a General Electric 8800 CT/N Scanner and imaged a single dried human mandible embedded in plastic and three frozen cadaver heads. Sixteen observers measured inter- and extra-condylar distances, transverse condylar dimension, condylar angulation, and the plastic base of the specimen. They found intra- and inter-observer variabilities to be lowest for the specimen base and highest for condylar angulation. While there were no significant differences between CT and macroscopic

measurement of the mandible, they found measurement of condyles with structural changes in the transaxial plane was subject to substantial error. They concluded that transaxial linear measurements of the condylar processes free of significant structural changes had an error and an accuracy well within acceptable limits. They also found that error for angular measurements was significantly greater than the error for linear measurements.

Waitzman *et al.,* (1992) compared 40 craniofacial measurements taken directly from five dry skulls (approximate ages: adults, over 18 years; child, 4 years; infant, 6 months) to transaxial CT scans and found excellent agreement between both measurements. The overall percent difference in total was less than 1% for 70% of the measurements; less than 1.5% for 80%; and less than 2% for 90%. Further, because patient positioning can alter CT results, they also evaluated the effect of head tilt on the accuracy of craniofacial measurements. They found that error was within clinically acceptable limits (less than 5%) if the head tilt angle was no more than $\pm 4^0$ from baseline.

For MPR images, results from the literature indicate that measurement accuracy is dependent on the orientation of the oblique scan and plane thickness as well as they type of scan used. Ahlqvist *et al.* (1998) identified the bony regions of the glenoid fossa where the risk of radiographic distortion is increased in conventional and computed tomography. Using 50 corrected coronal MR and 50 axial CT images and 200 sagittal cryosections of 50 TMJs, they found that the roof and posterior wall of the glenoid fossa (bordering the middle cranial fossa and the external auditory canal) had an inclination to the imaging planes used in TMJ radiography that makes them highly susceptible to

projection artifacts. They found that inclination of parts of the fossa roof exceeded the limit for reliable depiction in corrected sagittal and coronal planes in 40% and 8% of the joints respectively. The inclination of parts of the posterior wall of the fossa exceeded the limit for reliable depiction in corrected sagittal and in true sagittal planes in 100% and 84% of the joints respectively. In 84% of the joints the inclination exceeded the limit for reliable depiction in the axial plane. For both bone walls the regions with unfavorable inclination were in the medial part of the joint. They concluded that the oblique coronal projection is well suited for depiction of the roof of the fossa,is preferable to a sagittal projection, and an oblique axial projection is required to accurately depict the posterior wall.

Ahlqvist and Isberg evaluated the validity of MPR CT for depiction of the bone margins of the TMJ using 7 specimens. They compared measurements from coronal MPR images with bone dimensions as the full width at half maximum separating the TMJ from the middle cranial fossa, middle ear and external auditory canal. They found good agreement when the bone walls were thicker than 1 mm with accuracy influenced only by the angle of the bone wall to the scanning plane. Conversely, they found that bone walls thinner than 1 mm were reproduced with a magnification that increased with decreasing bone thickness. The difference increased further as the inclination of the bone wall became greater. They concluded that measurements were reliable within ± 10% for bone walls more than approximately 1 mm thick which form an angle of less than 35 degrees to the perpendicular of the scanning plane. They concluded that the accuracy of measurement depends, because of partial volume averaging effects, on scanning plane

and thickness with poorer agreement for thicknesses less than 1mm and inclination of the articular eminence exceeding 35 degrees.

Naitoh et al., (2004) recently evaluated the measurement accuracy of double-oblique reconstructed images (oblique orthogonal slices to oblique MPR along the dental arch) in multi-slice helical CT. They measured mandibular height from the alveolar crest immediately below an aluminum tube to the superior border of the mandibular canal using the double-oblique reconstructed images and the micro-CT average images of three semi-lateral dried mandibles. They reported a mean of the differences between the double-oblique reconstructed images with a table pitch of 1.5 in a helical scan and the micro-CT average images was 0.31 mm. They concluded that oblique coronal 2D reconstructed images from helical CT in the posterior mandible were highly accurate.

Most recently investigators have investigated the comparative accuracy of 3D reconstructed imaging. Cavalcanti and Vannier (1998) investigated the relative accuracy of craniofacial measurements (n=28) comprised of unique (n=7) and conventional craniometric anatomical landmarks (n=23). Measurements were obtained from volumetric spiral CT 2D and 3D reconstructed images by imaging 9 cadaver heads with spiral CT at 3 mm collimation with 2 mm/sec table feed. They found that the accuracy for 3DCT was higher than 2DCT images for seven of 28 measurements. In addition they found 25% of the 2DCT measurements to be significantly different from the physical measurements. They concluded, however, that all measurements with 3DCT were found to have satisfactory accuracy in comparison with physical measurements. In a follow up study on the measurement accuracy of 3D images from spiral CT, Cavalcanti et al., (1999) imaged 9 cadaver heads subjected to blunt trauma to simulate traumatic

craniofacial fractures. Measurements were made on the images twice by two observers, based on conventional craniofacial anatomic landmarks and compared with repeated dimensions on the cadaver heads obtained with an electromagnetic digitizer. They found the mean difference between the image and real measurements was less than 2 mm in all instances and no statistically significant differences between the 3D-CT and the physical measurements.

Using 4 phantom objects, Lo et al., (2000) evaluated the errors of 3-D measurements made by CT imaging by comparing the images to physical measurements. Linear, area, and volume measurement differences were statistically insignificant and ranged from 0% to 2.57%.

Most recently, Cavalcanti et al., (2004) performed physical measurements on 13 cadaver heads and examined them with spiral CT to determine the precision and accuracy of anthropometric measurements using 3D-CT. Linear measurements were based upon conventional craniometric anatomical landmarks, were identified by two radiologists twice each independently, and were then performed by 3D-CT. They found no statistically significant difference between inter-observer and intra-observer measurements or between imaging and physical measurements in both 3D-CT. The standard error was found to be between 0.45% and 1.44% for all the measurements in both protocols, indicating a high level of precision. The error between the mean actual and mean 3D-based linear measurements was 0.83% for bone and 1.78% for soft tissue measurements, demonstrating high accuracy of both 3D-CT protocols. They concluded that 3D-CT volume rendering images using craniometric measurements can be used for

anthropological studies involving craniofacial applications with a high level of accuracy (mean error 0.83%)

CBCT Imaging Accuracy

Manufacturers of digital volume tomography machines (CBCT) state that their machines offer no discernible distortion of anatomical images (accurate to 0.1mm) and produce a digital representation of the patient's anatomy as it exists in nature (anatomic truth).

The first CBCT dedicated to dento-maxillo-facial imaging (NewTom 9000 [(Quantitative Radiology, Verona, Italy)], was introduced to aid in planning for implant placement. The accuracy in 2D cross-sectional implant measurement was clinically acceptable and varied from 0.8-1% for width measurements and 2.2% for height measurements.

For implant radiography, limited field CBCT (LCBCT) was compared to spiral computerized tomography using 5 cadaver mandibles. The vertical distance from the alveolar ridge to a reference point was measured by caliper and compared to measurements obtained from the CT images. Measurement error on the LCBCT was minimal (0.01-.65mm or .1 to 5.2%).

Lascala et al. evaluated the reliability of the linear measurements obtained in CBCT images using a NewTom QR-DVT 9000 ((Quantitative Radiology, Verona, Italy) by comparing thirteen measurements. The measurements of internal and external anatomical structures were obtained in eight dried skulls using a pachymeter and were compared to those obtained from the analysis of axial, sagittal or coronal reconstruction images. The anatomical structures were: frontozygomatic suture; infra-orbital foramen;

anterior and posterior nasal spine; lateral pterygoid lamina; occipital condyle; groove for superior petrosol sinus; posterior and posterior clinoid process. He found that the real measures were always larger than those derived from the images, however these differences were only significant (p<0.05) for measurements of the internal structures of the skull base. He concluded that, although the CBCT images underestimate the real measurements between skull structures, this technique can be safely indicated for linear evaluation of skull structures, except for structures of the base skull. This results in no discernible error (accuracy to 0.1mm).[26, 30] Araki et al. presented the configuration and physical properties of the new iCAT system in 2004. Three patient cases were presented to display the ease in which developmental pathology could be detected.

TMJ Imaging

TMJ imaging accuracy is important not only to discern disease processes within the TMJ during routine examination, but also to detect when the roof and posterior walls of the glenoid fossa have developmental defects or thin walls in which adjacent structures may be penetrated during invasive procedures. In addition, when surgical reconstruction of the TMJ is contemplated with the use of SLA and TMJ implants, accuracy is paramount

The application of CBCT to image the TMJ was first reported by and imaging protocols (providing corrected sagittal and coronal multi-planar reformatted (MPR) views and 3D reconstructions of the TMJ) have been described. The technique is reported to provide high diagnostic quality images of the bony components of the TMJ while offering a shorter examination time and lower patient dose than that of the conventional CT.

Recently Beason and Brooks evaluated the accuracy of measurements made with the prototype i-CAT (called DentoCAT™; Xoran Technologies, Ann Arbor) on cross-sectional images of 13 pairs of condyles (N=26) as compared to physical measurements, as well as the presence of osseous changes. They used a scanning protocol consisting of placing nine condyles at a time on a platform and scanned all condyles as a group. Imaging factors used were 120 kVp, 90 mAs, 11 cm field of view, 600 images in a single revolution, high acquisition mode, and both high and default resolution image reconstruction (0.2 mm, 0.4 mm voxel size respectively). One observer (un-blinded) measured the length, width, and height of the condyles 3 times for each condyle with similar measurements made on the condyles using a digital caliper. The presence of erosions and osteophytes was also evaluated on both images and specimens. They found that measurements made from 2D image recontrustion were statistically smaller than physical measurements. They also noted that more erosions and osteophytes were noted physically than in the images. They proposed that the reasons for the statistically significant difference could be calibration of the reconstruction program and ability to select the correct slice in the reconstruction program.

Preliminary Data

The i-CAT (Imaging Science International, Hatfield, PA) CBCT unit was installed in Radiology and Imaging Sciences, Dept. of Surgical/Hospital Dentistry, ULSD in July, 2004. The most recent software upgrade (Version 1.3) allows oblique linear bilateral slice selection with variable slice width. This modality can be applied to the TMJ to provide axial, corrected coronal and serial corrected sagittal images of the TMJ articulation (Figure 8).
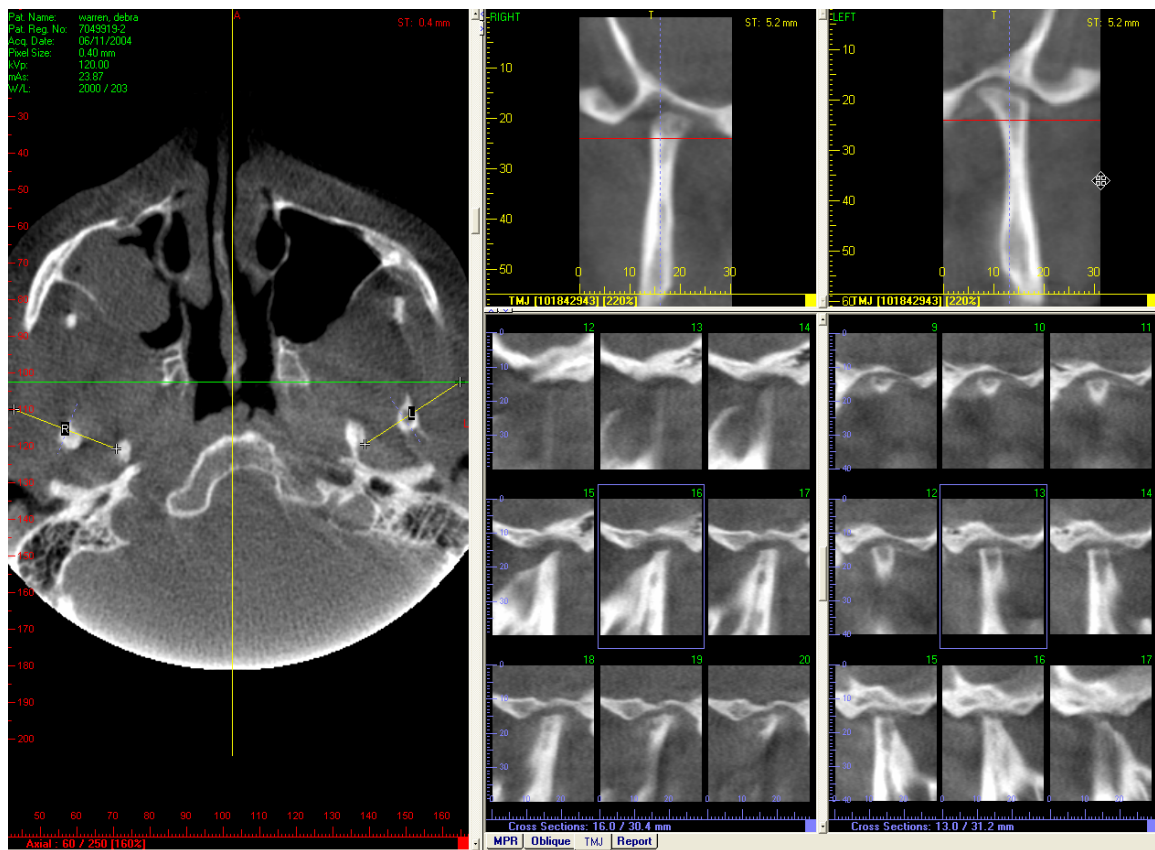
Figure 8. iCAT™ TMJ MPR imaging display protocol of a 46-year old female patient presenting with advanced rheumatoid arthritis affecting the TMJ. Axial image is shown on the left, corrected coronal images are shown on the upper right and sequential corrected sagittal slices are on the lower right

While our group has had considerable experience with imaging of the TMJ, we have also had occasion to have 3D images developed for a patient with rheumatoid arthritis, specifically for consideration of bilateral TMJ titanium replacement. Conversations with the company who manufacture such prostheses (TMJ Concepts, Ventura, CA) indicated that they have had no experience with the accuracy of the CBCT

images and recommended rescanning the patient according to their recommended CT protocol. This particular case accelerated the current interest in assessing the accuracy of TMJ measurements derived from CBCT iCAT images.

a.   b.
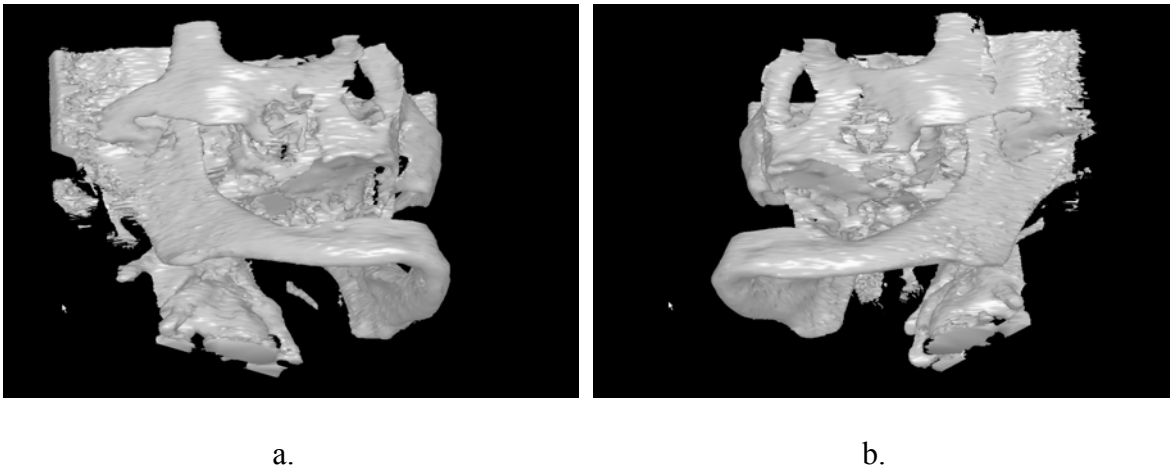
Figure 9. 3D reconstructed image from DICOM iCAT™ data of patient as described in Fig 8.

Therefore, we aim to determine whether CBCT produces accurate MPR images of a patient's TMJ articulation. More specifically, we hypothesize that the iCAT™ accurately produces an anatomically correct image in a 1:1 relationship to the true TMJ anatomy.

METHODS AND MATERIALS

This investigation was designed as an *in vitro* prospective self-controlled un-blinded experimental study. The sample was a group of skulls (n=25) which were imaged using CBCT and 3 digitally acquired extraoral cephalometric skull projections (lateral cephalometric, posterior-anterior cephalometric and submentovertex). Cone beam CT MPR projections were developed to demonstrate TMJ morphology and selected mandibular relationships. Ten TMJ and mandibular dimensions were measured on the skulls with a digital caliper and compared to magnification corrected measurements obtained from displayed images for each of the 4 modalities. A single rater (PI) performed the measurements on 3 independent occasions and the mean measurements and standard deviations compared with ANOVA with *post hoc* Dunnett *"t"* test.

Sample

Twenty-five intact dentate skulls (*n=25*) were obtained through the Department of Anatomical Sciences and Neurobiology at the University of Louisville. No demographic data was available on the available human remains so therefore the sample was not identified by age, gender or ethnic group. The Human Remains Committee within the Department of Anatomical Sciences and Neurobiology at the University of Louisville approved the study on September 1st, 2004.

The TMJ articulations (*n=50*) of all available skulls were inspected and digital photographic records taken. All condyles were essentially intact however because the

sample is used as teaching material some lateral and medial poles were slightly damaged. This consisted of minor loss of cortical material and a resultant defect. Retrospective visual audit of the human skulls was performed by 3 observers (PI, WCS OB), who reached a consensus as to the condition of the condyle via the Delphi method. The distribution of these defects in the sample is shown in Table 1. There were 20 condyles with lateral pole defects, 3 condyles with medial pole defects, 3 condyles with defects on both poles, and 24 of the condyles were completely intact. An example of this presentation is shown in Figure 10.

Table 1. Distribution of Condyle Defects in Skull Specimens.

Skull Designation	Condyle Status*		Skull Designation	Condyle Status*	
	Left	Right		Left	Right
D1	LP	LP	D43	I	LP
D7	LP	LP	D50	LP	LP
D13	MP	LP	D51	I	LP
D14	LP	LP	D56	I	I
D15	I	BP	D57	I	I
D22	MP	MP	D63	LP	LP
D24	I	LP	D66	BP	LP
D27	I	LP	D74	LP	LP
D29	LP	LP	D83	I	I
D31	I	I	D86	I	I
D34	BP	I	D89	I	I
D41	I	I	D105	I	I
			D107	I	I

* I = Intact; LP = lateral pole defect; MP = Medial pole defect; BP = Both poles defective

Figure 10. Digital photographic records showing examples of intact and non-intact condyles. Magnified images of two right TMJ condyles demonstrating normal (b.) and altered morphology (a.) with a minor lateral defect. From left; sagittal (lateral), coronal (frontal), and axial (superior) views.

In order to provide some degree of attenuation, 2-3 latex balloons filled with water were placed in the cranial vault prior to imaging. To simulate the TMJ inter-articular space and separate the mandibular condyle from the temporal fossa, a 1.5mm thick foam wedge was placed in the temporomandibular joint space between the glenoid fossa and the condylar head. For all images the teeth were in centric occlusion (maximum intercuspation) and the skulls held closed by metal springs bilaterally. A plastic head holder was constructed to support the skulls for imaging which provided stability by inserting a PVC pipe into the foramen magnum.

Imaging

Four radiographic modalities were used to image the 25 skull specimens:

1.   Extraoral projection radiography was performed using a Quint Sectograph (Model QS 10-1627W; Denar Corporation) using a 10:1 parallel grid. This device maintains a source-to-mid-sagittal distance of 5 feet. Skulls were stabilized in a cephalostat in three positions. Exposure settings were at 78 kVp, 200 mA, and 2/15 sec.

    a. *Lateral cephalometric (LC).* The skull was stabilized by two ear pieces inserted into the external auditory meati of the skull and positioned such that the Franfort plane was parallel to the floor. The skull was oriented such that the sagittal plane was perpendicular to the x-ray beam with the left side of the specimen closest to the imaging detector. The central ray of the beam was directed at the right external auditory meatus.

    b. *Cephalometric posterior anterior (PA).* The skull was stabilized by two ear pieces inserted into the external auditory meati of the skull and positioned such that the Franfort plane was parallel to the floor. The skull was oriented such that the sagittal plane was parallel to the x-ray beam with the facial bones of the skull of the specimen closest to the imaging detector. The central ray of the beam was directed midway between the external auditory meati at the level of the nuchal line.

    c. *Submentovertex (SMV).* For this projection the skull was also stabilized by two ear pieces inserted into the external auditory meati of the skull and positioned such that the Franfort plane was perpendicular to the floor. This necessitated that the chin was raised. In addition the skull was oriented such that the sagittal plane was parallel to the x-ray beam

45

with front of the specimen's head facing the x-ray beam and the vertex of the skull closest to the imaging detector. The entrance projection of the central ray of the beam was directed approximately midway between the condyles.

2. *Cone beam computed tomography (CBCT).* CBCT images were acquired of the entire skull using the i-CAT™ CBCT unit (Imaging Sciences International, Hatfield, PA, USA). The device was operated at 1-3 mA and 120 kV using a high frequency, constant potential, fixed anode with a nominal focal spot size of 0.5mm. Each skull was positioned into the device supported by the constructed plastic head holder. The hard tissue chin of each skull was inserted into the chin holder and vertical and horizontal laser lights on the device used to position the head. The head was oriented such that the mid-sagittal was perpendicular to the floor and the horizontal laser reference was along an imaginary line at the intersection of the posterior maxillary teeth and alveolar ridge. Lateral scout radiographs were then taken and small adjustments made to the skull orientation such that discrepancies between bilateral structures (e.g. posterior and inferior border of the mandibular ramus, zygomatic arch) were less 5mm (Figure 11). This positioned the skull for imaging such that the minimal amount of distortion occurred and that analysis with the proprietary software could be facilitated.

A single 360 degree rotation 20 sec. scan comprising 306 projections was then taken for each skull with a "full" field of view (17cm (diameter) x 13.2cm (height)) using the iCAT™ software (Version 1.7.7). Primary reconstruction of the data was performed immediately after acquisition and took approximately 60 sec. Secondary reconstruction

occurs in "real time" and provides contiguous color correlated 0.4mm axial, coronal and sagittal default 2D MPR slices. This results in 330 individual 0.4mm slices in each plane(Figure 12).

a.   b.
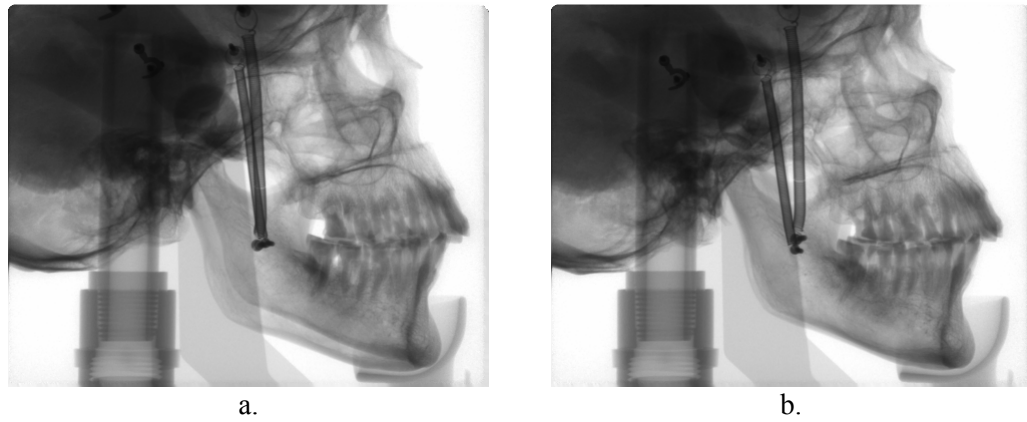
Figure 11. Scout images of a skull demonstrating initial position of specimen with excessive tilt (a.) and after adjustment immediately prior to scanning (b.)
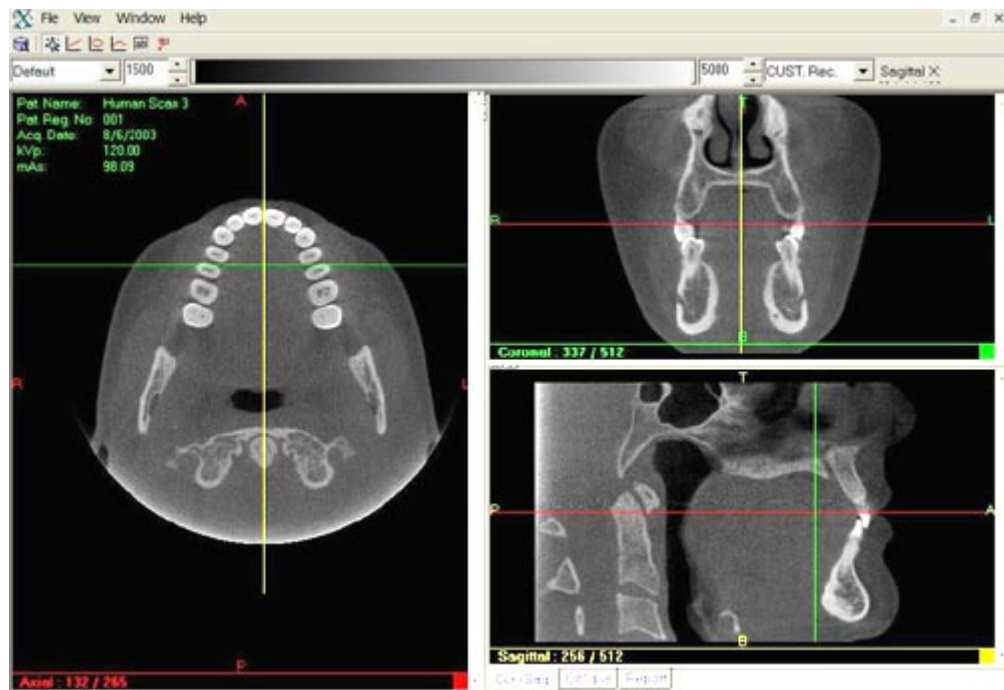
Figure 12. Default MPR iCAT™ display showing axial (left, color coded red), coronal

(top right, color coded green) and sagittal (lower right, color coded yellow) image slices.

Extraoral cephalometric images were acquired using an extra-oral photostimulable storage phosphor 8" x 10" imaging plate and scanned at 300dpi and 16-bit TIFF using the DenOptix™ Imaging system (Gendex/Kavo, Lake Zurich, IL, USA). The proprietary software used was VixWin™ 2000 (Version 1.2) digital imaging software (Gendex/Kavo, Lake Zurich, IL, USA). Images were exported from VixWin™ as lossless 16-bit TIF format without image enhancement. For display and analysis extraoral images were imported into a commercial photographic imaging software (Adobe Photoshop 7.0 2002; Adobe, 2002; San Jose, CA) and images equalized prior to measurement. This was performed to standardize post processing and image display rather than use the proprietary VixWin™ software equalization algorithm. Equalization redistributes the brightness values of pixels so that they more evenly represented over the entire range of brightness levels. After detecting the brightest and darkest values in the composite image, they are remapped such that the brightest value represents white and the darkest represents black. Brightness is then equalized by distributing the intermediate pixel values evenly through the gray scale (Figure 13).
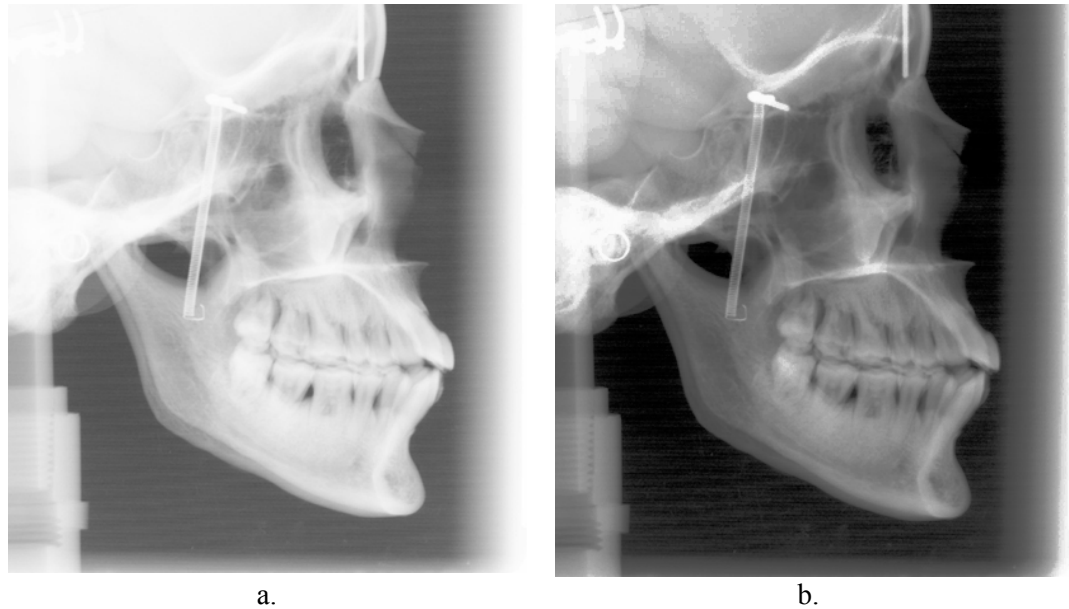
Figure 13. Example of effect of post processing using PhotoShop on a lateral
cephalometric image (a.) before and (b.) after image equalization.

CBCT images were acquired with a megapixel (1024 x 1024) flat-panel
hydrogenated amorphous silicon detector with cesium iodide scintillator and primary
reconstructed images reformatted from 306 projections providing a pixel matrix size of
0.4mm.

Measurement Analysis

On each skull specimen a number of anthropometric and/or cephalometric points
were identified and indelibly marked (Table 2). Operational definitions of these
landmarks were derived considering the vagaries of established definitions and in regard
to minimizing location subjectivity.

Ten linear measurements either directly characterizing the size of the individual
condyles (condylar width, length and height), or representative of intercondylar
(maximum lateral and maximum medial intercondylar distance), TMJ/mandible

(pogonion to condyle, pogonion to second molar, lateral mandibular condyle to gonion) or mandibular (maximum mandibular molar and maximum mandibular width) spatial relationship associated with the TMJ were then developed from a consideration of the operational definitions and with regard to coronal, axial and sagittal assessments provided by conventional extraoral plane projection imaging (Table C).

Table 2. Anatomical landmarks used as references for the measurements.

Landmark	Definition (Representative Figure)
Posterior mandibular condyle (PCo)	Most posterior extent of the mandibular condyle located 4mm inferior to the apex of the superior condylar surface (Fig. 14).
Anterior mandibular condyle (ACo)	Most anterior extent of the mandibular condyle located 4 mm inferior to the apex of the superior condylar surface (Fig. 14).
Lateral mandibular condyle (LCo)	Most lateral extent of the mandibular pole of the condyle viewed coronally (Fig. 15).
Medial mandibular condyle (MCo)	Most medial extent of the mandibular pole of the condyle viewed coronally (Fig. 15).
Superior mandible condyle (SCo)	Most superior apex on the concavity of the condylar head viewed sagittally (Fig. 14)
Inferior sigmoid notch (InfSig)	Most inferior apex on the concavity between the coronoid and condylar process of the mandible viewed sagittally (Fig. 14).
Pogonion (Pog)	Most anterior mid-sagittal point along the convexity of the chin of the mandible body viewed sagittally (Fig. 15).
Posterior superior mandibular condyle (PSCo)	Point along the posterior superior surface of the mandiblular condyle which is the greatest distance from Pogonion viewed sagittally (Fig.14).
Distal second molar (DM2)	Most superior distal contact point of the crown of the second mandibular molar relative to Pogonion in the sagittal plane (Fig. 14).
Mesial Second molar (MM2)	Most lingual mesial contact point of the crown of the second mandibular molar in the axial plane (Fig. 15).
Gonion (Go)	Point midway along the curvature of the angle of the mandible between the inferior border of the body and posterior border of the ramus of the mandible viewed sagittally (Fig. 14).
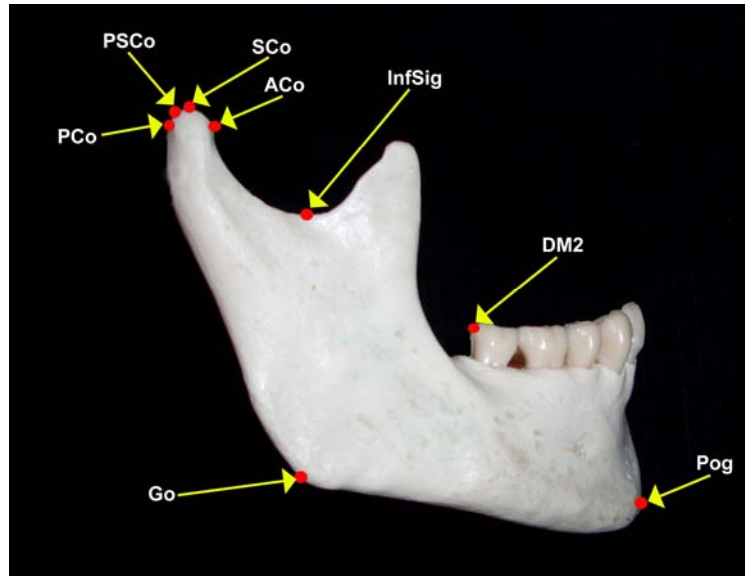
Figure 14. Anatomical Landmarks Sagittal View.
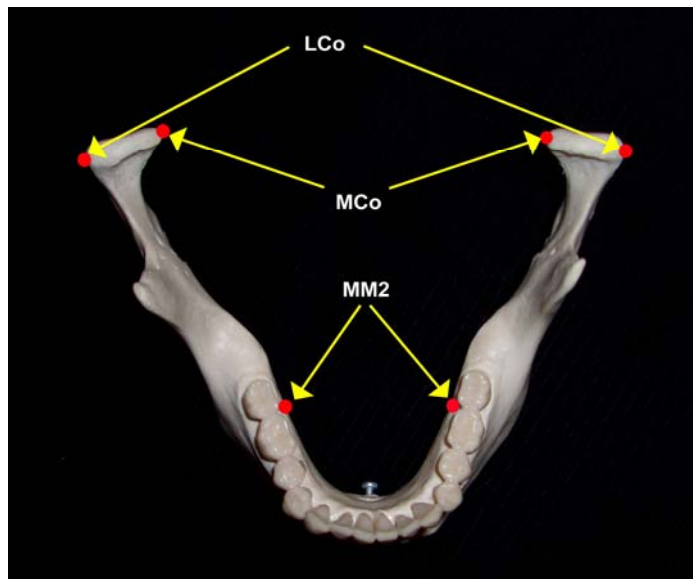
Figure 15. Anatomical Landmarks Axial View.

Table 3. TMJ specific and related measurements.

Measurement	Linear Distance (Figure)	Definition	Imaging Modality Procedure Figure			
			iCAT™	LC	PA	SMV
Condylar width	PC – AC (16)	Linear distance between the posterior mandibular condyle and anterior mandible condyle in the sagittal plane.	17	18	---	19
Condylar length	MCo – LCo (20)	Linear distance between the medial mandibular condyle and lateral mandible condyle in the coronal plane.	21	---	22	23
Condylar height	CoHt (24)	Perpendicular linear distance from the superior mandible condyle (SCo) to a tangent constructed between the most inferior point of the coronoid sigmoid notch (InfSig) perpendicular to a tangent of the posterior surface of the ramus in the sagittal plane.	25	26	---	---
Pogonion to Condyle	Pog – PSCo (27)	Linear distance between Pogonion and the posterior superior mandibular condyle in the sagittal plane.	28	29	---	---
Pogonion to Distal Second molar	Pog – DM2 (30)	Linear distance between Pogonion and the most distal superior point of the crown of the second mandibular molar in the sagittal plane.	31	32	---	---
Lateral mandibular condyle to Gonion	LCo – Go (33)	Linear distance between the lateral mandibular condyle and Gonion in the coronal plane.	34	35	36	---
Maximum lateral intercondylar distance	LCo – LCo (37)	Linear distance between the lateral mandibular condyles in the coronal plane.	38	---	39	40
Maximum medial intercondylar distance	MCo – MCo) (41)	Linear distance between the medial mandibular condyles in the coronal plane.	42	---	43	44

Table 3. (continued) TMJ specific and related measurements

Measurement	Linear Distance (Figure)	Definition	Imaging Modality Procedure Figure			
			iCAT™	LC	PA	SMV
Maximum mandibular molar width	M2 – M2 (45)	Linear distance between the most distal superior distal contact point of the second mandibular molars in the coronal plane	46	---	---	47
Maximum mandibular width	Go – Go (48)	Linear distance between gonion point in the coronal plane	49	---	50	51

To establish the true dimension of each linear measurement, 3 independent measurements were made directly on the skulls (true measurements) with a digital caliper (27-500-90, GAC). Representative images of these measurements are shown in Figures 16-49.

Measurements on digital extraoral images were performed by the PI on three separate occasions by importing the image files into a commercial photographic imaging software (Adobe Photoshop 7.0 2002; Adobe, 2002; San Jose, CA). After image enhancement by equalization (see previously), images were then magnified 200% and linear distances measured using the available cursor-driven measurement algorithm. The monitor used was a 17 in. (Proview, California) flat panel TFT color monitor with a screen resolution of 1280 x 1024 a 0.23 mm dot pitch set at an image quality of 32-bit.

While the measurement algorithm of the CBCT software is calibrated with respect to voxel dimensions, direct measurements from the extraoral projections are inherently magnified. To quantify the degree of radiographic magnification associated with each projection and to calculate a magnification factor to apply to the direct measurements, each of the radiographs was retaken for four skulls with a 100mm metal ruler placed in the mid-sagittal and perpendicular to the radiographic beam. Each ruler

was measured three times by the PI for each radiographic image and the mean radiographic distance determined (Table 4). Therefore all measured distances on the extraoral digital images were calibrated according to the calculated magnification. For LC the reduction factor was 9.92%, for SMV the reduction factor was 9.98% and for PA the reduction factor was 10.21%.

Table 4. Replicate Measurements (Mean ± Standard Deviation (SD)) of a 100 mm Ruler positioned in the Mid-sagittal of 4 Extraoral Digital Images (Lateral Cephalometric (LC), Cephalometric Submentovertex (SMV) and Posterior Anterior Cephalometric)

| Modality | Read | Specimen Identification | | | | Mean (mm) |
		D57	D63	D107	D14	
SMV	#1	111.4	110.6	110.9	111.7	
	#2	110.8	110.1	110.5	111.5	
	#3	111.4	110.8	111.3	111.1	
	Mean	111.20	110.50	110.90	111.43	111.01
	SD	0.35	0.36	0.40	0.31	0.40
LC	#1	110.8	111.1	112	110.7	
	#2	110.8	110.7	111.4	110.8	
	#3	111.4	110.6	111.2	111.3	
	Mean	111.00	110.80	111.53	110.93	111.07
	SD	0.35	0.26	0.42	0.32	0.32
PA	#1	111.5	111.5	111.7	111.2	
	#2	110.9	111.2	111.8	110.7	
	#3	111.4	111	112.1	111.3	
	Mean	111.27	111.23	111.87	111.07	111.36
	SD	0.32	0.25	0.21	0.32	0.35

A combination of 3 extraoral radiographic projections is necessary to provide visualization of the linear dimensions selected for the TMJ and mandibular measurements at least once. This is because the inherent nature of extraoral radiography provides 2D plane film projections. Cone beam CT however acquires 3D data during the acquisition process. Therefore based on choice of linear 2D MPR location and width it is

theoretically possible to provide multiple projections from which the same linear dimensions can be obtained. The iCAT™ CBCT default display provides perpendicular coronal, axial and sagittal 0.4mm wide image slices in the middle of the dataset. While the position of these default slices can be altered, it was necessary to develop 7 alternate projections using the available software. The projection construction and parameters used to provide appropriate images demonstrating the defined landmarks are summarized in Table 5 and detailed in Appendix A. The monitor used was a 17 in. (Proview, California) flat panel TFT color monitor with a screen resolution of 1280 x 1024 a 0.23 mm dot pitch set at an image quality of 32-bit.

Table 5. Description of Projections used to Measure TMJ and TMJ-related Linear

Dimensions.

Projection (s) Used	Image Projection Construction Method and Measurement (Slice thickness in mm)	Linear Dimension (s)
Limited area, trans oblique, narrow slice	Axial image is adjusted to image maximum medio-lateral condylar dimension. Oblique 2D MPR constructed along poles of condyle. Greatest dimension from multiple trans oblique limited MPR (1mm) recorded.	Condylar width
Limited area, trans oblique, narrow slice	Axial image is adjusted to image condyle and superior tip of coronoid process. Oblique 2D MPR constructed through tip of coronoid and anterior margin of external auditory meatus. Greatest dimension from multiple trans oblique limited MPR (1mm) recorded.	Condylar length
Wide area, oblique, medium slice	Axial image is adjusted to image condyle and superior tip of coronoid process. Oblique 2D MPR (10mm) constructed through tip of coronoid and anterior margin of external auditory meatus. Line constructed as per definition.	Condylar height
Wide area, oblique, medium slice	Axial image is adjusted to image condyle and superior tip of coronoid process. Oblique 2D MPR (12.4mm) constructed through posterior margin of external auditory meatus anteriorly through pogonion by scrolling axial image. Lines constructed as per definitions.	Pogonion to Condyle, Pogonion to Distal second molar
Wide area, oblique, wide slice	Axial image is adjusted to image condyle and superior tip of coronoid process. Oblique 2D MPR (28mm) constructed through anterior margin of condylar at junction of neck of condyle by scrolling axial image. Line constructed as per definition.	Lateral mandibular condyle to Gonion, maximum mandibular width
Wide area, oblique, medium slice	Axial image is adjusted to image condyle and superior tip of coronoid process. Oblique 2D MPR (10mm) constructed through lateral poles of both condyles. Lines constructed as per definitions.	Maximum lateral intercondylar distance, maximum medial intercondylar distance
Wide area, axial, narrow slice	Axial image is adjusted to image interproximal contact between the first and second mandibular molar. Line constructed as per definition	Maximum mandibular molar width

Figure: 16
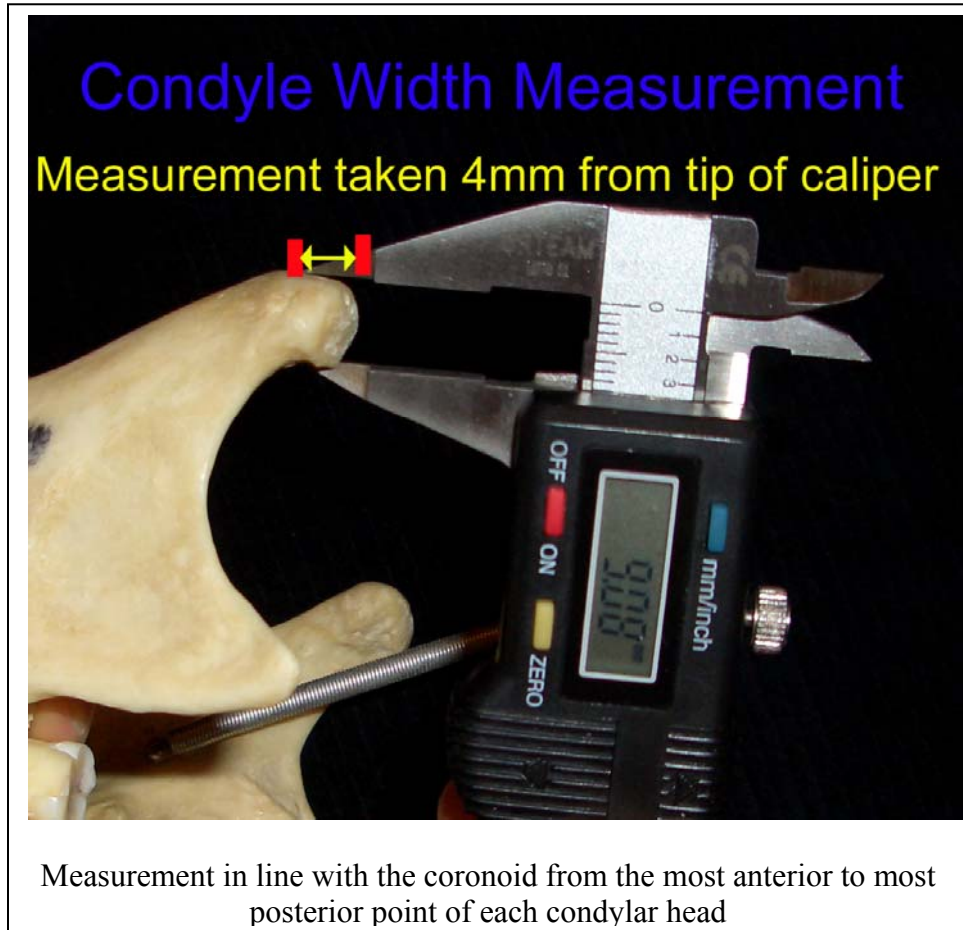
Measurement in line with the coronoid from the most anterior to most posterior point of each condylar head

Figure : 17

Measurement in line with the coronoid from the most anterior
to most posterior point of each condylar head using a slice in
the sagittal plane

Figure : 18

4mm From
Superior of Condyle

Condylar Width
Measurement

Measurement in line with the coronoid from the most anterior to most
posterior point of each condylar head
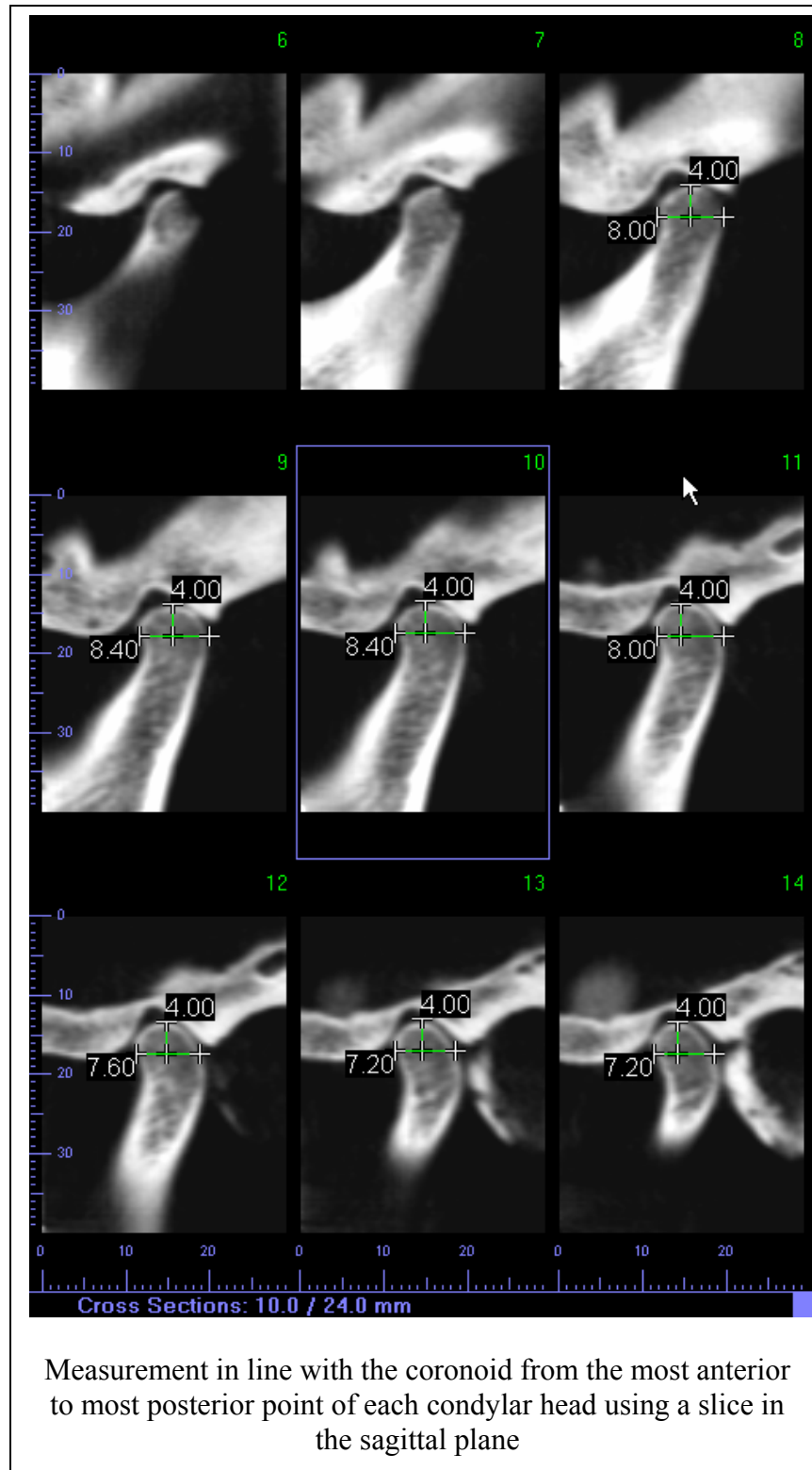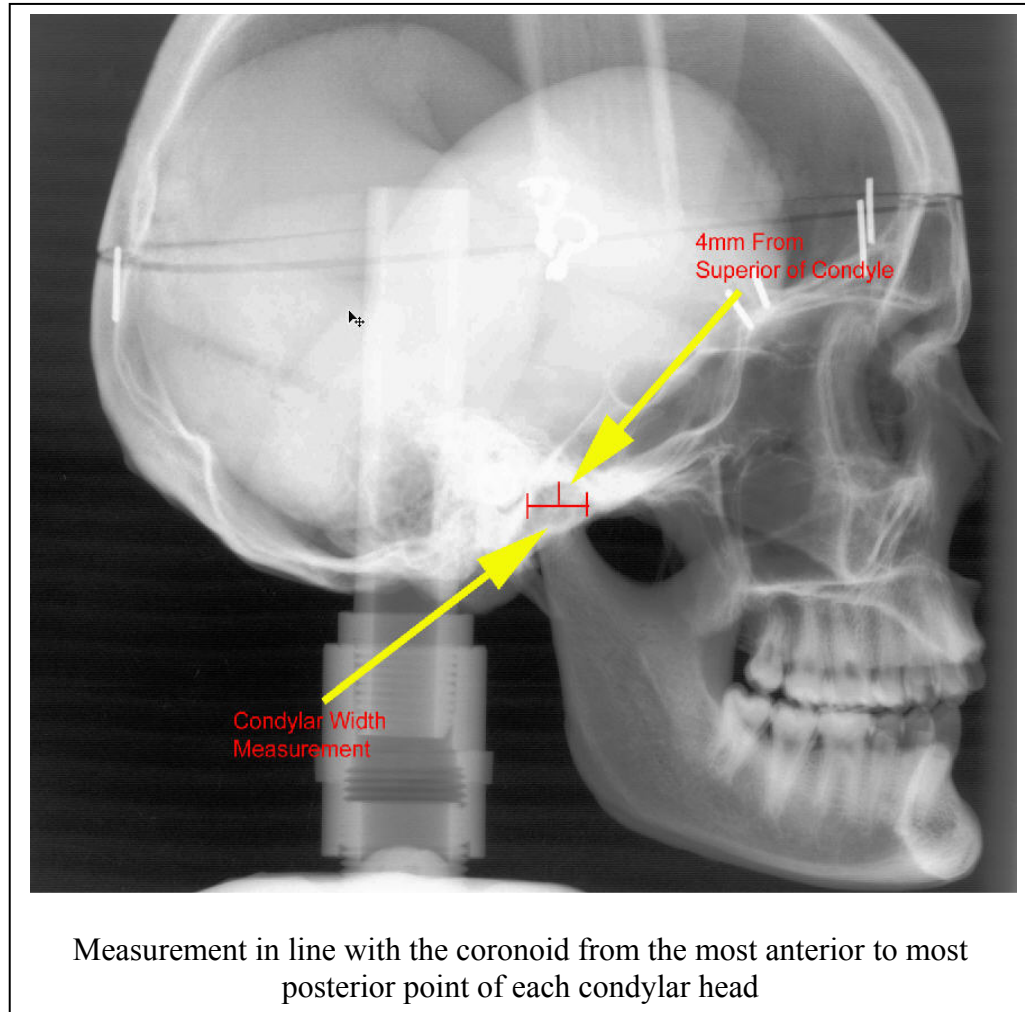
Figure : 19

SMV: CONDYLAR WIDTH MEASUREMENT
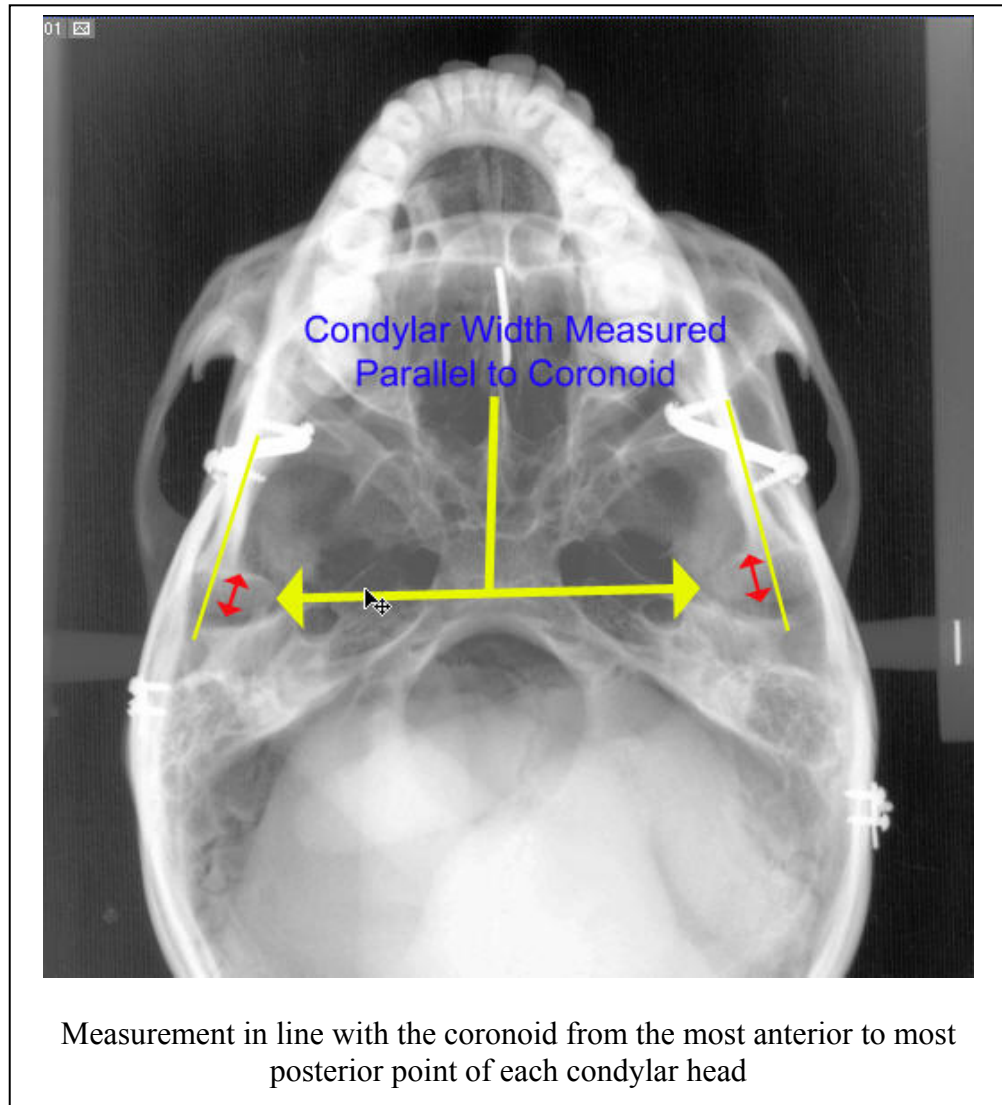
Measurement in line with the coronoid from the most anterior to most posterior point of each condylar head

Figure : 20

Most lateral to most medial point on each condyle

Figure : 21

Most lateral to most medial point on each condyle using a slice in the frontal plane
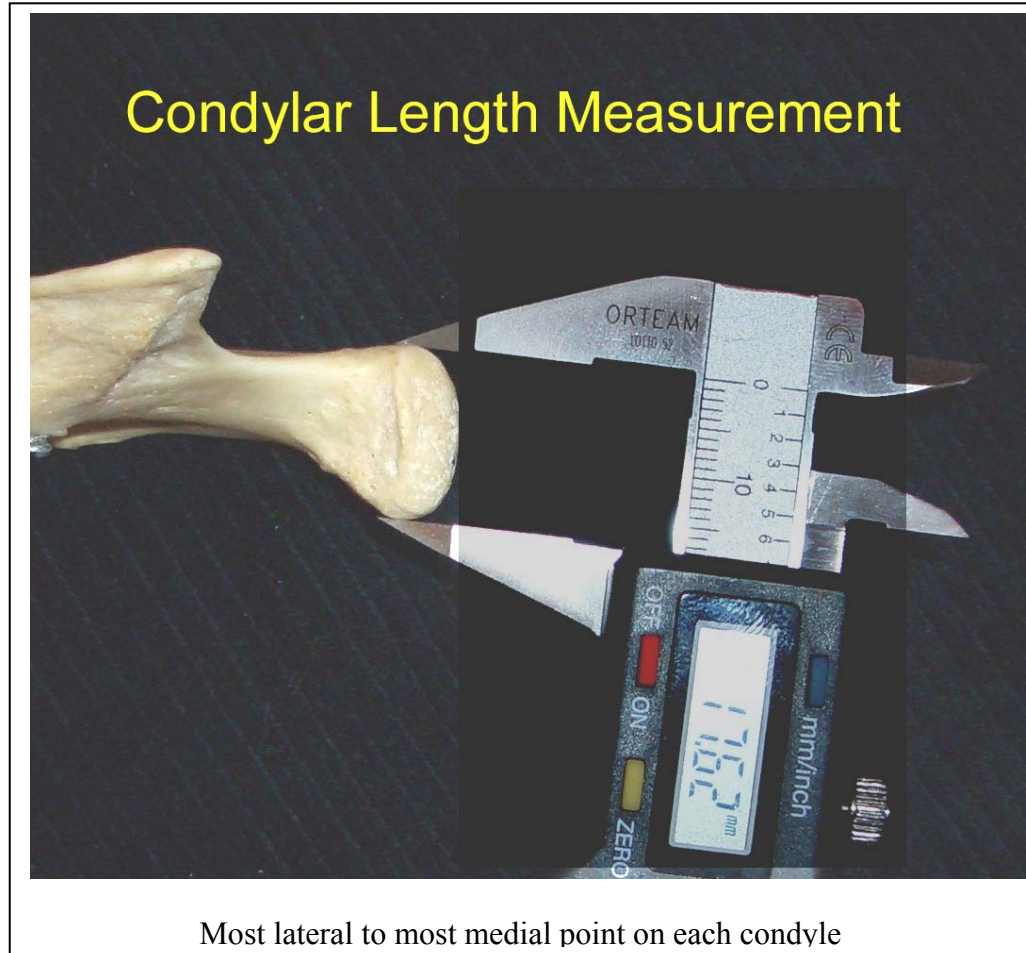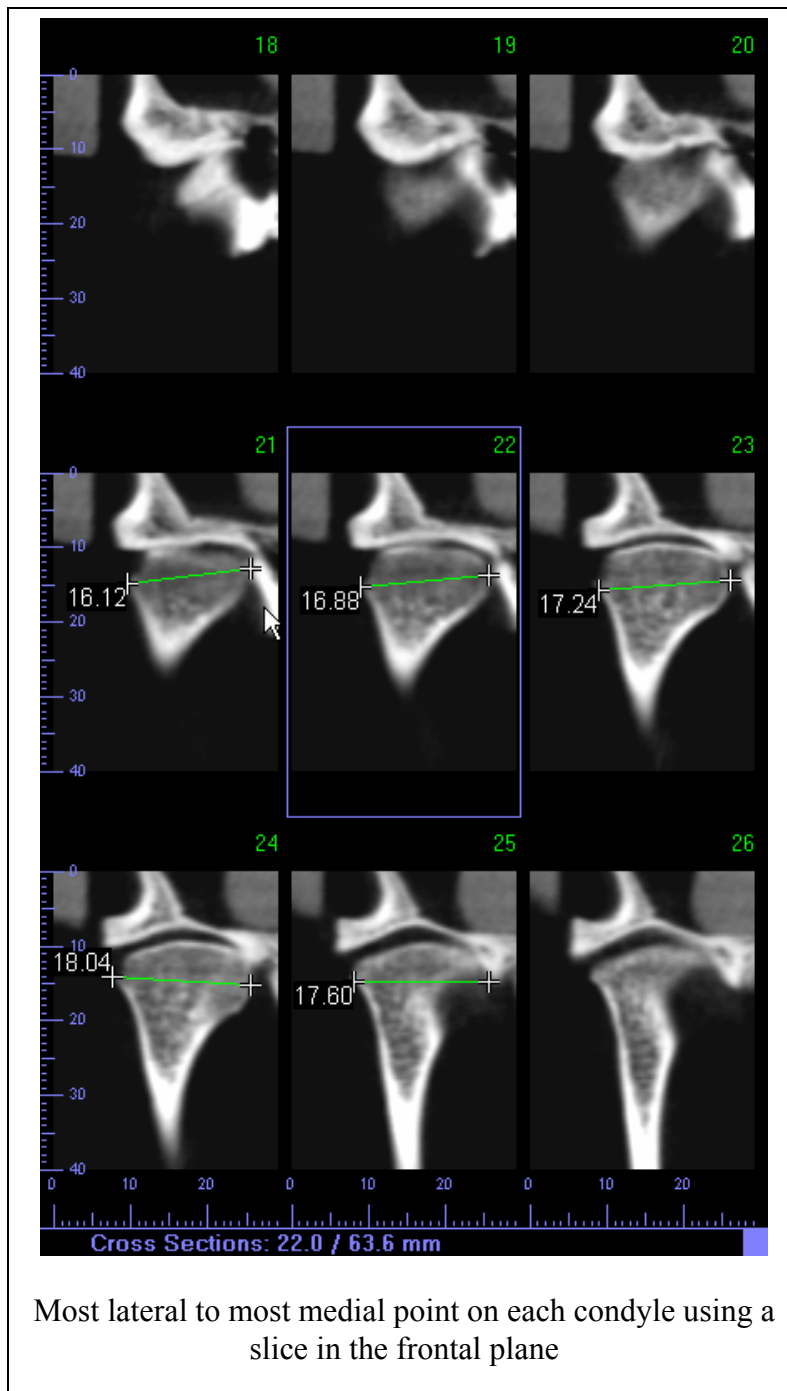
Figure : 22

PA: CONDYLAR LENGTH MEASUREMENT
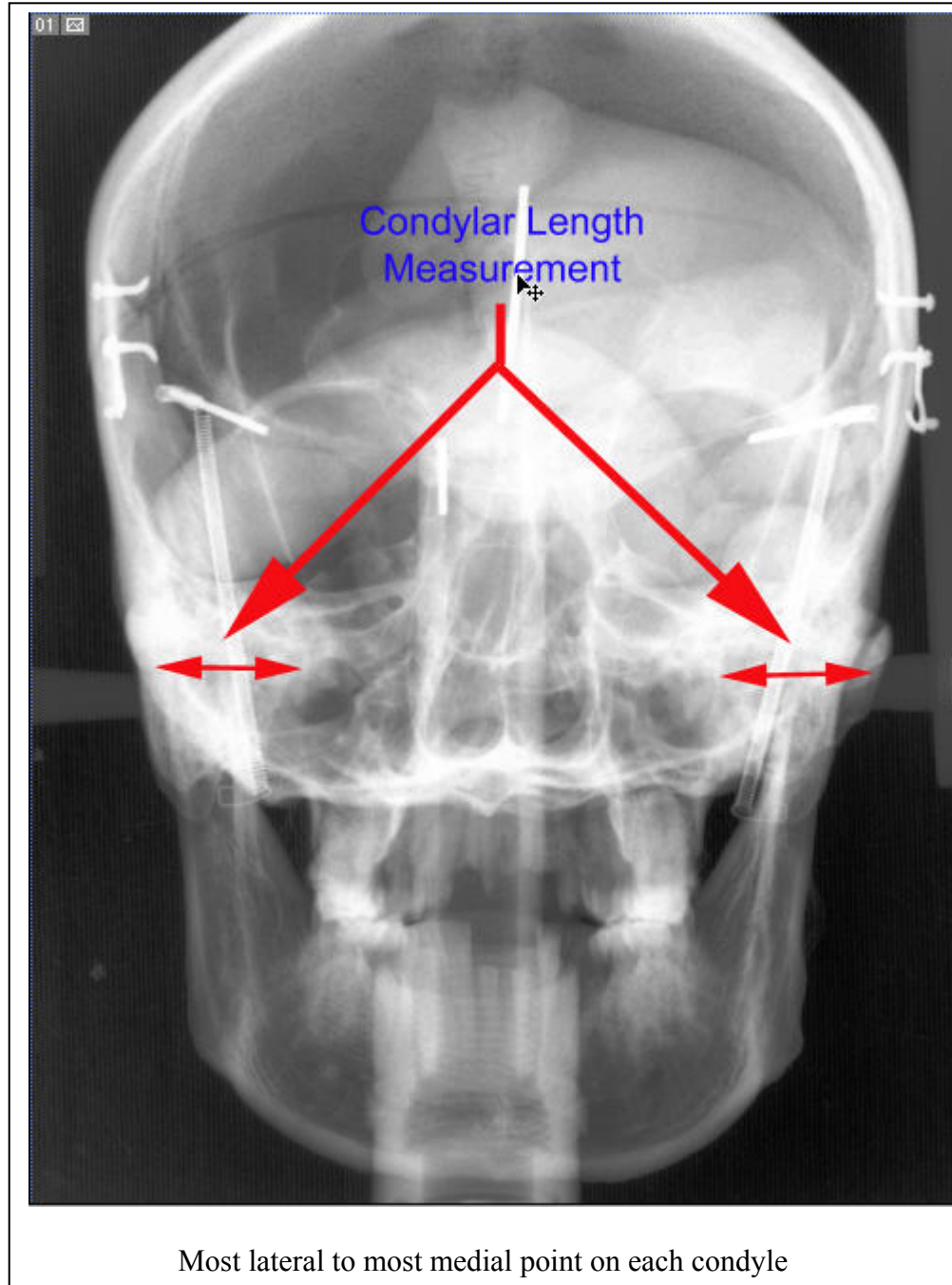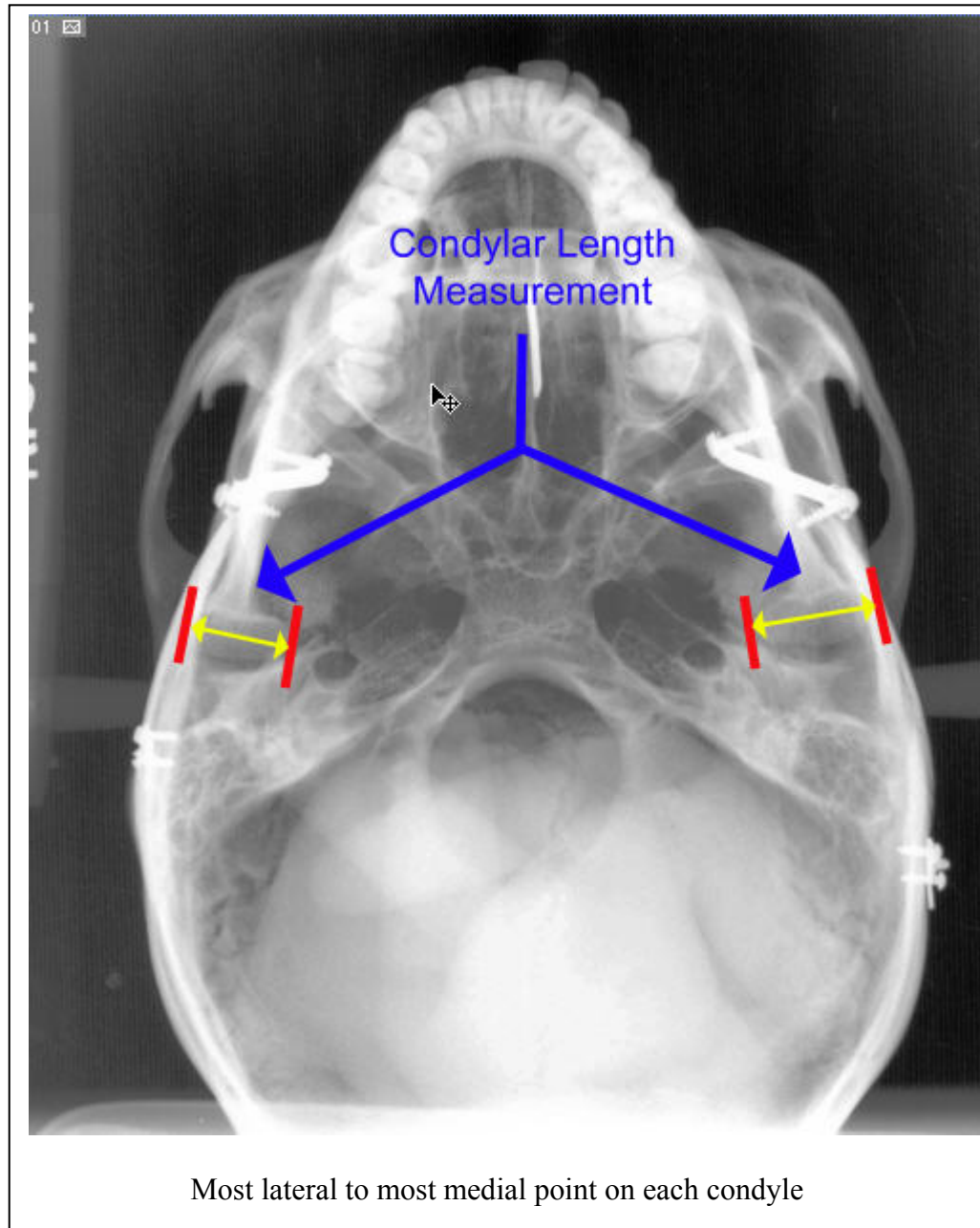
Most lateral to most medial point on each condyle

Figure : 23

Most lateral to most medial point on each condyle
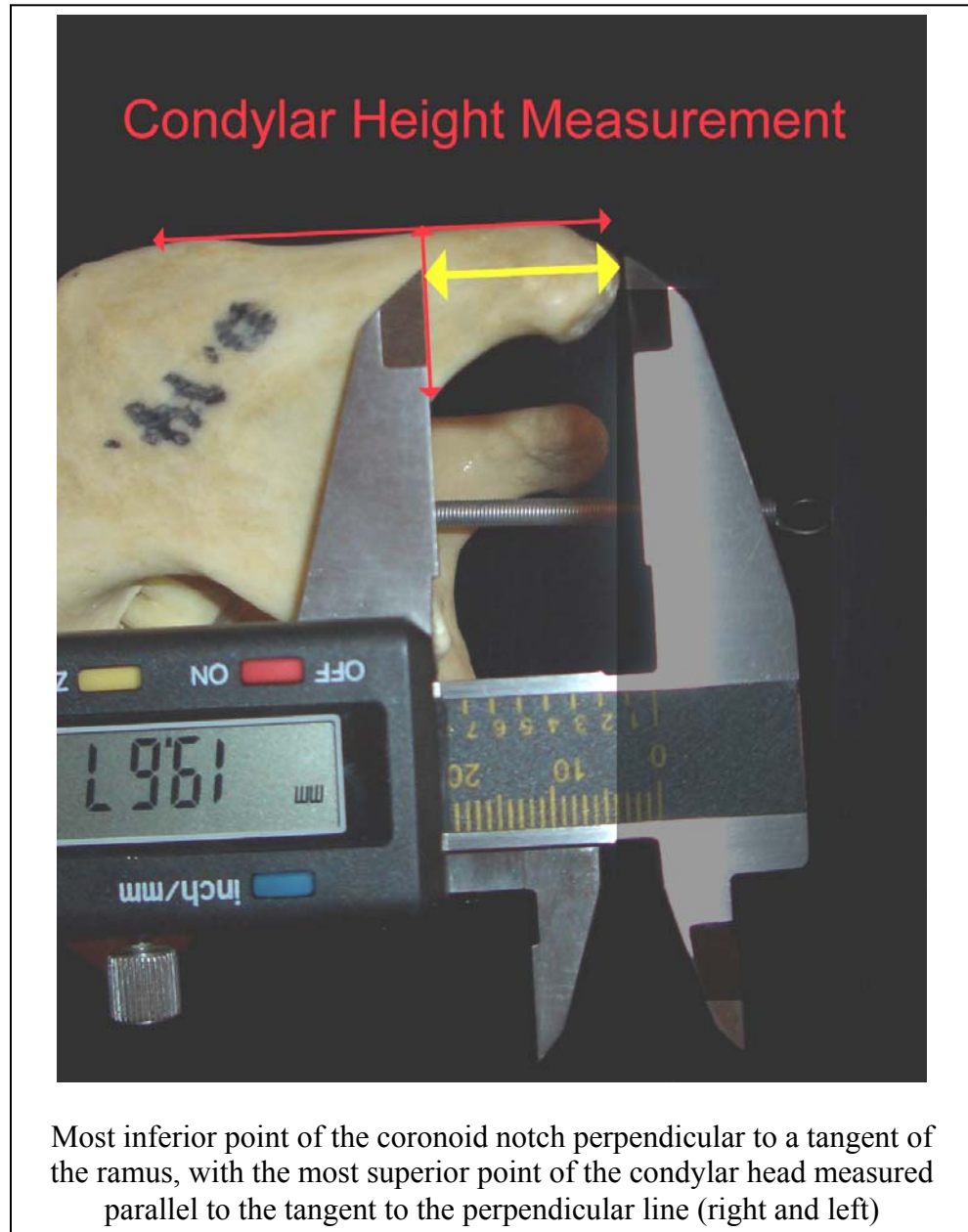
Figure : 24

Most inferior point of the coronoid notch perpendicular to a tangent of
the ramus, with the most superior point of the condylar head measured
parallel to the tangent to the perpendicular line (right and left)

Figure : 25

ICAT: CONDYLAR HEIGHT MEASUREMENT
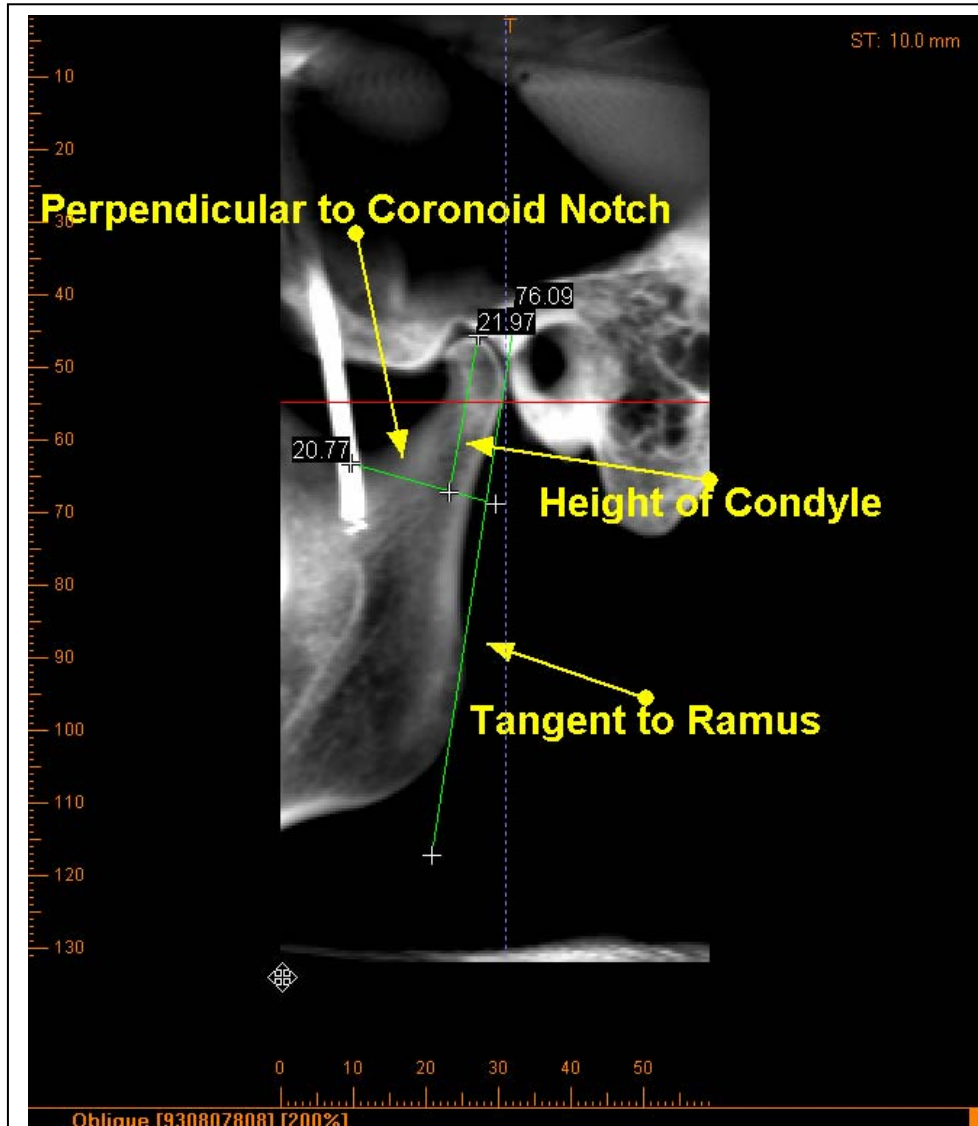
Most inferior point of the coronoid notch perpendicular to a tangent of the ramus, with the most superior point of the condylar head measured parallel to the tangent to the perpendicular line (right and left) using a sagittal slice

Figure : 26

CEPH: CONDYLAR HEIGHT MEASUREMENT
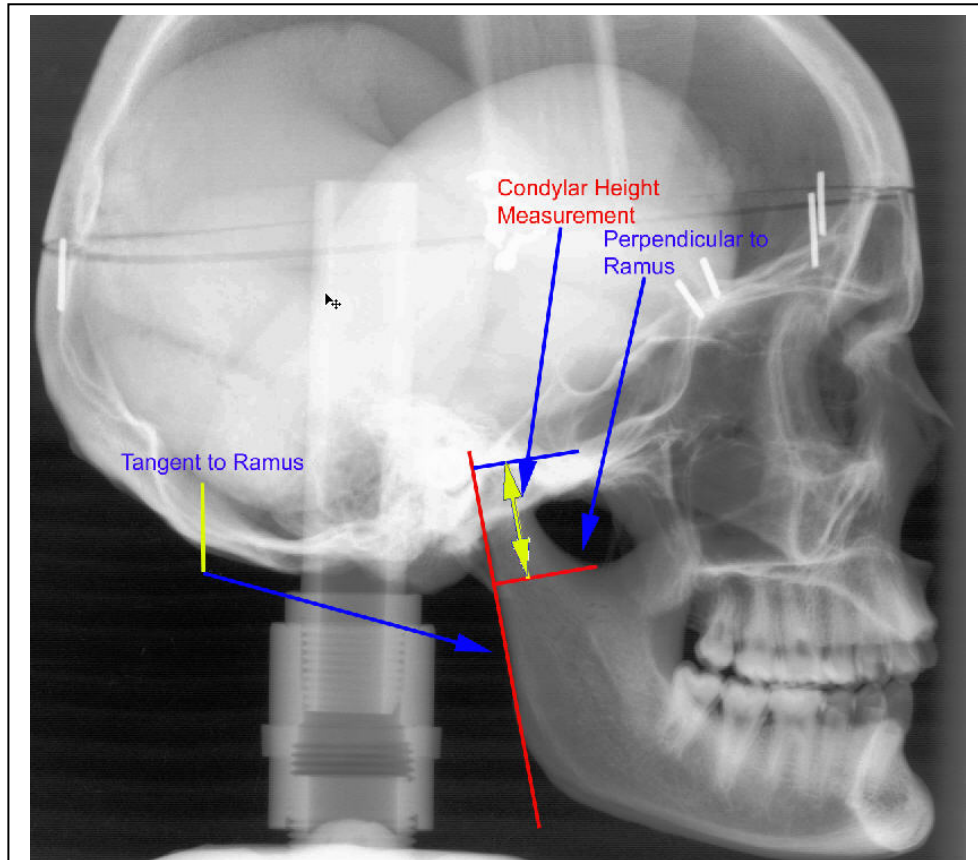
Most inferior point of the coronoid notch perpendicular to a tangent of the ramus, with the most superior point of the condylar head measured parallel to the tangent to the perpendicular line (right and left)

Figure : 27

TRUE: POGONION TO CONDYLE

Greatest distance from pogonion to the superior point
on the condylar head

Figure : 28

ICAT: POGONION TO CONDYLE

Greatest distance from pogonion to the superior point on the condylar head using sagittal slices through each condyle
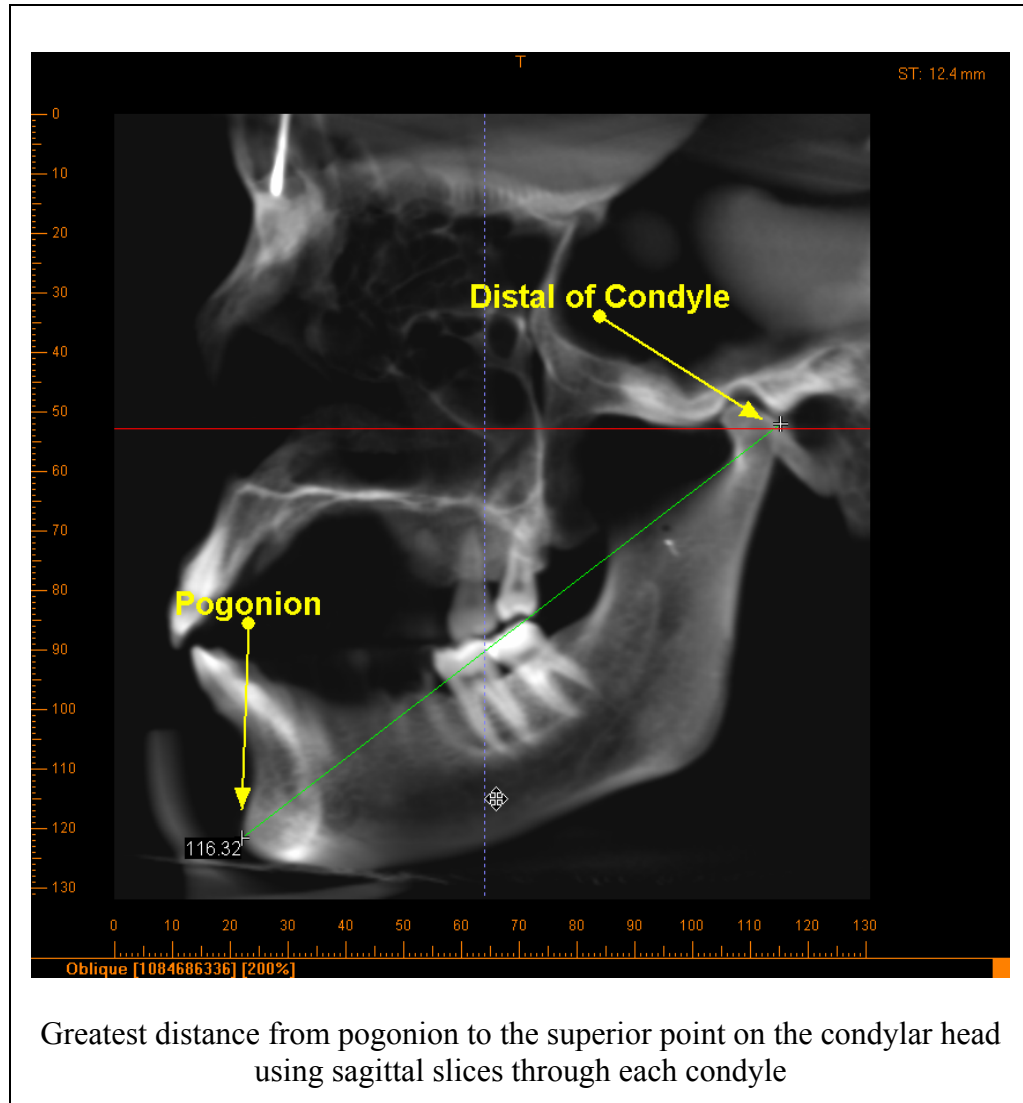
Figure : 29

CEPH: POGONION TO CONDYLE

Greatest distance from pogonion to the superior point on the condylar head
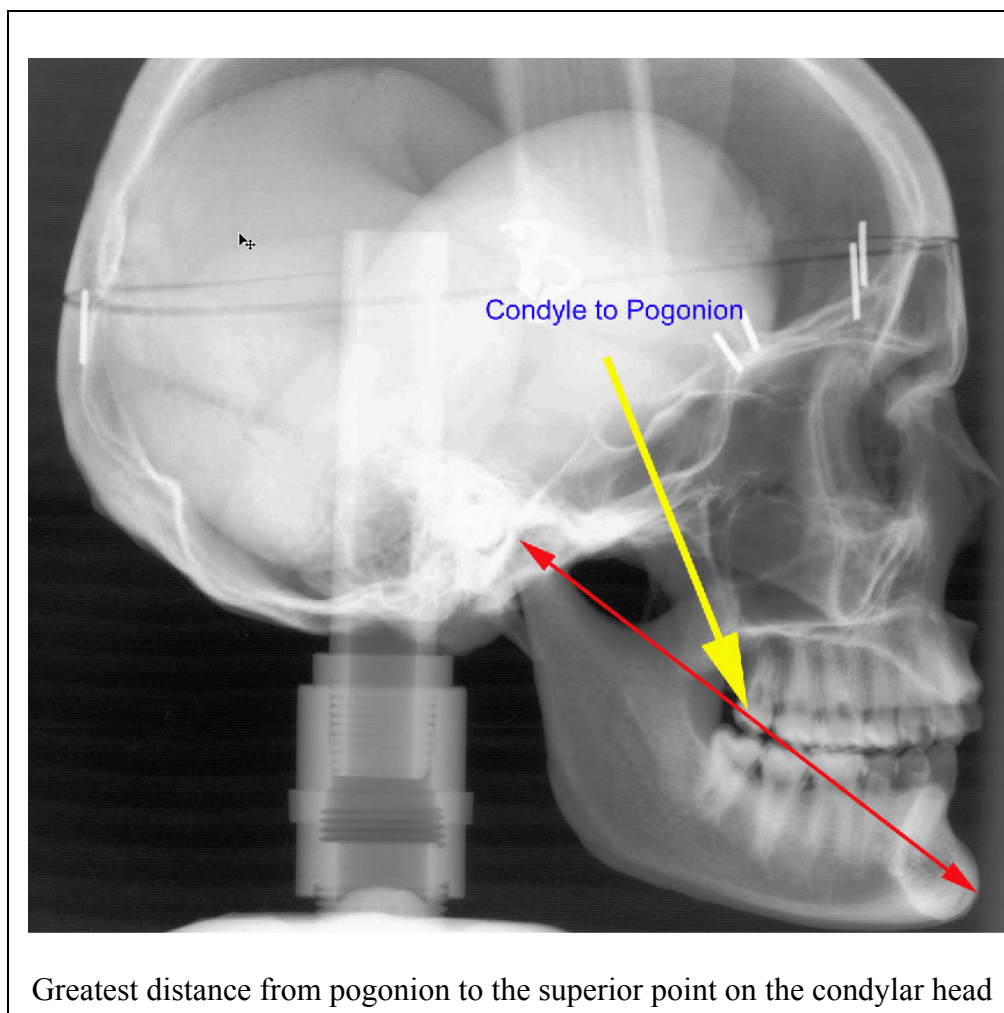
Figure : 30

TRUE: POGONION TO SECOND MOLAR

Pogonion to most distal point of the right and left twelve year molars
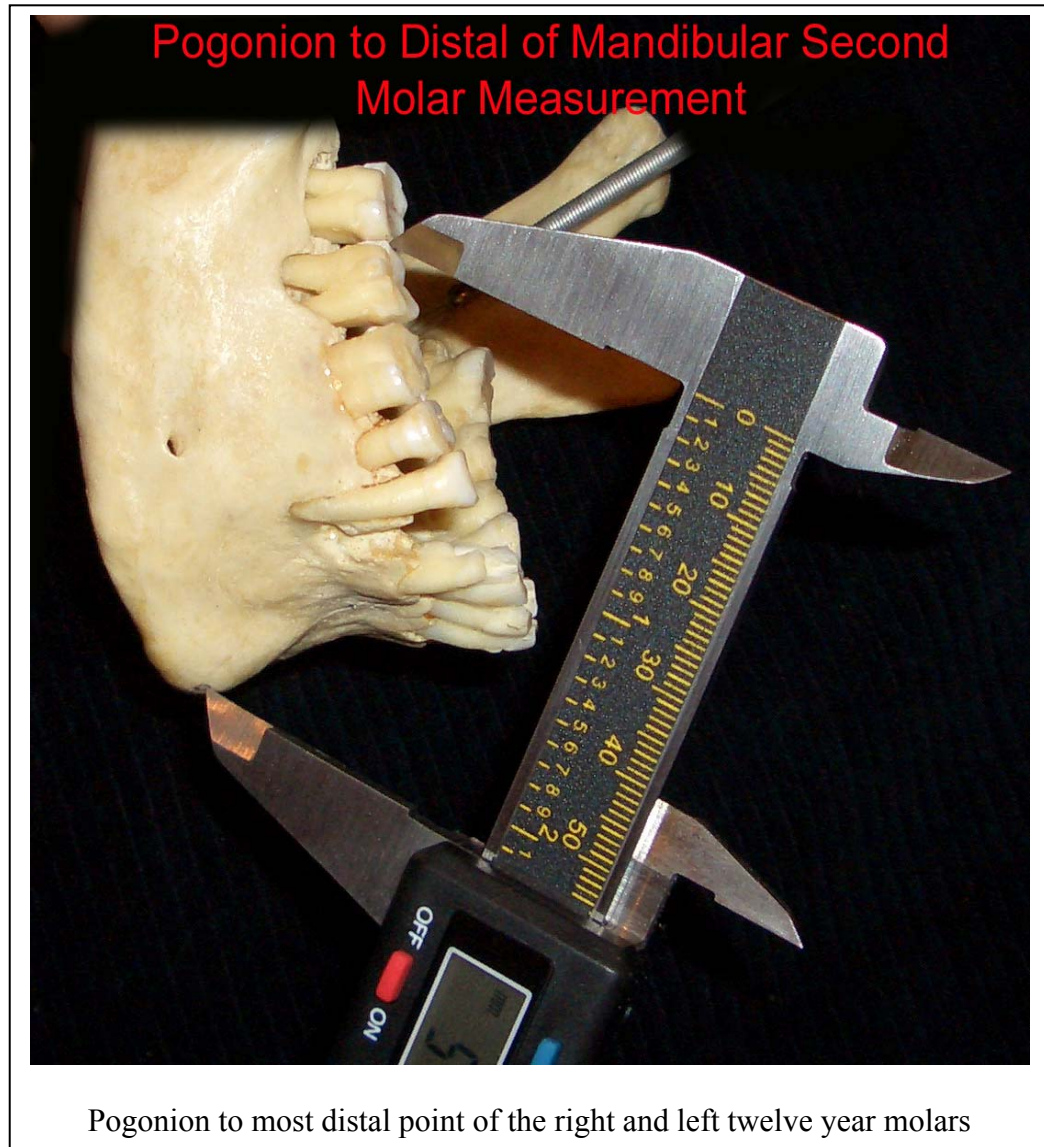
Figure : 31

ICAT: POGONION TO SECOND MOLAR

Pogonion to most distal point of the right and left twelve year molars using sagittal slices
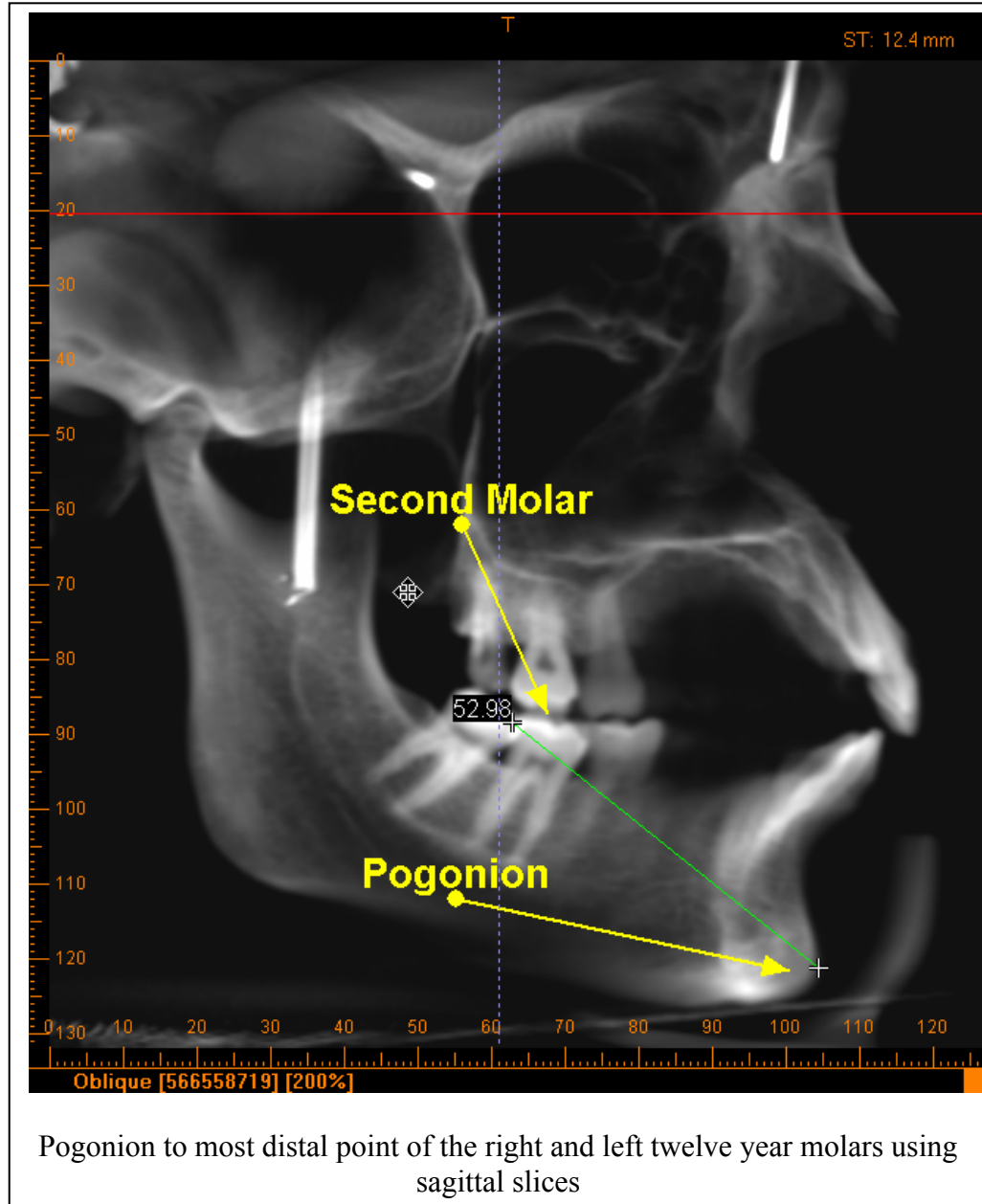
Figure : 32

<u>CEPH: POGONION TO SECOND MOLAR</u>

Pogonion to most distal point of the right and left twelve year molars
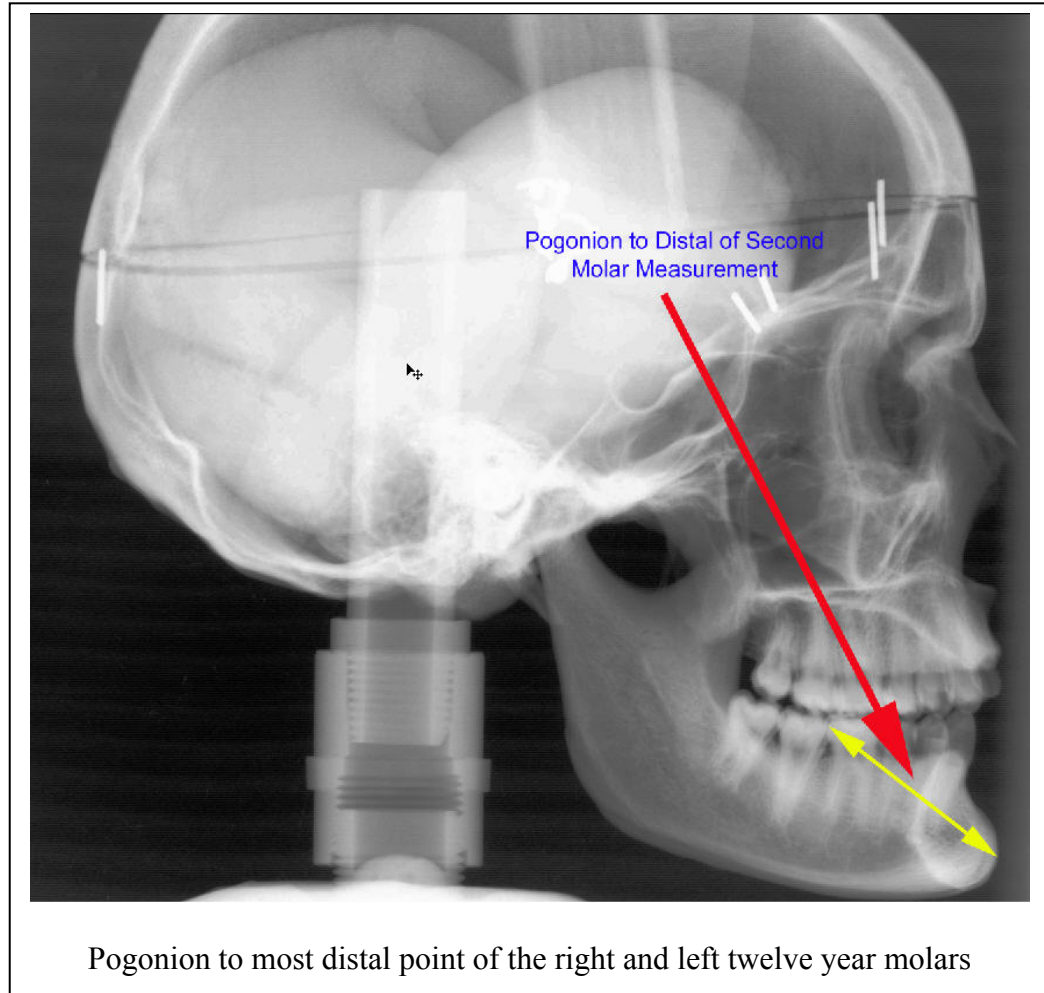
Figure : 33

Lateral pole of each condylar head to gonion

Figure : 34

ICAT: LATERAL POLE TO GONION

Lateral pole of each condylar head to gonion using a slice in the mid-
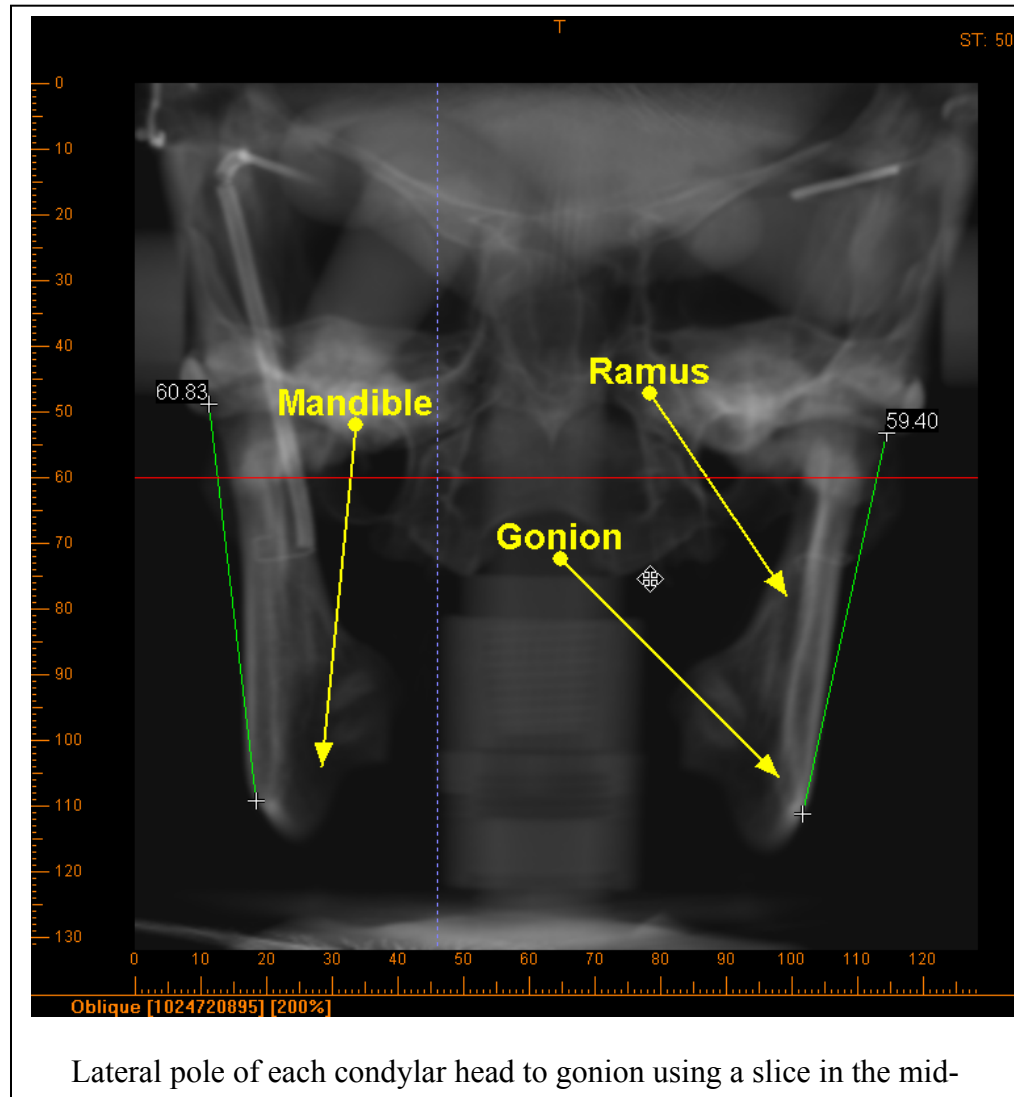
Figure : 35

<u>CEPH: LATERAL POLE TO GONION</u>

Lateral pole of each condylar head to gonion
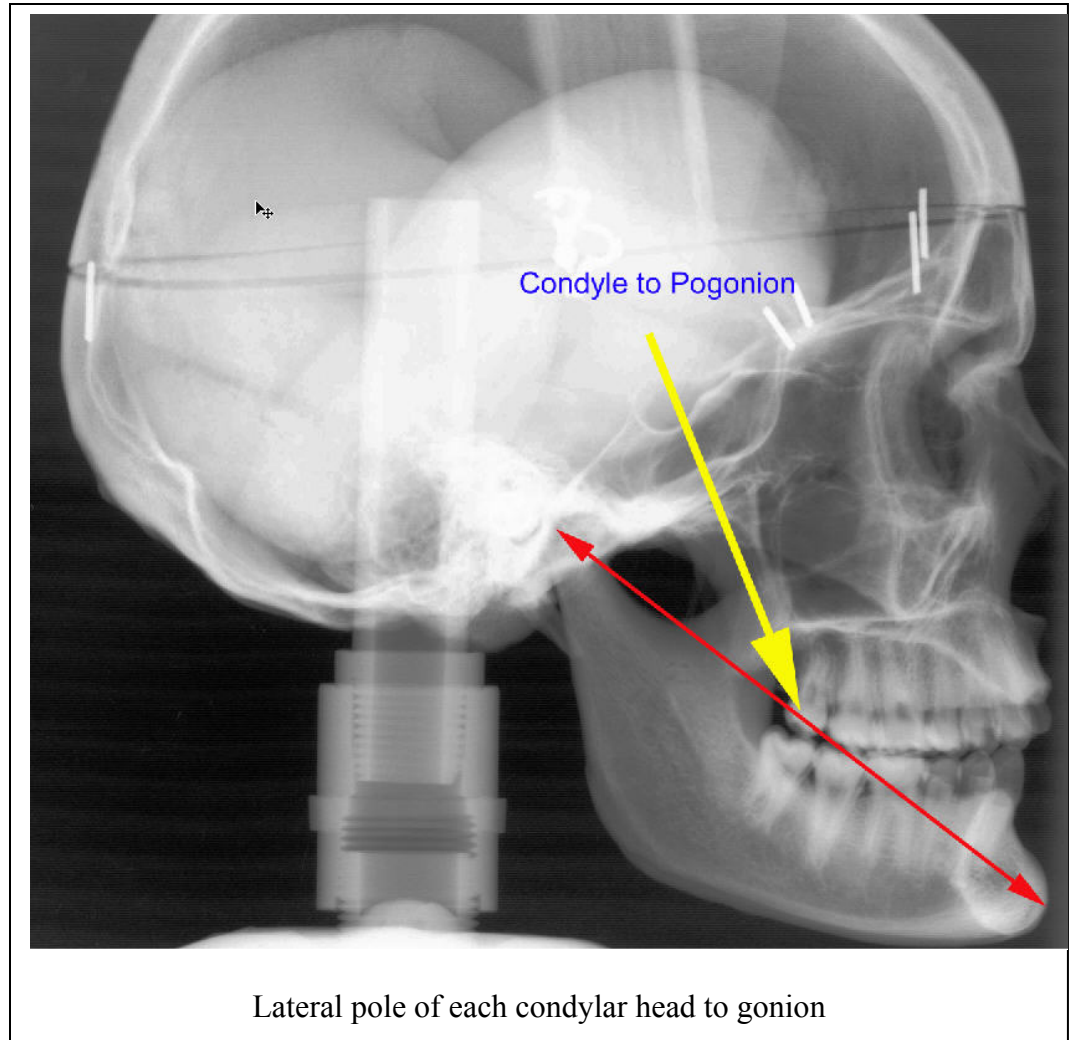
Figure : 36

Lateral pole of each condylar head to gonion
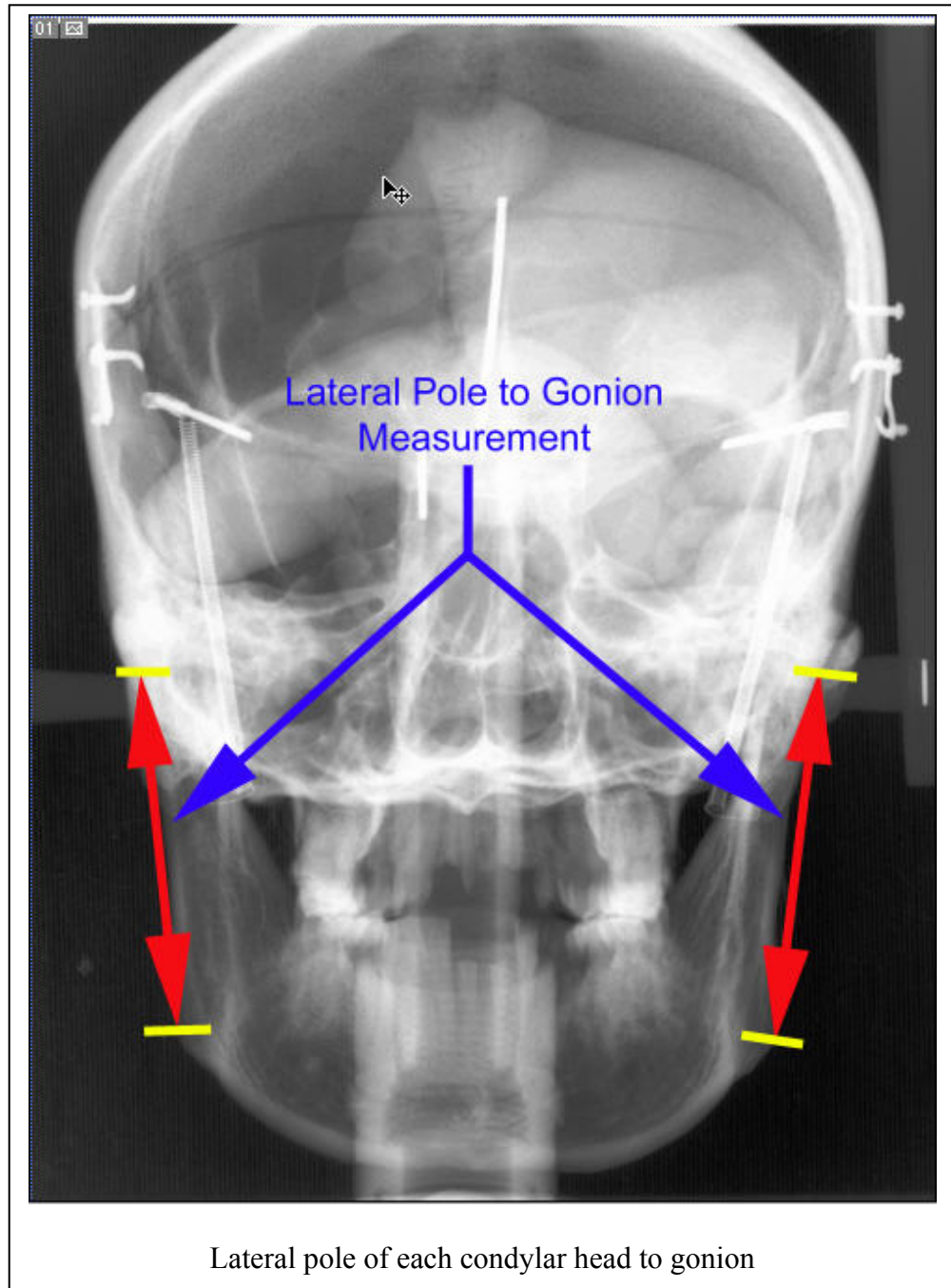
Figure : 37

<u>TRUE: LATERAL DISTANCE BETWEEN CONDYLES</u>

Condylar Length From Lateral Pole to Lateral Pole

Most lateral point on right condyle to most lateral point on left condyle
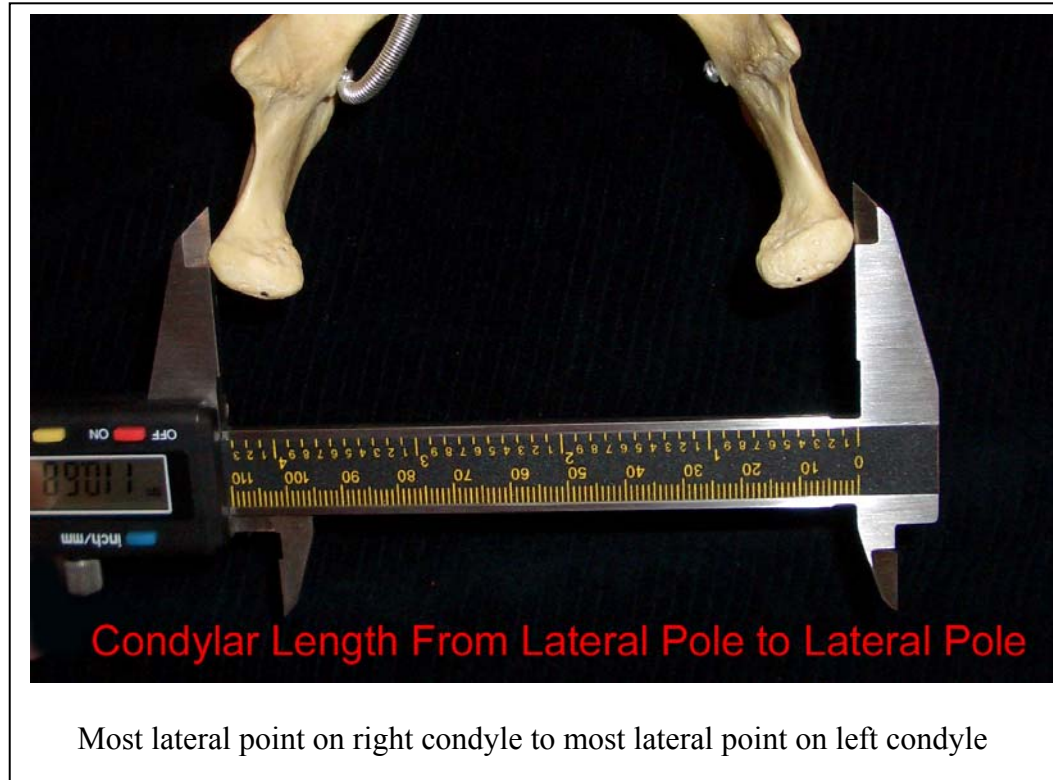
Figure : 38

ICAT: LATERAL DISTANCE BETWEEN CONDYLES

Most lateral point on right condylar head to most lateral point on left condylar head using a slice in the frontal plane
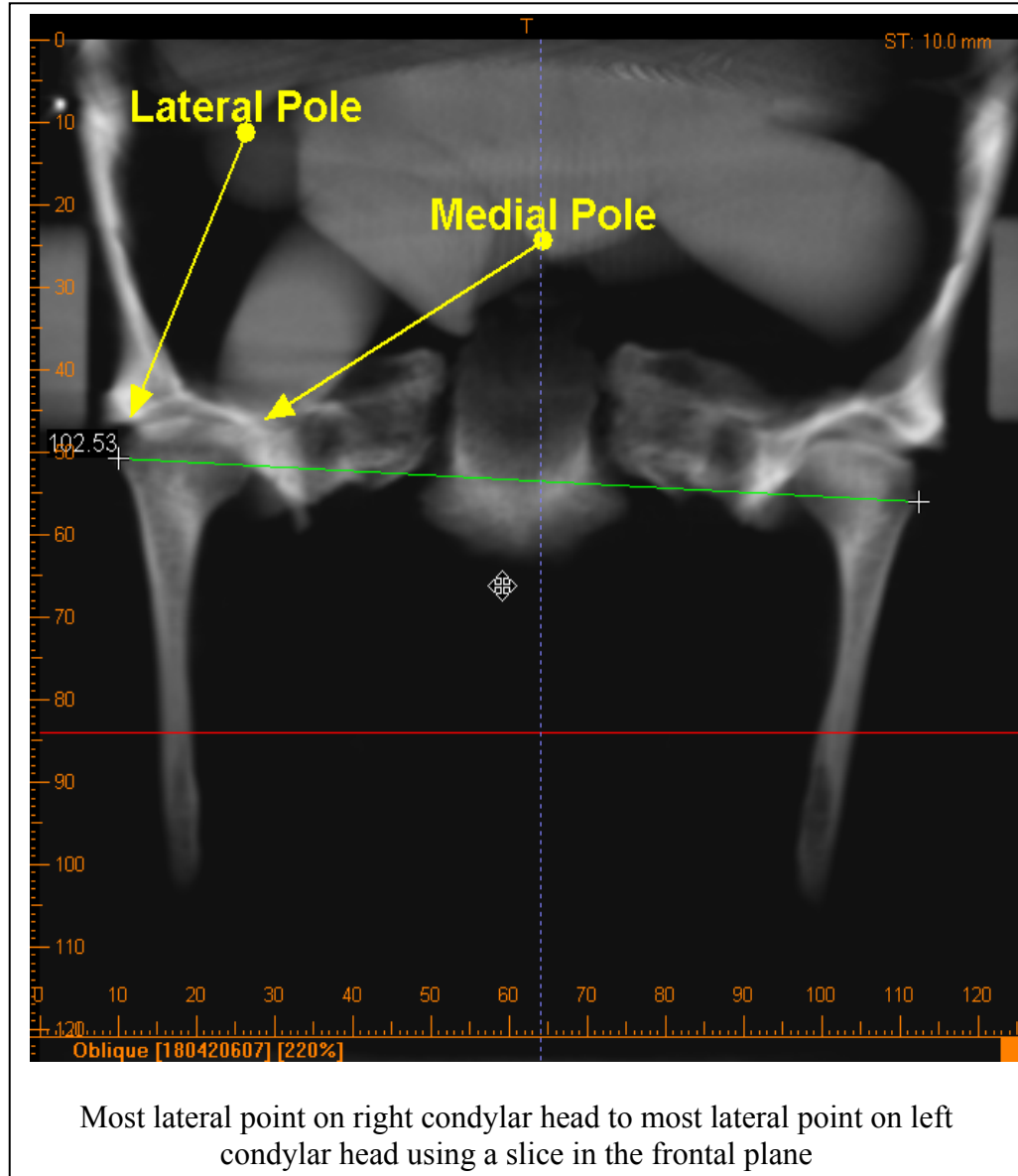
Figure : 39

PA: LATERAL DISTANCE BETWEEN CONDYLES
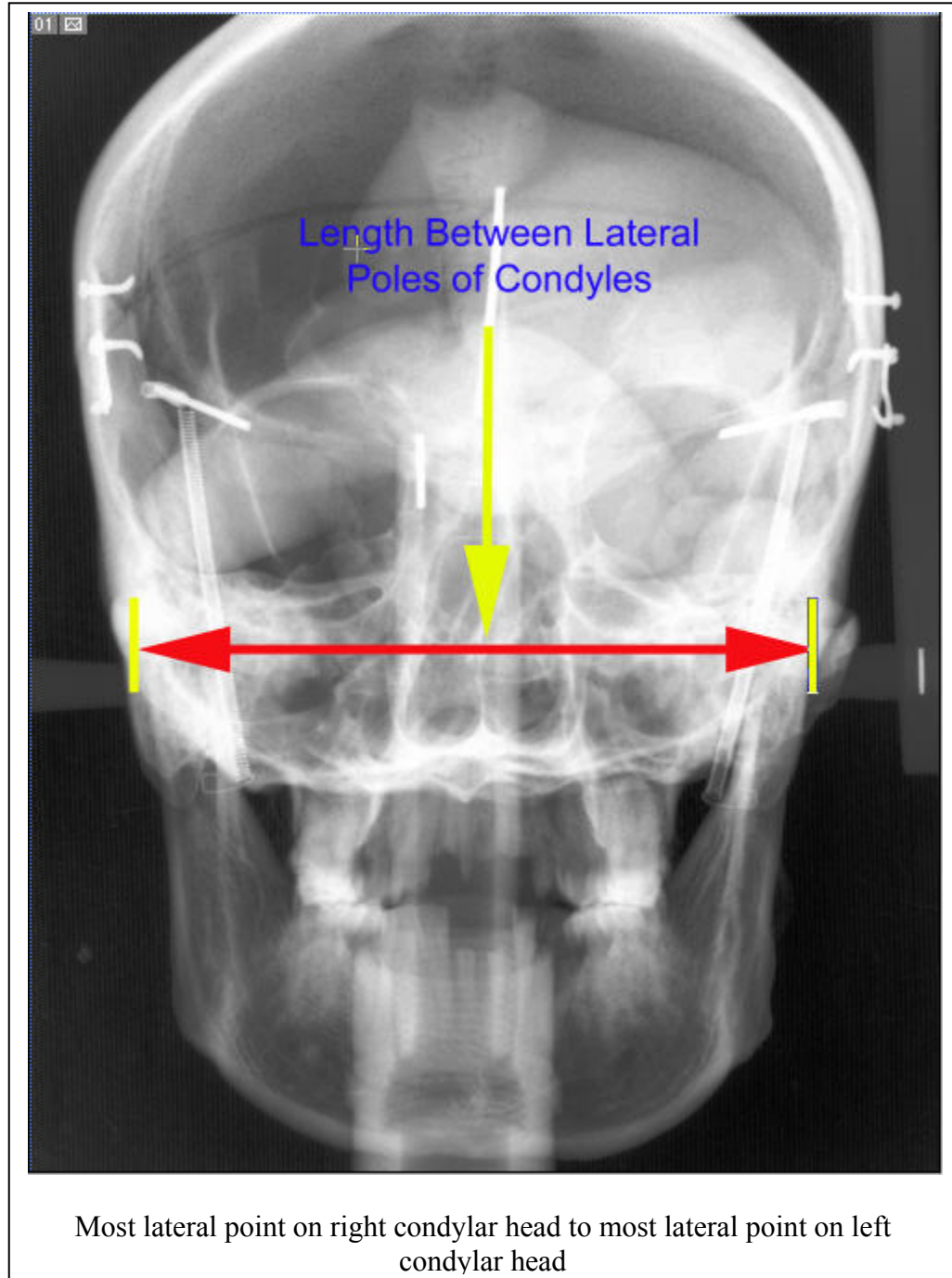
Most lateral point on right condylar head to most lateral point on left
condylar head

Figure : 40

Most lateral point on right condylar head to most lateral point on left
condylar head

Figure : 41

Condylar Length From Medial Pole to Medial Pole

Most medial point on right condyle to most medial point on right condyle
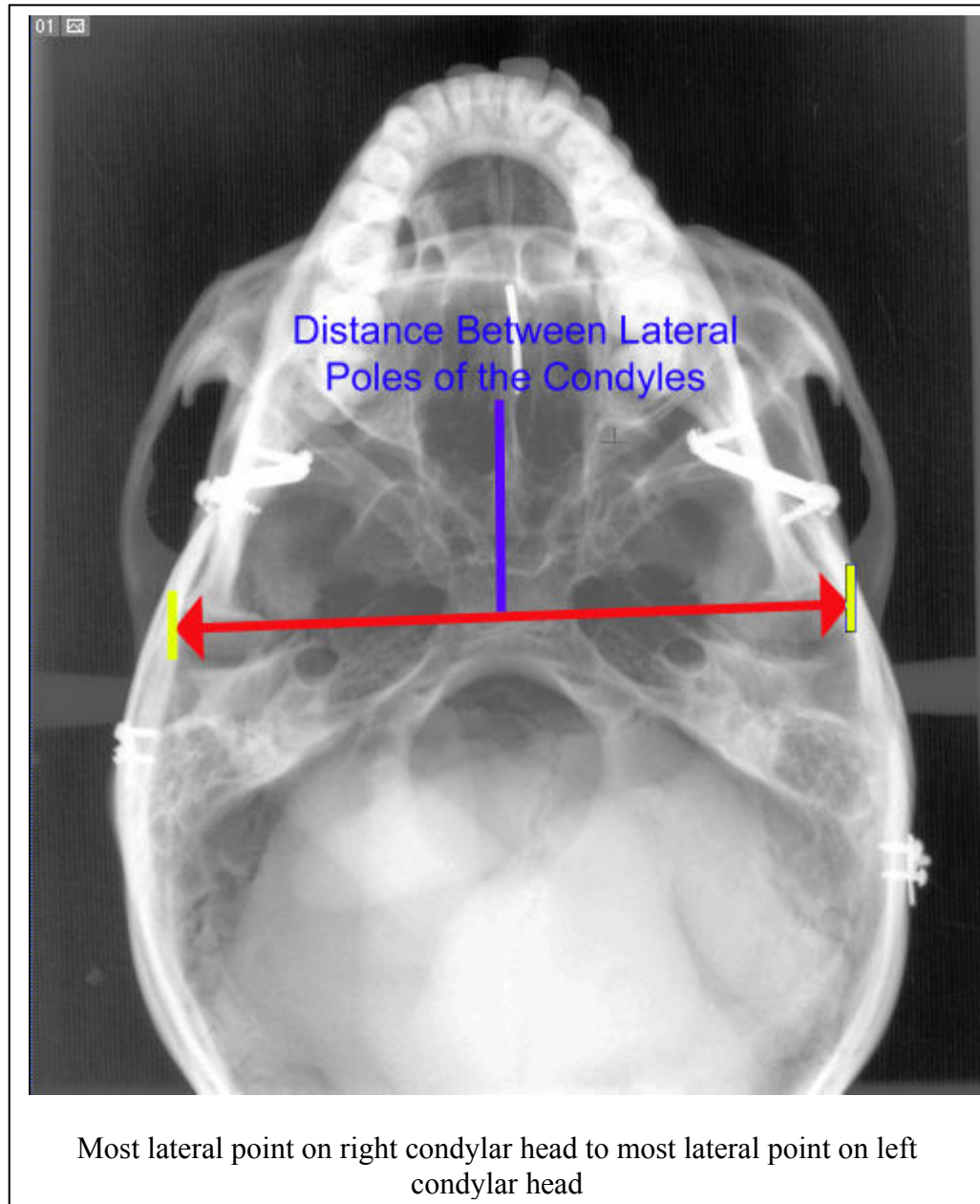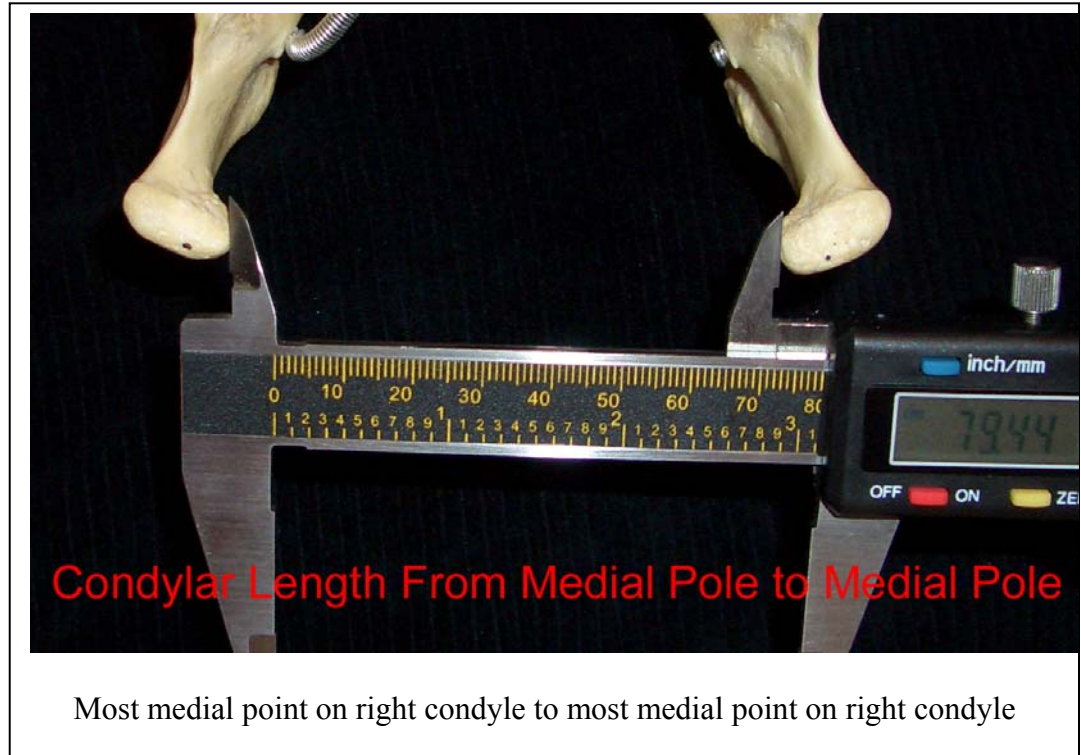
Figure : 42

ICAT: MEDIAL DISTANCE BETWEEN CONDYLES

Most medial point on right condyle to most medial point on right condyle using a slice in the frontal plane
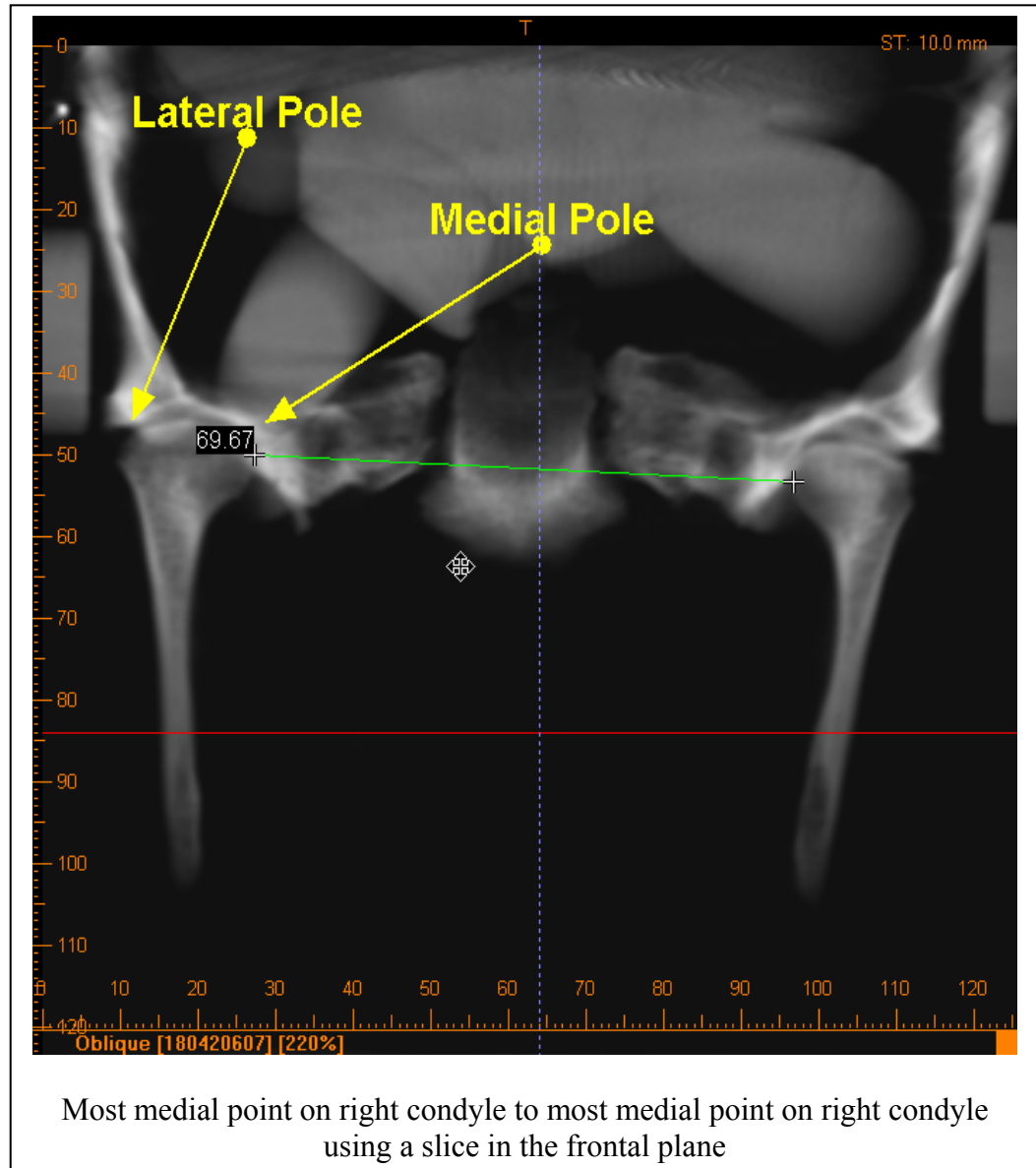
Figure : 43

PA: MEDIAL DISTANCE BETWEEN CONDYLES

Most medial point on right condyle to most medial point on right condyle

Figure : 44

Most medial point on right condyle to most medial point on right condyle
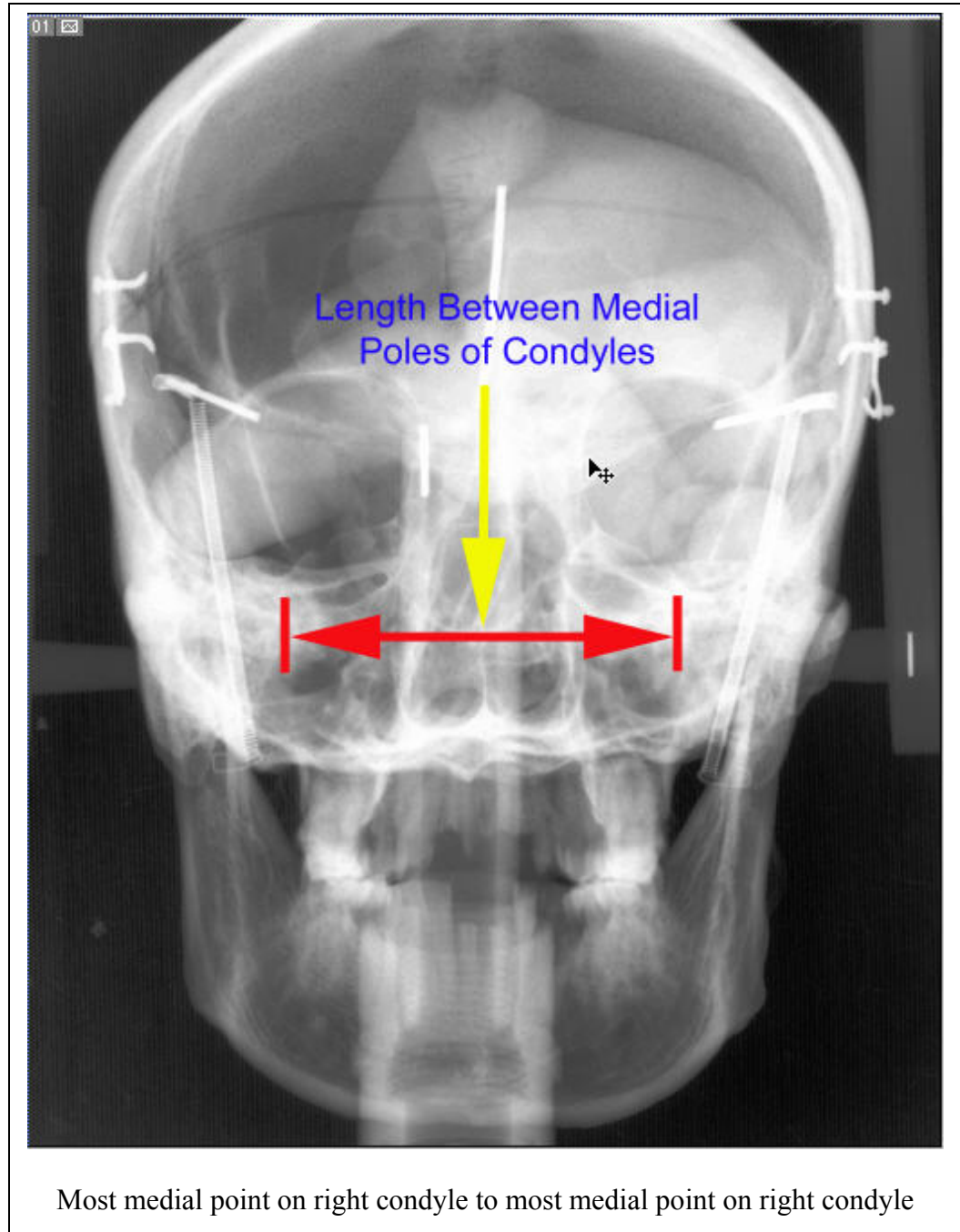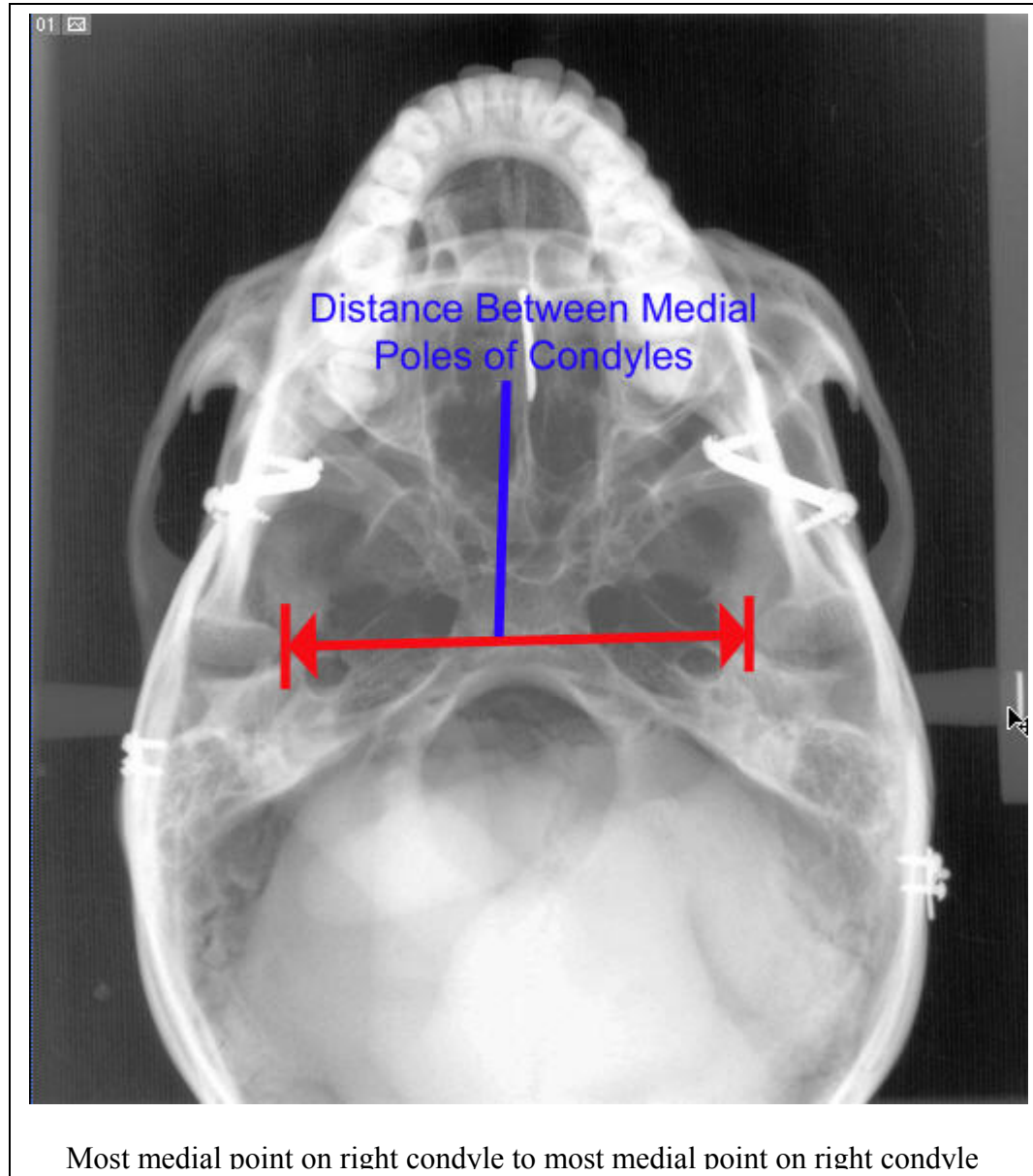
Figure : 45

TRUE: MAXIMUM MOLAR WIDTH

Transverse distance of the mandible lingually between distal interproximal
contact of the right six year molar and the distal interproximal contact of the
left six year molar
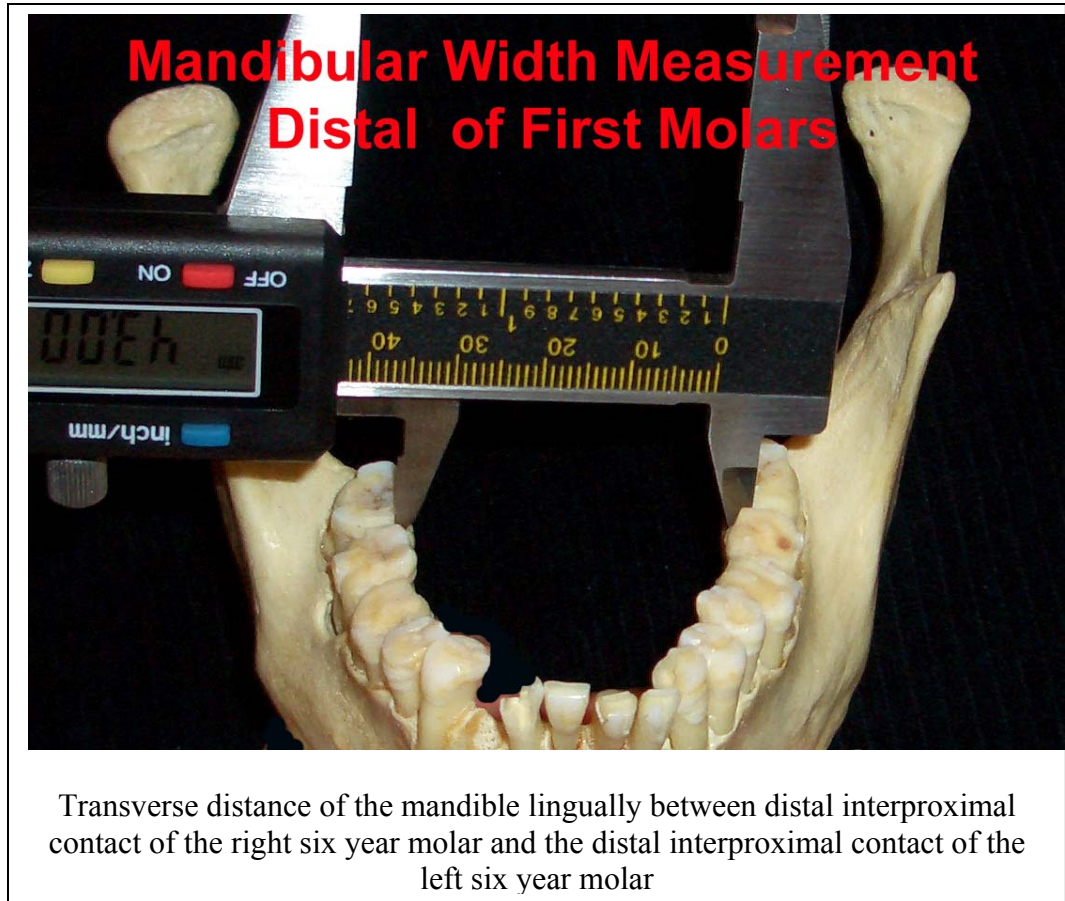
Figure : 46

<u>ICAT: MAXIMUM MOLAR WIDTH</u>
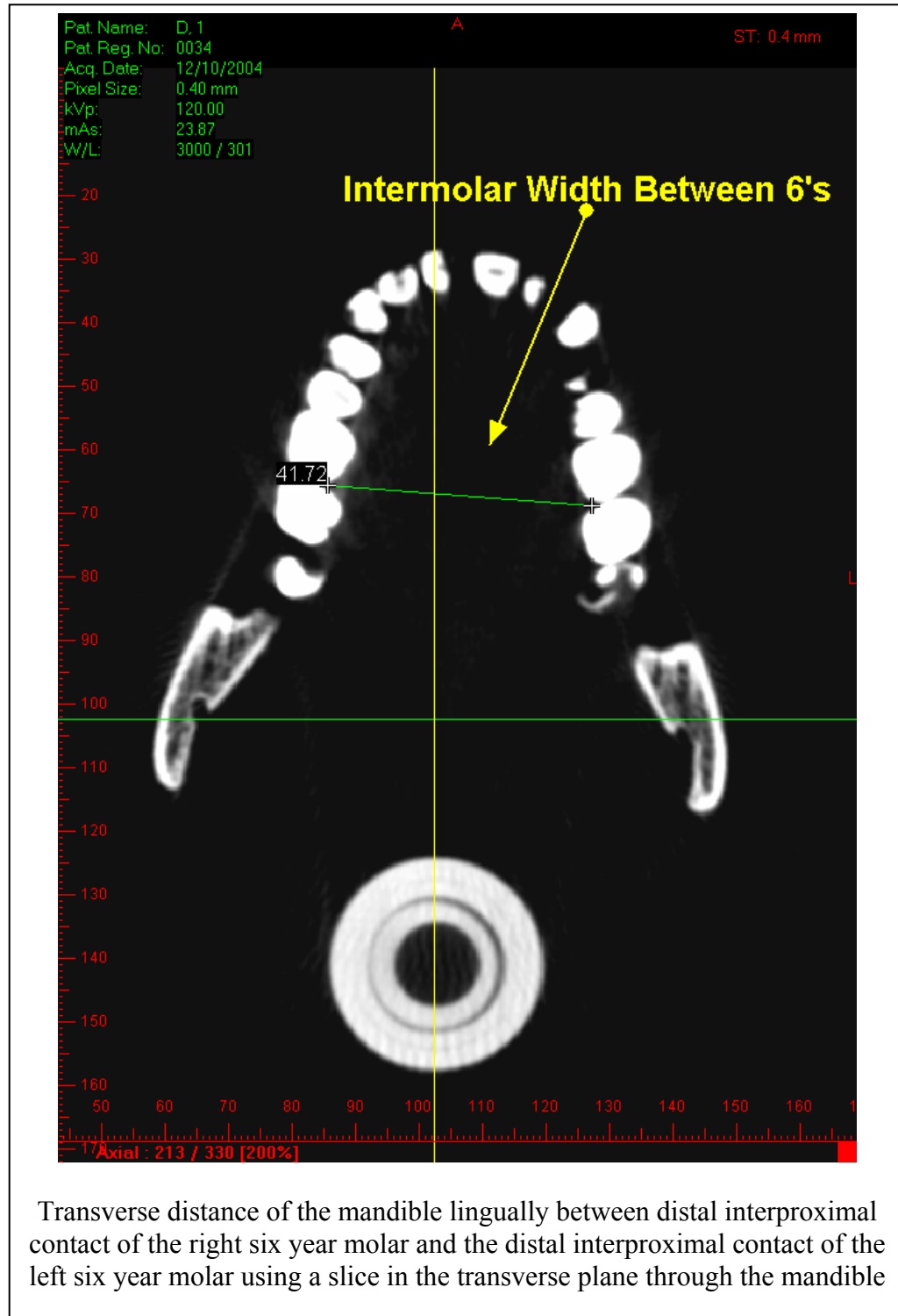
Transverse distance of the mandible lingually between distal interproximal contact of the right six year molar and the distal interproximal contact of the left six year molar using a slice in the transverse plane through the mandible

Figure : 47
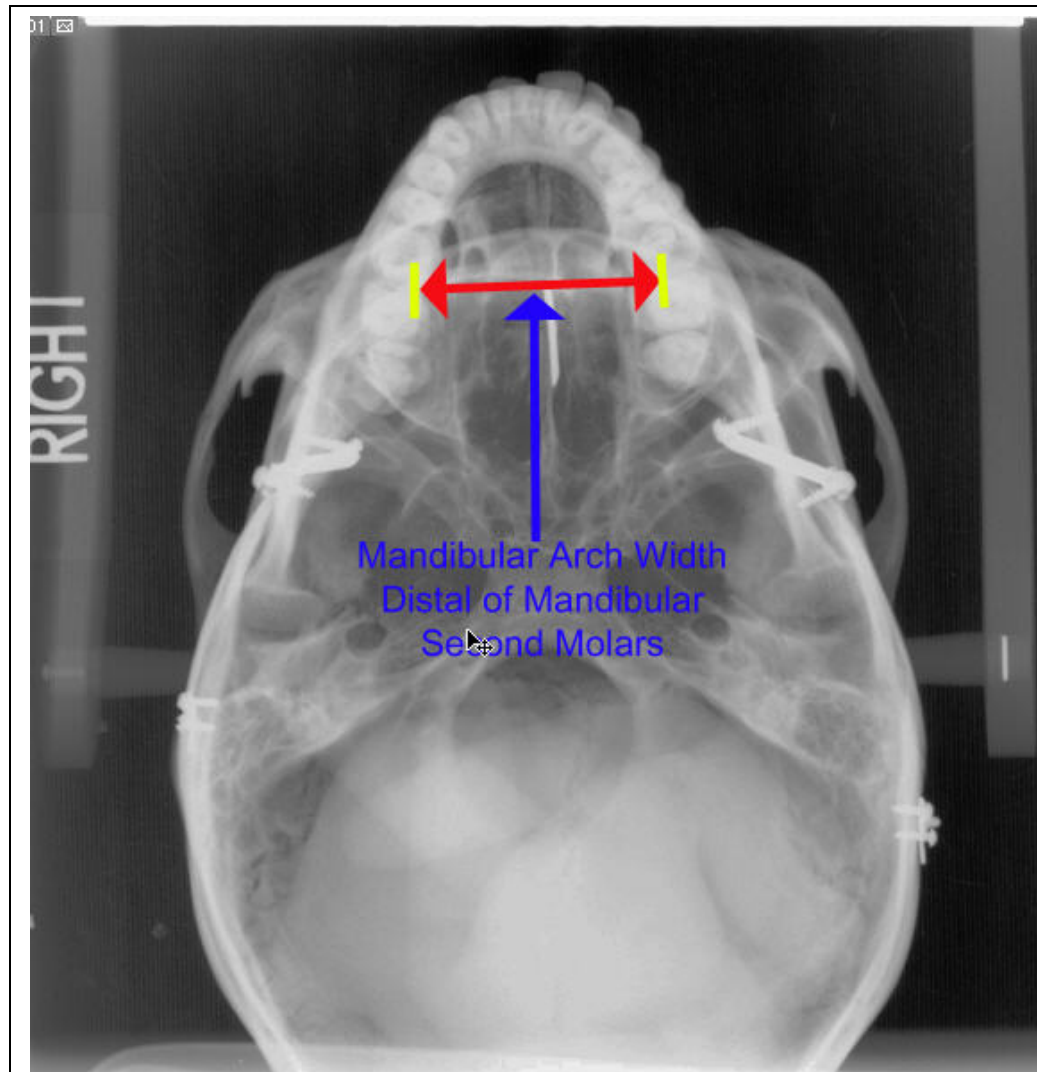
Transverse distance of the mandible lingually between distal interproximal contact of the right six year molar and the distal interproximal contact of the left six year molar

Figure : 48

TRUE: GONION TO GONION

Gonion to Gonion Measurement

Right gonion to left gonion

Figure : 49

Right gonion to left gonion using a slice in the frontal plane
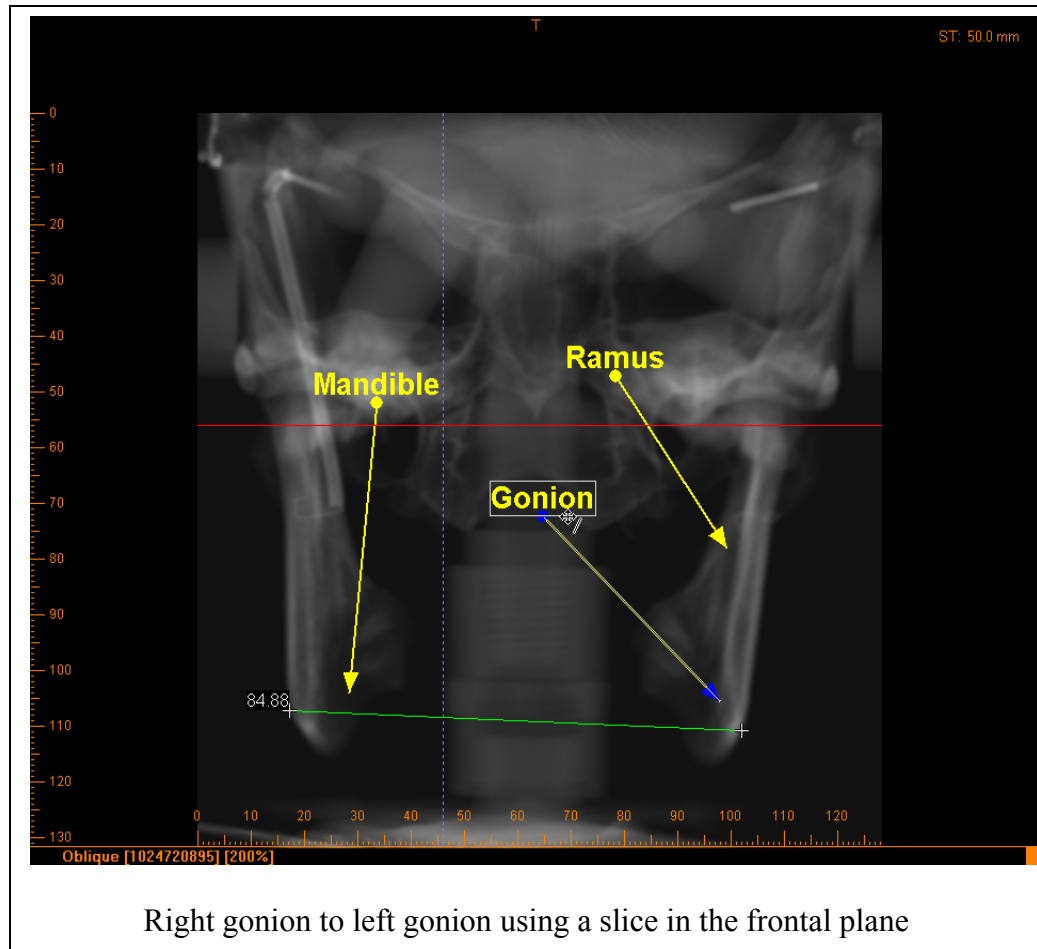
Figure : 50

PA: GONION TO GONION

Right gonion to left gonion
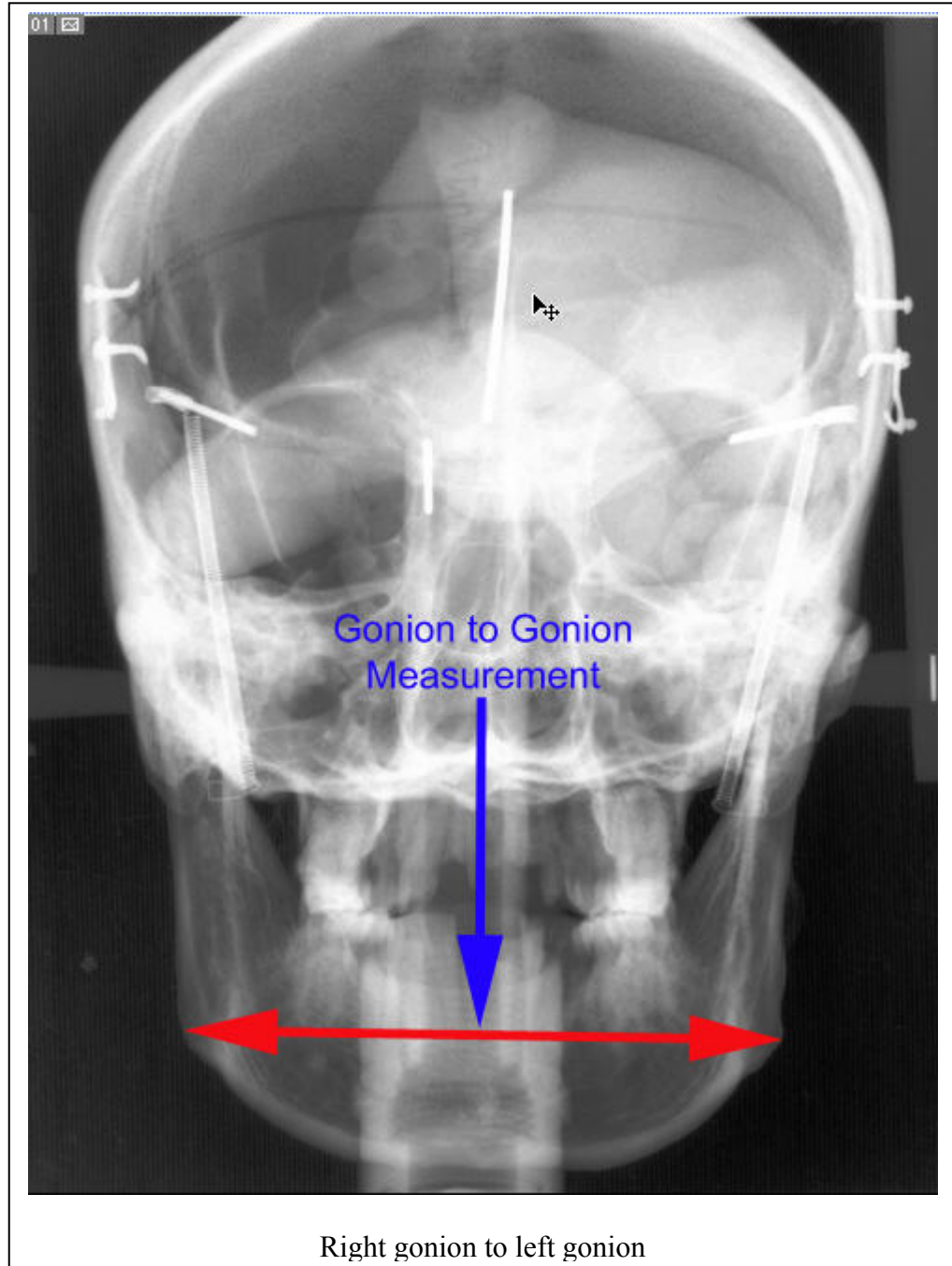
Figure : 51

Right gonion to left gonion
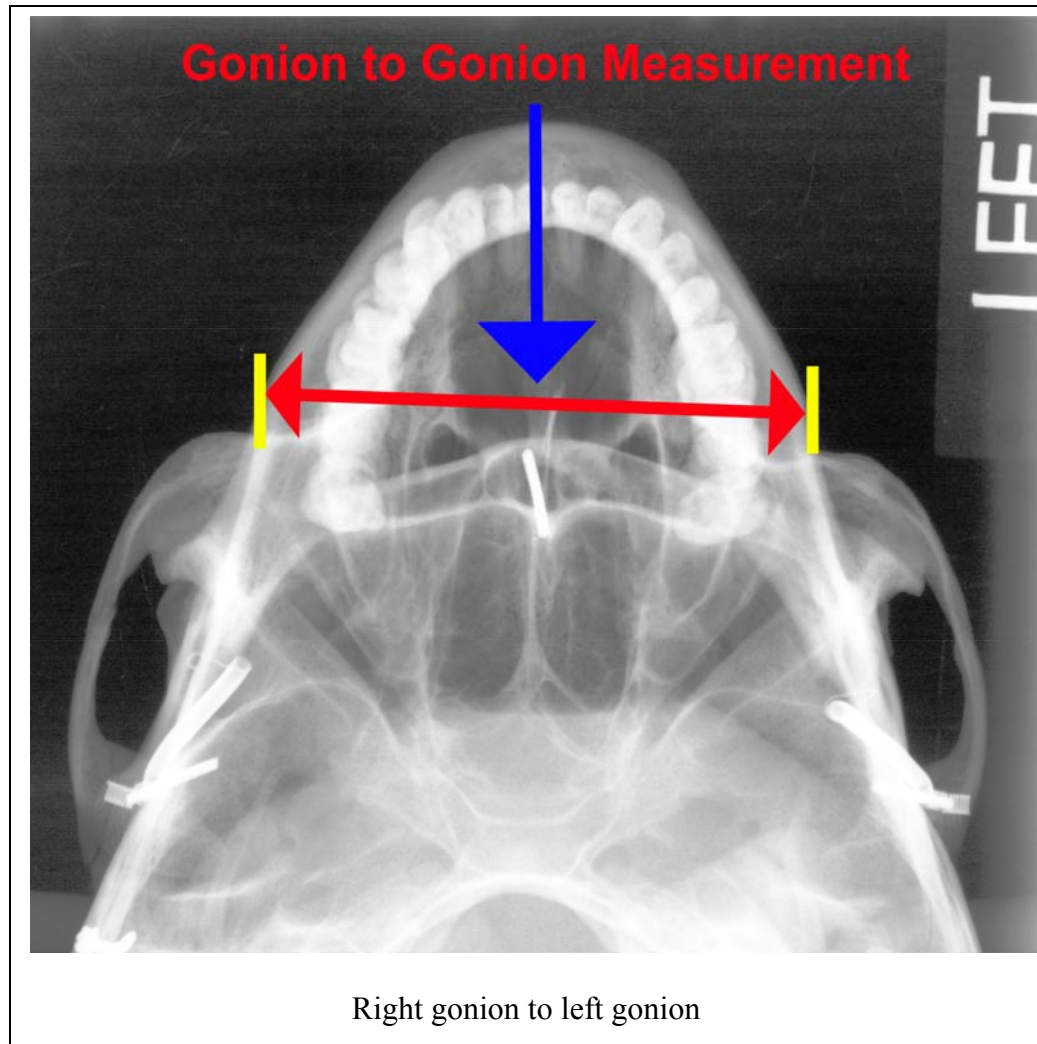
Data Collection

All measurements were entered into a Microsoft Excel 2003 (Microsoft, Redmond, WA, USA) database. Mean ± standard deviation of 3 independent replicates of the 10 measurements were calculated for each skull sample and modality. The data files were then coded for use with the Statistical Package for the Social Sciences software (SPSS, Version 12.0, SPSS, Inc., Chicago, IL, USA) which was used to conduct the analyses.

Statistical Analyses

Distributions from each measurement dimension (condylar width, condylar height, condylar length, etc.) were assessed and determined to be normally distributed. Therefore the mean of the 3 replicate measurements was used for statistical analysis. Analysis of the standard deviation of the replicate measurements did not demonstrate a normal distribution; therefore, the natural log of each standard deviation was used in the subsequent analysis. The statistical analysis consisted of a one way ANOVA for each measurement dimension as well as the natural log of the standard deviations. The *post hoc* survey utilized Dunnett's *'t'* Test with the actual dimensions as the control group. All other groups were compared against the control group. The *á priori* level of significance was set at $p \leq 0.05$. No power analysis was performed because no previous data was available. Some measurements were unable to be calculated from specific extraoral radiographic projections because the linear dimension was not in the image plane and therefore that modality omitted from the analysis.

RESULTS

For each of the 25 skull specimens, 10 measurements were obtained a series of 3 times for each modality (true measurement, iCAT, radiograph). A mean and standard deviation was calculated for the 3 measurements for each modality (see Table 2 for an example of the measurements made for the right condyle of 1 of the 25 skull specimens). Some measurements could only be obtained with 1 or 2 radiographs, while others could be measured using all three. For example, condylar width was measured using the skull specimen with calipers and using the iCAT, but only 2 types of radiographs could be used (ceph and SMV) due to the inability to make the measurement on the PA film. The mean and standard deviation for each type of measurement on each skull specimen were used for the statistical analysis.

Table 6:

CALCULATION OF COMPARATIVE LINEAR DIMENSIOS. EXAMPLE USING

CONDYLAR WIDTH REPLICATE MEASUREMENTS CALCULATING MEAN AND

STANDARD DEVIATION FOR SKULL SPECIMEN #1 RIGHT SIDE

Modality	Read #1	Read #2	Read #3	Mean	Standard Deviation
True	9.15	9.40	9.29	9.28	0.13
iCAT	8.99	8.95	8.80	8.91	0.10
Ceph	10.80	10.00	9.50	10.10	0.66
PA	---	---	---	---	---
SMV	8.90	8.70	8.20	8.60	0.36

Condylar Width

Table 7 shows the condylar width means and standard deviations for each skull specimen. Because each skull specimen had two condyles, bilateral measurements were made. For example, for skull specimen #1, the right condyle measured at 9.28mm (true), 8.91mm (iCAT), 10.10mm (ceph), and 8.60 mm(SMV). The condylar width could not be measured using the PA radiographic view. The standard deviation for the 3 times condylar width was measured for each modality was 0.13 (true), 0.10 (iCAT), 0.66 (ceph), and 0.36 (SMV).

Condylar Length

Table 8 describes the condylar length final means and standard deviations for each skull specimen. Because each skull specimen had two condyles, bilateral measurements were made. For example, for skull specimen #1, the right condyle measured at 15.79mm (true), 16.44mm (iCAT), 22.27mm (PA), and 20.11mm (SMV). The condylar length could not be measured using the cephalometric radiographic view. The standard deviation for the 3 times condylar length was measured for each modality on the right was 0.03mm (true), 0.14mm (iCAT), 0.78mm (PA), and 0.12 (SMV).

Condylar Height

Table 9 describes the condylar height final means and standard deviations for each skull specimen. Because each skull specimen had two condyles, bilateral measurements were made. For example, for skull specimen #1, the right condyle measured at 21.76mm (true), 20.87mm (iCAT), and 19.77mm (ceph). The condylar height could not be measured using the PA or SMV radiographic views. The standard deviation for the 3 times condylar height was measured for each modality was 0.10 (true), 0.31 (iCAT), and 0.45 (ceph).

Pogonion to Condyle

Table 10 describes the pogonion to condyle final means and standard deviations for each skull specimen. Because each skull specimen had two sides, bilateral measurements were made. For example, for skull specimen #1, the right side measured at 119.70mm (true), 119.40mm (iCAT), and 117.07mm (ceph). The measurement could not be made using the PA or SMV radiographic views. The standard deviations for the 3 times the measurement was made for each modality were 0.24 (true), 0.11 (iCAT), and 0.49 (ceph).

Pogonion to Distal Second Molar

Table 11 describes the pogonion to second molar final means and standard deviations for each skull specimen. Because each skull specimen had two sides, bilateral measurements were made. For example, for skull specimen #1, the right side measured at 55.05mm (true), 55.59mm (iCAT), and 63.31mm (ceph). The measurement could not be made using the PA or SMV radiographic views. The standard deviations for the 3 times the measurement was made for each modality were 0.14 (true), 0.18 (iCAT), and 0.81 (ceph).

Lateral Pole to Gonion

Table 12 describes the lateral pole to gonion final means and standard deviations for each skull specimen. Because each skull specimen had two sides, bilateral measurements were made. For example, for skull specimen #1, the right side measured at 46.74mm (true), 47.39mm (iCAT), 63.37mm (ceph), and 60.73 mm(SMV). The measurement could not be made using the PA radiographic view. The standard deviations for the 3 times the measurement was made for each modality were 0.25 (true), 0.19 (iCAT), 0.90 (ceph), and 1.51 (SMV).

Lateral Length Between Condyles

Table 13 describes the lateral length between condyles final means and standard deviations for each skull specimen. Because this was a midline measurement bilateral measurements were not made. For example, for skull specimen #1, the mean length measured at 99.06mm (true), 99.11mm (iCAT), 117.10mm (PA), and 119.23mm(SMV). The measurement could not be made using cephalometric radiographic view. The standard deviation for the 3 times lateral length was measured for each modality was 0.04 (true), 0.09 (iCAT), 0.36 (ceph), and 0.51 (SMV).

Median Length Between Condyles

Table 14 describes the median length between condyles final means and standard deviations for each skull specimen. Because this was a midline measurement bilateral measurements were not made. For example, for skull specimen #1, the mean length measured at 65.70mm (true), 65.90mm (iCAT), 77.90mm (PA), and 77.93mm(SMV). The measurement could not be made using the cephalometric radiographic view. The standard deviation for the 3 times lateral length was measured for each modality was 0.04 (true), 0.09 (iCAT), 0.36 (ceph), and 0.51 (SMV).

Molar Width

Table 15 describes the molar width final means and standard deviations for each skull specimen. Because this was a midline measurement bilateral measurements were not made. For example, for skull specimen #1, the mean width measured at 35.53mm (true), 36.12mm (iCAT), and 42.87mm (SMV). The measurement could not be made using the PA or cephalometric radiographic views. The standard deviation for the 3 times molar width was measured for each modality was 0.25 (true), 0.06 (iCAT), and 0.35 (SMV).

Mandibular Width

Table 16 describes the mandibular width final means and standard deviations for each skull specimen. Because this was a midline measurement bilateral measurements were not made. For example, for skull specimen #1, the mean width measured at 83.72mm (true), 83.10mm (iCAT), 92.87mm (PA), and 85.10mm(SMV). The measurement could not be made using the PA or cephalometric radiographic views. The standard deviation for the 3 times mandibular width was measured for each modality was 0.10 (true), 0.10 (iCAT), 0.25 (PA), and 0.46 (SMV).

Table 7:

CONDYLAR WIDTH MEASUREMENT MEANS AND STANDARD DEVIATION
MEANS BY MODALITY

	TRUE		*i-CAT*		*LC*		*SMV*	
Sample	*Mean*	*SD*	*Mean*	*SD*	*Mean*	*SD*	*Mean*	*SD*
1 R	9.28	0.13	8.91	0.10	10.10	0.66	8.60	0.36
1 L	10.42	0.26	10.26	0.04	11.33	0.51	9.20	0.44
2 R	9.74	0.07	10.22	0.07	10.70	0.46	8.60	0.44
2 L	10.27	0.13	10.01	0.11	10.97	0.21	10.73	0.47
3 R	8.34	0.27	8.54	0.12	12.03	0.35	10.07	0.23
3 L	8.57	0.04	8.68	0.02	10.43	0.21	11.17	0.35
4 R	7.88	0.10	7.97	0.03	10.07	0.29	8.53	0.35
4 L	9.14	0.07	8.91	0.08	9.40	0.36	8.90	0.36
5 R	9.36	0.11	9.49	0.05	13.77	0.35	9.17	0.21
5 L	10.56	0.09	10.29	0.07	12.50	0.30	9.23	0.15
6 R	10.37	0.16	10.17	0.10	10.93	0.45	9.13	0.31
6 L	9.55	0.18	9.75	0.08	10.33	0.25	8.40	0.26
7 R	8.31	0.07	8.49	0.04	12.63	0.55	8.43	0.32
7 L	8.86	0.14	8.92	0.06	11.93	0.38	9.03	0.38
8 R	8.86	0.05	8.74	0.05	12.63	0.60	9.57	0.21
8 L	9.42	0.06	9.31	0.08	12.43	0.40	10.40	0.17

9 R	9.19	0.15	9.32	0.04	12.47	0.21	9.57	0.21
9 L	9.52	0.02	9.51	0.07	12.20	0.30	10.57	0.32
10 R	7.81	0.28	8.02	0.08	13.37	0.55	8.63	0.23
10 L	8.87	0.06	8.99	0.07	12.63	0.32	9.00	0.20
11 R	6.74	0.06	6.63	0.11	10.20	0.56	6.67	0.25
11 L	7.20	0.06	7.37	0.07	11.23	0.15	6.97	0.21
12 R	9.94	0.07	9.96	0.11	11.13	0.29	10.57	0.31
12 L	10.14	0.12	10.25	0.05	10.70	0.26	10.47	0.15
13 R	9.39	0.18	9.48	0.07	11.63	0.70	9.33	0.15
13 L	10.59	0.06	10.68	0.08	11.27	0.47	11.77	0.25
14 R	6.77	0.02	6.94	0.07	9.57	0.57	7.10	0.26
14 L	6.74	0.05	6.81	0.09	9.13	0.25	9.57	0.06
15 R	7.14	0.10	7.26	0.09	12.43	0.61	7.13	0.15
15 L	7.86	0.07	7.91	0.08	11.93	0.15	7.50	0.26
16 R	8.30	0.18	8.14	0.08	10.53	0.57	9.23	0.25
16 L	9.16	0.09	9.12	0.09	10.13	0.40	9.40	0.36
17 R	8.96	0.17	8.77	0.08	10.37	0.38	11.10	0.36
17 L	8.93	0.11	8.96	0.08	9.97	0.15	10.47	0.25
18 R	8.88	0.20	8.81	0.07	11.07	0.74	8.30	0.26
18 L	8.73	0.05	8.68	0.14	10.63	0.21	8.67	0.38
19 R	8.73	0.02	8.73	0.09	12.80	0.20	9.40	0.44
19 L	9.33	0.16	9.39	0.05	12.30	0.26	9.80	0.30
20 R	9.99	0.17	10.09	0.05	11.13	0.32	10.00	0.26
20 L	9.90	0.16	9.92	0.17	11.17	0.40	9.53	0.40
21 R	6.00	0.28	5.88	0.12	9.37	0.45	7.20	0.26
21 L	7.11	0.08	7.18	0.03	9.33	0.35	7.70	0.26
22 R	7.76	0.07	7.82	0.05	11.03	0.32	8.13	0.21
22 L	8.93	0.30	8.89	0.15	11.17	0.49	8.40	0.36
23 R	7.08	0.06	7.11	0.04	8.33	0.15	7.30	0.26
23 L	7.94	0.19	7.98	0.16	8.37	0.25	9.07	0.21
24 R	6.89	0.20	6.78	0.07	10.20	0.30	8.57	0.49
24 L	9.32	0.15	9.21	0.08	9.87	0.38	9.67	0.45
25 R	9.90	0.30	10.08	0.03	12.20	0.36	11.47	0.25
25 L	11.38	0.27	11.17	0.16	12.07	0.31	11.47	0.15

Table 8:

CONDYLAR LENGTH: MEASUREMENT MEANS AND STANDARD DEVIATION MEANS

	TRUE		i-CAT		PA		SMV	
Sample	Mean	SD	Mean	SD	Mean	SD	Mean	SD
1 R	15.79	0.03	16.44	0.14	22.27	0.78	20.11	0.12
1 L	17.28	0.06	18.43	0.02	18.90	0.66	18.17	0.31
2 R	20.34	0.04	20.56	0.08	23.43	0.76	21.20	0.20
2 L	20.64	0.06	20.21	0.05	20.30	0.50	21.27	0.21
3 R	16.26	0.02	16.76	0.08	20.10	0.61	21.27	0.60
3 L	18.39	0.04	18.36	0.12	21.30	0.62	22.53	0.21
4 R	18.04	0.01	18.10	0.17	20.43	0.25	20.20	0.10
4 L	19.53	0.04	19.49	0.13	21.20	0.36	19.93	0.38
5 R	17.18	0.01	17.15	0.05	19.80	0.26	19.13	0.21
5 L	17.71	0.05	18.06	0.06	22.93	0.64	19.80	0.36
6 R	20.74	0.04	20.65	0.06	24.33	0.83	21.63	0.35
6 L	19.82	0.02	19.93	0.10	23.50	0.62	20.17	0.31
7 R	16.48	0.02	16.52	0.18	18.90	0.53	18.33	0.25
7 L	16.91	0.04	17.15	0.24	18.73	0.21	17.67	0.06
8 R	21.29	0.02	21.29	0.03	22.47	1.20	21.53	0.23
8 L	23.16	0.01	23.35	0.20	26.17	0.31	25.47	0.12
9 R	16.22	0.02	16.66	0.39	21.77	0.64	17.73	0.32
9 L	16.20	0.02	16.37	0.32	18.53	0.55	17.40	0.17
10 R	17.82	0.06	17.75	0.20	19.17	0.31	18.07	0.15
10 L	17.85	0.04	17.81	0.04	19.57	0.25	19.27	0.21
11 R	17.79	0.02	17.76	0.05	24.80	1.04	18.43	0.47
11 L	20.14	0.02	20.19	0.05	26.80	0.90	19.23	0.21
12 R	17.81	0.01	17.75	0.13	21.37	0.57	18.40	0.46
12 L	17.59	0.05	17.53	0.10	18.93	0.40	18.40	0.10
13 R	17.83	0.04	17.81	0.03	24.83	0.95	19.47	0.25
13 L	18.79	0.06	18.73	0.11	23.63	0.42	18.60	0.36
14 R	19.10	0.04	19.15	0.05	18.13	0.81	19.50	0.30
14 L	19.19	0.02	19.13	0.07	16.10	0.30	20.30	0.36

15 R	16.24	0.05	16.20	0.04	19.90	1.25	19.10	0.60
15 L	16.87	0.02	16.83	0.03	21.00	0.20	19.20	0.26
16 R	21.35	0.04	21.34	0.10	20.40	0.72	23.70	0.20
16 L	21.34	0.04	21.42	0.08	20.23	1.00	21.17	0.59
17 R	14.55	0.06	14.62	0.07	14.37	0.32	16.27	0.32
17 L	14.39	0.02	14.43	0.10	14.47	0.60	15.10	0.36
18 R	17.08	0.01	17.13	0.08	23.13	0.55	18.97	0.25
18 L	16.57	0.04	16.59	0.11	18.73	1.07	18.47	0.32
19 R	20.64	0.05	20.58	0.06	18.80	0.46	21.57	0.25
19 L	19.36	0.04	19.39	0.03	20.63	0.40	20.40	0.20
20 R	19.13	0.03	19.18	0.05	19.97	0.72	19.40	0.26
20 L	18.29	0.04	18.35	0.06	22.23	0.49	18.10	0.26
21 R	21.78	0.04	21.72	0.05	19.57	0.71	23.97	0.57
21 L	21.48	0.02	21.51	0.03	19.23	0.61	24.03	0.57
22 R	19.33	0.02	19.40	0.07	24.10	0.40	21.70	0.30
22 L	20.40	0.03	20.39	0.06	19.60	0.26	21.33	0.49
23 R	21.72	0.03	21.70	0.09	18.83	0.25	21.20	0.40
23 L	22.51	0.07	22.56	0.05	18.77	0.15	23.23	0.45
24 R	19.52	0.03	19.64	0.10	25.67	0.83	21.47	0.47
24 L	19.28	0.00	19.31	0.04	24.10	0.61	21.53	0.60
25 R	20.89	0.05	20.75	0.16	18.90	0.26	22.17	0.55
25 L	19.17	0.02	19.24	0.08	18.47	0.47	18.93	0.15

Table 9:

CONDYLAR HEIGHT MEASUREMENT MEANS AND STANDARD DEVIATION MEANS

Sample	TRUE Mean	SD	i-CAT Mean	SD	LC Mean	SD
1 R	21.76	0.10	20.87	0.31	19.77	0.45
1 L	22.10	0.05	22.39	0.25	17.00	0.44
2 R	17.46	0.20	17.64	0.12	20.70	0.46
2 L	13.93	0.09	14.25	0.11	20.40	0.46
3 R	15.71	0.11	16.12	0.09	16.90	0.26
3 L	18.28	0.16	18.24	0.06	18.87	0.32
4 R	16.95	0.02	17.22	0.14	19.53	0.57
4 L	17.48	0.14	17.50	0.15	22.27	0.45
5 R	22.12	0.05	22.16	0.03	23.80	0.40
5 L	24.13	0.04	23.52	0.08	25.33	0.42
6 R	27.31	0.16	26.36	0.17	24.07	0.31
6 L	25.40	0.05	25.74	0.10	23.93	0.51
7 R	17.77	0.07	17.81	0.15	19.40	0.44
7 L	15.33	0.06	15.14	0.07	19.27	0.47
8 R	14.49	0.08	14.66	0.11	16.20	0.26
8 L	13.03	0.17	13.10	0.13	16.70	0.44
9 R	22.46	0.04	22.36	0.22	25.07	0.65
9 L	22.05	0.08	22.04	0.14	26.43	0.35
10 R	19.21	0.06	19.59	0.14	22.37	0.50
10 L	18.19	0.13	18.56	0.13	24.47	0.55
11 R	17.04	0.05	17.62	0.28	19.17	0.38
11 L	14.84	0.13	14.20	0.20	17.13	0.35
12 R	16.83	0.10	16.95	0.36	22.07	0.40
12 L	20.10	0.06	21.22	0.35	23.67	0.61
13 R	18.54	0.12	18.60	0.24	18.83	0.35
13 L	17.15	0.05	17.82	0.24	20.33	0.25

14 R	16.83	0.06	16.79	0.26	17.50	0.17
14 L	17.65	0.06	18.50	0.26	17.60	0.52
15 R	24.51	0.14	24.80	0.12	27.33	0.21
15 L	24.72	0.12	23.77	0.10	27.40	0.53
16 R	19.84	0.13	20.16	0.07	16.63	0.47
16 L	17.20	0.07	17.75	0.16	18.30	0.44
17 R	19.92	0.08	20.02	0.14	21.47	0.47
17 L	20.70	0.11	20.96	0.17	21.30	0.35
18 R	17.32	0.10	17.31	0.14	21.47	0.59
18 L	18.73	0.14	18.30	0.20	20.97	0.67
19 R	19.03	0.07	19.26	0.17	21.03	0.40
19 L	20.00	0.09	20.00	0.15	21.30	0.20
20 R	22.38	0.10	22.16	0.16	26.60	0.72
20 L	22.39	0.11	22.37	0.17	25.60	0.30
21 R	18.40	0.08	18.55	0.18	19.80	0.46
21 L	16.50	0.16	16.78	0.18	20.40	0.20
22 R	22.29	0.06	22.67	0.08	24.37	0.15
22 L	24.23	0.10	24.32	0.17	25.57	0.50
23 R	17.46	0.14	17.73	0.06	19.50	0.40
23 L	17.80	0.09	17.85	0.13	21.30	0.60
24 R	21.62	0.84	21.86	0.23	21.73	0.40
24 L	19.47	0.07	19.66	0.22	23.00	0.60
25 R	21.78	0.11	21.93	0.22	23.73	0.35
25 L	22.76	0.18	22.73	0.13	23.87	0.35

Table 10:

POGONION TO CONDYLE MEASUREMENT MEANS AND STANDARD DEVIATION

MEANS BY MODALITY

	TRUE		i-CAT		LC	
Sample	Mean	SD	Mean	SD	Mean	SD
1 R	119.70	0.24	119.40	0.11	117.07	0.49
1 L	121.81	0.14	121.84	0.10	116.47	0.65
2 R	116.03	0.50	116.91	0.05	120.90	0.50
2 L	115.07	0.32	115.40	0.12	123.13	0.31
3 R	111.44	0.55	111.23	0.04	120.80	0.70
3 L	115.51	0.35	115.14	0.06	117.93	0.21
4 R	116.99	0.58	117.44	0.12	118.23	0.42
4 L	116.34	0.55	116.27	0.04	118.63	0.49
5 R	120.32	0.14	122.03	0.10	123.10	0.61
5 L	121.55	0.30	121.76	0.05	121.20	0.26
6 R	115.32	0.08	116.39	0.22	114.60	0.50
6 L	119.38	0.16	119.10	0.04	116.13	0.31
7 R	109.44	0.54	108.56	0.08	110.87	0.71
7 L	107.32	0.19	106.72	0.15	109.87	0.31
8 R	120.08	0.23	120.67	0.04	121.50	0.26
8 L	119.85	0.40	121.49	0.06	122.10	0.35
9 R	115.55	0.64	115.13	0.09	120.67	0.38
9 L	118.07	0.66	119.35	0.20	120.43	0.35
10 R	118.20	0.14	119.55	0.08	120.63	0.45
10 L	117.58	0.25	117.17	0.11	120.17	0.60
11 R	108.62	0.42	108.98	0.07	108.93	0.35
11 L	110.22	0.74	110.27	0.07	111.97	0.49
12 R	116.84	0.40	118.36	0.15	120.73	0.75
12 L	120.09	0.18	121.01	0.11	123.10	0.30
13 R	121.52	1.31	121.16	0.22	124.83	0.45
13 L	122.68	1.07	123.10	0.06	122.97	0.57
14 R	107.97	0.85	106.17	0.08	108.80	0.30
14 L	112.92	0.42	112.27	0.11	115.40	0.44

15 R	121.16	0.80	120.40	0.07	124.03	0.21
15 L	119.46	0.35	118.92	0.04	123.00	0.40
16 R	118.20	0.77	120.41	0.07	121.60	0.40
16 L	120.79	0.69	120.74	0.10	120.90	0.26
17 R	106.70	0.32	107.10	0.13	109.20	0.20
17 L	108.03	0.28	109.18	0.15	110.27	0.55
18 R	111.58	0.61	110.68	0.08	111.83	0.29
18 L	113.78	1.00	115.17	0.17	113.27	0.50
19 R	121.74	0.86	121.47	0.13	123.80	0.66
19 L	121.52	0.48	122.69	0.08	123.50	0.30
20 R	122.65	0.55	123.82	0.10	127.03	0.45
20 L	122.41	0.26	124.84	0.11	127.10	0.53
21 R	114.90	0.04	114.95	0.03	116.67	0.46
21 L	119.32	0.30	117.83	0.06	119.50	0.44
22 R	123.12	0.25	125.12	0.06	124.77	0.67
22 L	123.93	0.42	124.26	0.10	124.53	0.31
23 R	108.45	0.11	110.79	0.02	110.30	0.36
23 L	108.95	0.44	110.28	0.10	110.67	0.35
24 R	123.19	0.34	124.32	0.07	127.70	0.40
24 L	121.98	0.58	122.25	0.05	128.57	0.21
25 R	123.19	0.64	122.73	0.16	126.13	0.93
25 L	123.57	0.60	125.00	0.09	130.97	0.42

Table 11:

POGONION TO DISTAL SECOND MOLAR MEASUREMENT MEANS AND STANDARD

DEVIATION MEANS BY MODALITY

	TRUE		i-CAT		LC	
Sample	*Mean*	*SD*	*Mean*	*SD*	*Mean*	*SD*
1 R	55.05	0.14	55.59	0.18	63.31	0.81
1 L	56.03	0.04	55.41	0.16	63.63	0.91
2 R	55.37	0.53	56.70	0.05	56.42	0.32
2 L	54.16	0.44	55.39	0.16	56.83	0.32
3 R	50.69	0.04	50.79	0.09	53.87	0.38
3 L	48.98	0.35	49.66	0.11	53.53	0.51
4 R	55.10	0.31	55.93	0.07	53.42	0.42
4 L	54.53	0.99	54.85	0.15	54.03	0.15
5 R	50.69	0.09	51.34	0.09	57.45	0.36
5 L	51.34	0.12	52.18	0.03	57.03	0.25
6 R	53.77	0.11	53.37	0.23	53.51	0.46
6 L	59.22	0.18	58.80	0.15	53.67	0.45
7 R	53.78	0.40	54.20	0.05	51.29	0.17
7 L	51.79	0.46	50.37	0.12	50.93	0.21
8 R	56.50	0.42	57.75	0.08	53.82	0.30
8 L	56.37	0.38	56.96	0.10	54.57	0.47
9 R	55.37	0.51	57.08	0.15	51.13	0.36
9 L	53.07	0.22	53.97	0.10	51.17	0.25
10 R	52.44	0.46	51.93	0.04	51.63	0.37
10 L	52.31	0.41	52.39	0.15	51.43	0.21
11 R	56.92	0.44	57.67	0.06	46.61	0.38
11 L	57.27	0.27	57.59	0.07	46.33	0.35
12 R	51.66	0.45	51.31	0.09	52.74	0.32
12 L	51.77	0.45	51.72	0.09	52.70	0.44
13 R	55.22	0.29	56.18	0.08	53.37	0.63
13 L	54.57	0.40	55.36	0.17	53.33	0.61
14 R	51.44	0.33	52.28	0.07	48.54	0.37

14 L	52.04	0.48	52.33	0.17	48.27	0.42
15 R	57.53	0.12	57.26	0.16	55.48	0.48
15 L	57.13	0.18	57.36	0.12	55.90	0.40
16 R	54.13	0.42	55.42	0.10	51.12	0.53
16 L	54.21	0.68	55.34	0.04	51.03	0.47
17 R	56.19	0.27	57.42	0.14	51.72	0.19
17 L	56.14	0.41	56.25	0.18	51.93	0.59
18 R	53.52	0.15	53.52	0.09	54.92	0.26
18 L	55.19	0.21	56.11	0.09	54.80	0.20
19 R	57.24	0.53	57.78	0.07	56.81	0.11
19 L	55.94	0.22	55.28	0.13	56.47	0.32
20 R	56.64	0.71	57.38	0.18	56.62	0.37
20 L	57.06	0.43	56.15	0.08	57.00	0.46
21 R	56.96	0.11	56.90	0.09	56.55	0.27
21 L	58.40	0.23	58.09	0.22	56.83	0.25
22 R	56.92	0.20	57.56	0.12	57.63	0.39
22 L	57.96	0.75	58.59	0.20	57.83	0.31
23 R	52.18	0.19	51.90	0.08	48.62	0.41
23 L	51.59	0.39	52.56	0.11	48.91	0.62
24 R	61.45	0.48	62.36	0.19	56.70	0.71
24 L	59.32	0.46	60.50	0.14	56.73	0.36
25 R	53.56	0.56	52.19	0.03	52.36	0.27
25 L	52.57	0.43	52.42	0.09	52.07	0.47

Table 12:

LATERAL POLE TO GONION MEASUREMENT MEANS AND STANDARD DEVIATION

	TRUE		i-CAT		LC		SMV	
Sample	*Mean*	*SD*	*Mean*	*SD*	*Mean*	*SD*	*Mean*	*SD*
1 R	46.74	0.25	47.39	0.19	63.37	0.90	60.73	1.51
1 L	48.27	0.37	47.01	0.17	60.03	0.21	57.37	0.55
2 R	55.97	0.35	57.06	0.10	56.60	0.70	51.90	1.35
2 L	55.97	0.67	55.40	0.20	55.80	0.60	55.33	0.51
3 R	50.73	0.14	49.80	0.08	62.80	0.89	64.80	0.36
3 L	52.84	0.13	55.46	0.08	62.27	0.71	63.83	0.59
4 R	52.59	0.64	52.29	0.14	57.13	0.65	54.70	0.56
4 L	51.43	0.32	51.19	0.18	60.13	0.74	56.27	0.42
5 R	53.73	0.05	53.20	0.17	56.97	0.72	65.63	0.96
5 L	52.16	0.13	52.46	0.19	55.83	0.51	66.83	0.35
6 R	51.09	0.07	51.08	0.13	63.73	0.76	62.37	0.51
6 L	53.03	0.06	52.71	0.20	62.90	0.62	62.07	0.74
7 R	47.28	0.23	48.16	0.17	57.70	0.87	54.33	1.10
7 L	49.74	0.31	50.71	0.09	60.57	0.60	53.30	0.78
8 R	55.26	0.39	54.19	0.07	60.23	0.84	57.90	0.40
8 L	53.18	0.57	53.20	0.06	59.13	0.50	57.40	0.70
9 R	54.60	0.45	53.68	0.17	64.77	0.25	58.70	0.46
9 L	52.29	0.56	52.95	0.09	62.77	0.42	57.27	0.25
10 R	53.41	0.27	54.54	0.20	64.80	0.50	55.23	0.21
10 L	52.85	0.30	53.87	0.10	64.47	0.29	57.37	0.51
11 R	46.09	0.52	46.45	0.09	54.10	0.70	53.37	0.38
11 L	46.10	0.35	48.33	0.08	53.20	0.26	56.33	0.80
12 R	53.63	0.34	55.14	0.14	63.63	0.87	59.30	0.35
12 L	54.29	0.33	55.74	0.13	67.47	0.50	57.53	0.80
13 R	56.29	0.56	55.91	0.08	66.00	0.70	66.03	0.31
13 L	57.21	0.55	56.86	0.06	65.20	0.53	62.03	0.35
14 R	50.59	0.59	49.24	0.12	64.97	0.49	57.23	0.49
14 L	54.46	0.41	53.48	0.21	58.90	0.36	58.43	0.49

15 R	50.72	0.43	51.30	0.15	63.13	0.40	59.57	0.83
15 L	56.57	0.38	55.87	0.11	64.17	0.29	57.03	0.40
16 R	51.46	0.27	51.49	0.18	57.07	0.31	54.10	0.36
16 L	49.82	0.29	50.24	0.10	56.27	0.40	59.10	0.87
17 R	44.27	0.25	44.97	0.08	52.10	0.26	46.80	0.10
17 L	45.36	0.93	43.80	0.13	53.07	0.42	47.47	0.31
18 R	48.51	0.38	50.06	0.17	56.63	0.76	58.80	1.32
18 L	48.70	0.20	48.37	0.17	56.60	0.78	61.70	0.85
19 R	52.14	0.37	53.06	0.07	67.63	0.93	62.60	1.15
19 L	56.45	0.20	55.36	0.13	67.17	0.60	64.47	0.74
20 R	53.56	0.24	52.44	0.10	66.37	0.50	60.80	0.36
20 L	54.76	0.13	55.76	0.11	65.77	0.55	63.60	0.36
21 R	46.13	0.78	46.40	0.11	51.23	0.38	51.20	0.79
21 L	44.52	0.57	45.17	0.08	52.70	0.36	52.87	0.64
22 R	49.98	0.19	51.17	0.14	58.70	0.70	60.13	0.61
22 L	52.81	0.04	51.81	0.17	57.10	0.46	53.20	0.36
23 R	43.54	0.50	44.54	0.13	57.00	0.60	56.83	0.47
23 L	42.20	0.23	42.88	0.22	56.43	0.81	52.83	0.55
24 R	55.03	0.16	53.46	0.10	67.87	0.81	60.27	1.08
24 L	55.21	0.04	54.61	0.19	67.23	0.49	60.73	0.47
25 R	55.26	0.25	54.71	0.16	59.40	1.04	62.47	0.31
25 L	53.35	0.43	54.54	0.15	62.30	0.44	62.83	0.81

Table 13:

LATERAL LENGTH BETWEEN CONDYLES MEASUREMENT MEANS AND STANDARD

DEVIATION MEANS BY MODALITY

	TRUE		*i-CAT*		*LC*		*SMV*	
Sample	*Mean*	*SD*	*Mean*	*SD*	*Mean*	*SD*	*Mean*	*SD*
1	99.06	0.04	99.11	0.09	117.10	0.36	119.23	0.51
2	112.73	0.13	112.92	0.03	112.03	0.87	114.67	0.14
3	103.20	0.02	103.12	0.09	110.31	0.06	109.44	0.11
4	105.88	0.03	105.94	0.06	116.30	0.79	115.97	0.35
5	109.87	0.12	109.75	0.09	125.63	0.55	122.20	0.30
6	113.86	0.02	113.93	0.06	123.43	0.80	122.17	0.47
7	100.90	0.04	100.88	0.06	115.03	0.76	111.10	0.36
8	117.97	0.02	118.05	0.05	120.63	0.91	129.40	0.36
9	106.20	0.03	106.00	0.17	116.37	0.45	118.10	0.20
10	108.69	0.01	108.70	0.04	120.80	0.50	120.30	0.20
11	102.24	0.02	102.34	0.09	117.20	0.53	109.77	0.38
12	112.73	0.06	112.81	0.06	124.27	0.35	125.90	0.20
13	106.53	0.04	106.59	0.08	121.77	0.59	117.10	0.44
14	111.63	0.04	111.62	0.07	116.73	0.35	119.47	0.31
15	105.64	0.09	105.69	0.10	119.73	1.10	117.77	0.57
16	120.13	0.02	121.11	0.02	131.73	0.97	131.60	0.26
17	101.21	0.03	101.23	0.06	108.87	0.32	112.00	0.50
18	107.07	0.02	107.09	0.13	121.53	1.72	117.27	0.21
19	109.75	0.06	110.02	0.19	122.60	0.26	121.53	0.25
20	109.73	0.04	109.77	0.05	122.50	0.89	118.80	0.44
23	123.99	0.03	124.08	0.15	127.00	0.72	137.17	0.85
22	112.83	0.05	112.80	0.08	117.10	0.44	125.23	0.60
23	112.80	0.05	112.80	0.05	122.30	0.50	122.03	0.55
24	108.01	0.02	108.00	0.05	123.33	0.90	118.40	0.10
25	107.80	0.05	107.69	0.08	113.53	0.35	120.23	0.32

Table 14:

MEDIAN LENGTH BETWEEN CONDYLES MEASUREMENT MEANS AND STANDARD

DEVIATION MEANS BY MODALITY

Sample	TRUE		i-CAT		PA		SMV	
	Mean	SD	Mean	SD	Mean	SD	Mean	SD
1	65.70	0.02	65.90	0.11	77.90	0.36	77.93	0.31
2	72.19	0.03	71.86	0.05	70.47	0.45	82.67	0.21
3	70.08	0.03	70.16	0.04	78.30	0.62	81.20	0.20
4	68.74	0.08	68.70	0.07	78.73	0.67	75.80	0.26
5	77.94	0.08	77.68	0.09	82.07	0.42	86.30	0.30
6	74.36	0.06	74.39	0.05	74.90	0.50	82.23	0.15
7	68.14	0.01	68.23	0.03	75.73	0.31	75.80	0.17
8	74.49	0.09	74.55	0.05	82.07	0.80	82.60	0.26
9	74.78	0.11	74.76	0.06	83.50	0.62	83.37	0.15
10	74.22	0.04	74.25	0.03	85.37	0.55	83.57	0.15
11	65.60	0.07	65.50	0.08	69.57	0.84	73.03	0.15
12	78.22	0.07	78.26	0.05	85.33	0.25	87.20	0.10
13	71.03	0.03	71.11	0.08	74.00	0.92	79.30	0.26
14	75.61	0.04	75.64	0.09	84.77	0.51	83.83	0.23
15	74.37	0.13	74.29	0.07	80.13	0.35	82.33	0.15
16	79.08	0.02	79.03	0.06	88.20	0.75	87.37	0.32
17	72.58	0.10	72.68	0.12	81.17	0.45	80.47	0.21
18	74.28	0.11	74.41	0.03	75.90	0.62	81.57	0.25
19	72.96	0.01	72.91	0.06	83.77	0.40	82.47	0.55
20	73.22	0.11	73.18	0.05	79.60	0.62	82.57	0.42
23	82.56	0.04	82.49	0.17	90.33	1.11	91.13	0.35
22	75.04	0.04	75.10	0.05	83.47	0.45	83.30	0.17
23	71.69	0.05	71.71	0.05	85.67	0.55	80.90	0.26
24	70.94	0.03	71.02	0.08	74.87	0.42	79.30	0.20
25	70.41	0.04	70.47	0.06	77.47	0.47	79.13	0.35

Table 15:

MOLAR WIDTH MEASUREMENT MEANS AND STANDARD DEVIATION MEANS BY

MODALITY

	TRUE		*i-CAT*		*SMV*	
Sample	*Mean*	*SD*	*Mean*	*SD*	*Mean*	*SD*
1	35.53	0.25	36.12	0.06	42.87	0.35
2	39.47	0.21	39.55	0.12	42.77	0.12
3	35.72	0.07	36.13	0.06	44.03	0.57
4	36.55	0.27	36.68	0.07	41.23	0.75
5	39.91	0.11	39.64	0.06	47.23	0.74
6	37.77	0.11	37.32	0.11	42.07	0.75
7	38.96	0.10	38.94	0.11	42.63	0.51
8	38.44	0.18	38.29	0.10	42.23	0.40
9	37.25	0.19	37.07	0.10	44.27	0.32
10	38.40	0.16	38.27	0.08	44.07	0.91
11	41.11	0.03	41.44	0.16	46.43	0.15
12	36.80	0.11	36.64	0.10	42.47	0.31
13	37.78	0.16	37.55	0.13	44.33	0.40
14	38.89	0.16	38.53	0.12	45.83	0.72
15	38.86	0.51	39.09	0.04	42.80	0.87
16	39.49	0.14	39.58	0.08	45.03	0.38
17	38.47	0.49	38.20	0.05	43.33	0.60
18	34.77	0.03	34.81	0.05	40.53	0.51
19	38.80	0.10	39.04	0.07	42.07	0.31
20	40.33	0.11	40.37	0.12	46.47	0.58
23	43.02	0.12	43.43	0.20	50.67	0.35
22	42.38	0.39	43.26	0.05	50.23	0.49
23	41.62	0.21	42.20	0.17	45.73	0.31
24	46.38	0.24	45.69	0.11	53.30	0.56
25	34.33	0.16	34.13	0.05	40.23	0.32

Table 16:

MANDIBULAR WIDTH MEASUREMENT MEANS AND STANDARD DEVIATION

MEANS BY MODALITY

	TRUE		*i-CAT*		*PA*		*SMV*	
Sample	*Mean*	*SD*	*Mean*	*SD*	*Mean*	*SD*	*Mean*	*SD*
1	83.72	0.10	83.10	0.10	92.87	0.25	85.10	0.46
2	96.84	0.03	94.84	0.03	91.73	0.60	91.40	0.36
3	87.11	0.46	86.18	0.10	103.67	0.50	93.67	0.25
4	94.49	0.35	93.49	0.23	99.93	0.80	86.40	0.26
5	85.44	0.22	83.89	0.46	88.17	0.71	88.63	0.46
6	86.21	0.07	86.01	0.70	96.00	0.46	81.33	0.12
7	81.84	0.10	81.74	0.23	87.80	0.56	83.97	0.23
8	99.98	0.11	99.05	0.61	108.93	0.61	90.03	0.59
9	85.55	0.14	85.91	0.61	91.70	0.40	79.40	0.69
10	94.62	0.32	94.87	0.24	103.03	0.15	94.10	0.26
11	85.45	0.19	84.67	0.46	91.50	0.82	92.57	0.15
12	93.23	0.11	94.22	0.20	101.73	0.31	86.57	0.15
13	87.32	0.23	86.80	0.01	93.43	0.40	84.97	0.31
14	90.75	0.03	90.43	0.16	96.80	0.36	83.80	0.36
15	87.19	0.36	87.00	0.04	92.80	0.66	82.77	0.35
16	101.52	0.12	101.97	0.19	108.77	0.25	94.97	0.47
17	87.02	0.17	86.74	0.10	92.97	0.25	85.77	0.29
18	77.02	0.05	75.60	0.24	84.23	0.15	78.63	0.15
19	97.49	0.13	96.79	0.45	102.53	0.99	92.90	1.08
20	95.67	0.26	94.86	0.42	102.83	0.84	95.37	0.45
23	91.88	0.05	89.81	0.19	98.70	0.75	94.20	0.30
22	100.82	0.14	99.51	0.26	106.80	0.30	93.77	0.25
23	89.25	0.10	89.81	0.25	95.70	0.10	83.90	0.26
24	90.10	0.02	89.02	0.24	97.27	0.35	86.23	0.72
25	96.77	0.13	92.27	0.47	103.57	0.47	98.27	0.61

Differences in Measurements by Modality

Table 17 describes the several statistically significant differences which were evident between each modality measurement and the true measurement (directly made on the skull specimens). When using the cephalometric radiograph, condylar width (p<0.001), condylar height (p<0.01), and the lateral pole to gonion (p< 0.001) measurements all differed significantly from anatomic truth. The PA measurements differed significantly for condylar length (p<0.001), lateral distance between condyles (p<0.001), medial distance between condyles (p<0.001), and gonion to gonion (p<0.05). The SMV measurements differed significantly for condylar height (p<0.01), lateral distance between condyles (p<0.001), medial distance between condyles (p<0.001), and maximum molar width (p<0.001). All measurements made using the iCAT did not differ significantly from anatomic truth.

Table 17:

STATISTICAL DIFFERENCES IN MODALITY MEASURMENTS TO TRUE

MEASUREMENTS (ANATOMIC TRUTH)

	N	*True Mean*	*iCAT Mean*	*Ceph Mean*	*PA Mean*	*SMV Mean*
Condylar Width	50	8.80	8.81	11.08***		9.18
Condylar Length	50	18.76	18.83		20.79***	20.08**
Condylar Height	50	19.46	19.56	21.43**		
Pogonion to Condyle	50	117.10	117.52	119.33		
Pogonion to Second Molar	50	54.79	55.15	53.85		
Lateral Pole to Gonion	50	51.44	51.59	60.43***	58.26	
Lateral Distance Between Condyles	25	109.22	109.28		119.51***	119.87***
Medial Distance Between Condyles	25	73.13	73.13		80.13***	81.81***
Maximum Molar Width	25	38.84	38.88			44.51***
Gonion to Gonion	25	90.69	89.94		97.34*	88.35

*p<0.05, **p<0.01, ***p<0.001

Differences in Standard Deviation by Modality

Table 18 describes the several statistically significant differences which were evident

between each modality standard deviation and the true standard deviation (measurements made

directly on the skull specimens). The mean standard deviation ranged from 0.01 to 0.18 for the

true measurements, while the standard deviation mean ranged from 0.07 to 0.28 for the iCAT,

0.37 to 0.58 for the ceph, 0.48 to 0.64 for the PA, and 0.25 to 0.49mm for the SMV. For the iCAT

standard deviations from the condylar width ($p<0.01$), condylar length ($p<0.001$), condylar height

($p<0.001$), pogonion to condyle ($p<0.001$), pogonion to second molar ($p<0.001$), lateral pole to

gonion ($p<0.001$), lateral distance between condyles ($p<0.001$), and maximum molar width

($p<0.001$) differed significantly from those measurements made directly on the skull specimens

(true standard deviation), although the magnitude of difference was extremely small and likely

insignificant clinically. For the ceph, standard deviations from the condylar width, condylar

height, and lateral pole to gonion differed significantly ($p<0.001$) from that made directly on the

skull specimens (true standard deviations). For the PA, standard deviations from the condylar

length, lateral pole to gonion, lateral distance between condyles, medial distance between

condyles, and gonion to gonion differed significantly ($p<0.001$) from that of measurements made

directly on the skull specimens (true standard deviation). For the SMV, standard deviations from

the condylar width, condylar length, lateral distance to condyles, medial distance to condyles,

maximum molar width, and gonion to gonion differed significantly ($p< 0.001$) from that of

measurements made directly on the skull specimens (true standard deviation).

Table 18:

STATISTICAL DIFFERENCES IN MEASUREMENT STANDARD DEVIATIONS

BETWEEN MODALITY AND ANATOMIC TRUTH

	N	*True s.d. Mean (mm)*	*iCAT s.d. Mean (mm)*	*Ceph s.d. Mean (mm)*	*PA s.d. Mean (mm)*	*SMV s.d. Mean (mm)*
Condylar Width	50	0.13	0.08**	0.37***		0.28***
Condylar Length	50	0.03	0.10***		0.57***	0.32***
Condylar Height	50	.01	0.16***	0.42***		
Pogonion to Condyle	50	.05	0.09***	0.44		
Pogonion to Second Molar	50	0.36	0.11***	0.39		
Lateral Pole to Gonion	50	.034	0.13***	0.58***	0.61***	
Lateral Distance Between Condyles	25	0.04	0.08***		0.64***	0.36***
Medial Distance Between Condyles	25	0.06	0.07		0.56***	0.25***
Maximum Molar Width	25	0.18	0.09**			0.49***
Gonion to Gonion	25	0.16	0.28		0.48***	0.38***

*p<0.05, **p<0.01, ***p<0.001

DISCUSSION

A number of imaging techniques have been developed to provide accurate imaging of the temporomandibular joint (TMJ). Currently, there is no single technique that provides accurate imaging of all anatomical aspects of the TMJ complex. Conventional radiographic modalities such as SMV, Cephalogram, or PA radiographs do not accurately assess the TMJ in all three planes of space. Modern modalities, such as MRI and CT, are being used more frequently in TMJ evaluation, but they are sophisticated and costly when considering their routine use by orthodontists. Conversely, CBCT gives an accurate representation of the TMJ, but offers several advantages over the traditional CT. First, the patient is exposed to less radiation than with conventional orthodontic radiographs or conventional CT, while CBCT provides all of the diagnostic information afforded by both. Second, dentomaxillofacial CBCT is more affordable and more practical, as it allows the patient to sit upright during the scan (iCAT), requires less space, and requires a shorter examination time than that of traditional CT. Finally, CBCT provides reconstructed images of high diagnostic quality which offer much more information than that of traditional orthodontic radiographs. Unfortunately, while several authors claim that CBCT offers high accuracy, no study has demonstrated the reconstructions as a 1:1 relationship to the true TMJ anatomy. Therefore, we performed a study to assess this relationship.

Ten linear TMJ measurements were made on the CBCT, Cephalogram, PA, and SMV images from 25 human skull specimens. The same measurements were also made directly on the skull specimens ("true" measures). Comparisons between the true measurements and the radiographic measurements were then made. None of the linear measurements of the CBCT varied significantly from the true measurements taken on the skulls, while 3 out of 5 measurements performed using the cephalogram significantly differed from the true measurements. Similarly, 4 out of the 5 PA measurements and 4 out of the 6 SMV measurements varied significantly. In fact, when using modalities other than CBCT, eight measurements collectively taken varied significantly. The only two measurements in which the CBCT was not significantly more accurate were the measurements pogonion to condyle and pogonion to the second molar. This may have occurred because these particular two measurements evaluated anatomical locations that were easily recognizable for all of the modalities evaluated.

When evaluated by modality, the means of the ten measurements for all 25 skull specimens varied. For example, the iCAT measurements varied from true by 0.00 to .36 mm, while the PA varied from 2.03 to 10.29 mm. The SMV varied from 0.38 to 10.65 mm and the Ceph from 0.94 to 8.94mm. On average, the difference between mean measurements between the iCAT and the true measurement was only 0.20mm, while the Ceph was 3.28mm, the PA 6.56 mm, and the SMV 4.84mm. This is both clinically and statistically significant, as the iCAT allows for a nearly 1:1 reconstruction of the TMJ complex in all dimensions. Previous studies of conventional CT have stated that error within 5% is clinically acceptable. Not only does this allow for more accurate diagnosis

to be performed, but this allows the reconstruction to be used to fabricate a synthetic joint prosthesis prior to reconstructive joint surgery.

Prior to orthodontic treatment, the iCAT is a useful modality for not only TMJ evaluation but also to acquire the diagnostic records necessary for the orthodontic diagnosis and treatment plan. Currently, dimensional assessment of the TMJ related orthodontic dimensions requires the use of 3 plane film projections (cephalogram, PA, and SMV). The 20 second iCAT reconstruction provides a perfect cephalometric view as well as any other view or "slice" that is desired. Further, in one scan the technique provides all information (aside from photographs) normally collected through cephalometric radiographs, posterior-anterior radiographs, panoramic radiographs, and tomograms. Potentially, this technique could eliminate the need for casts (the author is currently evaluating this) and the CT has been used to more accurately make linear measurements than that of a cephalogram. The scan can be stored easily on a DVD and accessed later, thus providing a perfect archive in a very small amount of space. Finally, the iCAT offers important medicolegal protection. As previously stated, a large number of malpractice claims against orthodontists are TMD related. Unfortunately, in an asymptomatic patient who has pathological changes in his/her TMJ, one cannot rule out the possibility that the orthodontic treatment resulted in TMD symptoms without a proper evaluation of the TMJ prior to orthodontic treatment. Typically, orthodontists use panoramic images to evaluate the TMJ, but this has been shown to be inadequate due to magnification and distortion of the image. Using the iCAT the resulting perfect 3D image of the joint allows orthodontists to more accurately asses the TMJ and to properly inform their patients of any abnormalities and potential complications prior to treatment.

Unfortunately, one author has discouraged the routine use of the PA, tomogram, and occlusal radiographs prior to the initiation of orthodontic treatment. This, however, puts the treating orthodontist at risk for litigation should a patient with subclinical TMD begin to manifest symptoms post orthodontic treatment.

Conventional CT is technique sensitive. Head tilt of ±4 degrees can affect CT measurements. Further, magnification effects are seen in the conventional CT scans of bone thinner than 1mm and thicker than 1mm with an inclination greater than 35 degrees. Additionally partial volume effects result in a progressively increasing magnification of bone thickness. Previously, no projection error was found with the CBCT, but such error did exist when using the conventional CT which could significantly affect proper diagnosis of the TMJ. Distortions were seen in the glenoid fossa and in the linear and angular measurements.

In comparison to conventional CT and traditional extraoral radiographs such as the panoramic and cephalogram, patient positioning is not as critical when using the iCAT. When taking a slice of the reconstruction, the image can be moved into any direction for improved positioning. This was done throughout this study and resulted in no error in the iCAT measurements.

Previously, reconstructed 2D images obtained by multi-slice helical computed tomography were shown to be accurate for the imaging diagnosis in dental implant treatment. However, in comparison to 2D CT, 3D spiral CT has been shown to more accurately distinguish craniofacial anatomy as well to allow for more accurate volume rendering techniques for craniometric measurements. Although we did not make comparisons to the 3D spiral CT, the CBCT is a more efficient use of x radiation, and is

faster in volumetric data acquisition. Rather than stack slices to obtain a 3D image, the CBCT makes a single scan to capture an object with a cone of X-rays. Studies performed on first dentomaxillofacial CBCT, the Newtom 9000, demonstrated that the CBCT measurements were consistently smaller for the internal structures than that of the true measurements (also made on skulls). Similar to the current study, the Newtom was reliable for linear measurements of more external structures which are more closely associated with dentomaxillofacial imaging.

Unfortunately, while the iCAT provides state of the art imaging of hard tissues, deficiencies do exist. Currently, the iCAT provides little differentiation between soft tissues. While it can contribute to the diagnosis of problems within soft tissues, such as the articular disc of the TMJ, the resolution is lacking. Further, as the scan penetrates completely through a cranium superimpositions can make differentiation of particular landmarks difficult.   While our study utilized important landmarks within orthodontic diagnosis, the images made of the skulls were high in contrast. This was done in order to clearly visualize the landmarks; however, at this level of contrast, soft tissue points used in cephalometric analyses may not be evident. If a clinician were using the iCAT to also perform a soft tissue analysis, the hard tissue anatomic landmarks may not be as readily evident at the reduced contrast.

We found that the measurements made using the iCAT were reproducible. The mean standard deviation when repeating measurements ranged from 0.01 to 0.36mm for the true measurements, 0.07 to 0.28mm for the iCAT, 0.37 to 0.58mm for the ceph, 0.48 to 0.64 mm for the PA, and 0.25 to 0.49mm for the SMV. When repeating the measures using the iCAT, each slice was saved and the measurement was later recalculated from

123

the same slice. This could slightly overestimate the reproducibility of the measures, since each slice may slightly vary.

We found the iCAT to accurately allow for linear measurements of skulls to be made; however, all 25 skulls in our study had healthy condyles. Although this was not tested, the iCAT should accurately depict arthritic changes in condyles.

Further research in this area is indicated. Our results indicate that linear dimensions are highly accurate using the iCAT. Chidiac et al., evaluated CBCT angle measurement and found no difference between it and the cephalogram. At this point, it is now necessary to investigate whether the spatial inter-relationship of these landmarks is maintained by this imaging modality.

The level of accuracy and reliability afforded by CBCT now enables the measurement of various parameters that may be affected by orthodontic/orthopedic intervention. For example, studies can now be performed to examine the relationship between occlusal changes and their effect on the TMJ, the effect of appliance therapy on the TMJ, the effect of surgery on the TMJ, and the effect of mandibular width on the TMJ. CBCT software algorithms will lead to a better understanding of the effect of orthodontic /orthopedic intervention on facial appearance. This could allow practitioners to better anticipate such changes and make the appropriate alterations in treatment.

CBCT with the iCAT facilitates patient data orientation. Therefore, further studies are warranted to investigate the effect of patient head tilt on linear accuracy. Currently, technology is being used to provide coronal, cross sectional imaging. However, at present "conventional" projections from available CBCT data are not developed. We attempted

to develop oblique MPR's which provided orthodontic specific landmarks in 3D. Our results indicate that the measurements are highly accurate.

Finally, 3D imaging has long been proposed as the "ideal" cephalometric image; however, the user interface with either the surface or volume rendered data has been limited. Emerging projections such as maximum intensity profile (MIP) provide possibilities for topographic analysis for general orthodontic practice. This particular data enhancement technique is less computational than traditional surface oblique volume rendering and can be potentially applied in clinical practice. Such 3D reconstruction gives a general overview of the TMJ which could be useful for the surgical reconstruction of the TMJ.

SUMMARY AND CONCLUSIONS

Currently, dimensional assessment of TMJ related orthodontic dimensions requires the use of 3 plane film projections: the cephalogram, the panoramic radiograph, and the SMV. CBCT provides all of the information from the 3 plane film projections and more in only 1 scan. We found that CBCT, specifically the iCAT, accurately depicts the TMJ complex in 3D as a 1:1 relationship. Measurements were reproducible and significantly more accurate than those measured with other modalities such as the cephalogram, PA, and SMV.
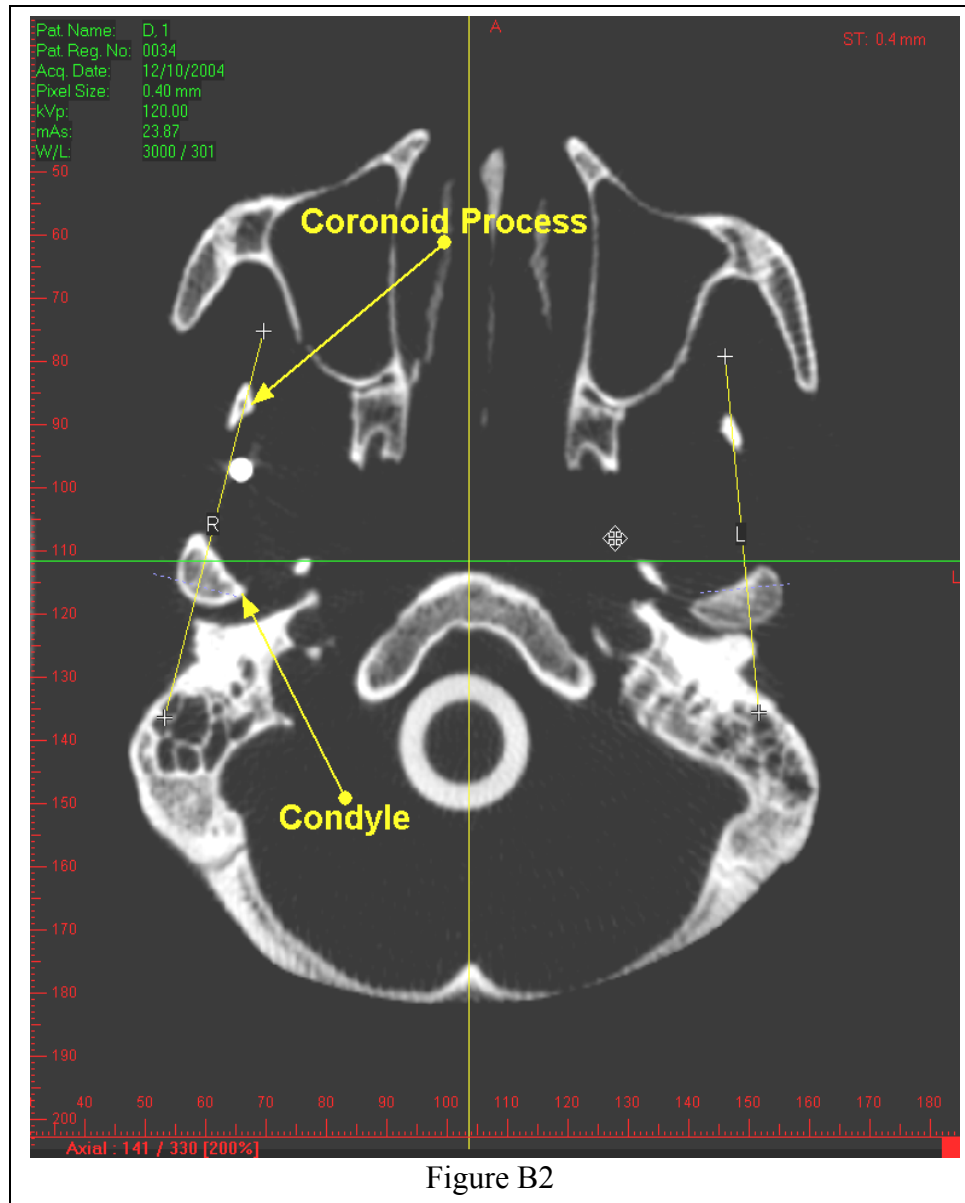
A. Condylar Width

1. Open image with iCAT software.

2. Interpolate image.

3. Set resolution to 3000/300.

4. Enlarged image 200%.

5. Maximized window.

6. Scrolled through transverse cross-section until condyle and coronoid process were visible (Figure A1).

7. Selected TMJ tool and placed separately but bilaterally through condyle from medial pole to lateral pole (Figure A2).

8. Selected sagittal images and enlarged to 200%.

9. Changed thickness of slice to 6.4 mm.

10. Select measure tool.

11. Measure from the superior part of the condyle down four millimeters with measure tool.

12. Measure condylar width at the four millilmeter mark on each of the six sections and record the largest measurement from the posterior part of the condyle to the anterior part of the condyle. Greatest anterior to posterior measurement (Figure A3).
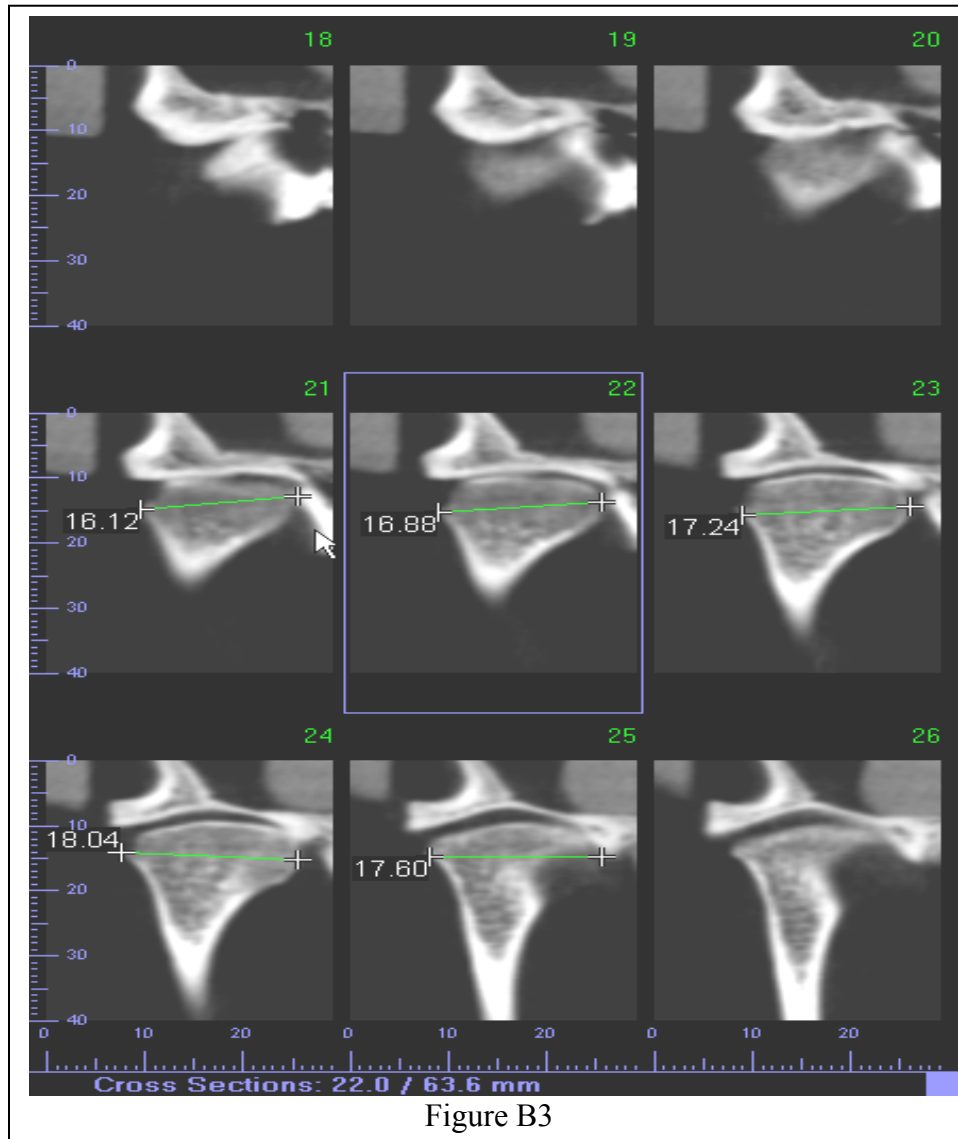
Figure A1

Figure A2

Figure A3
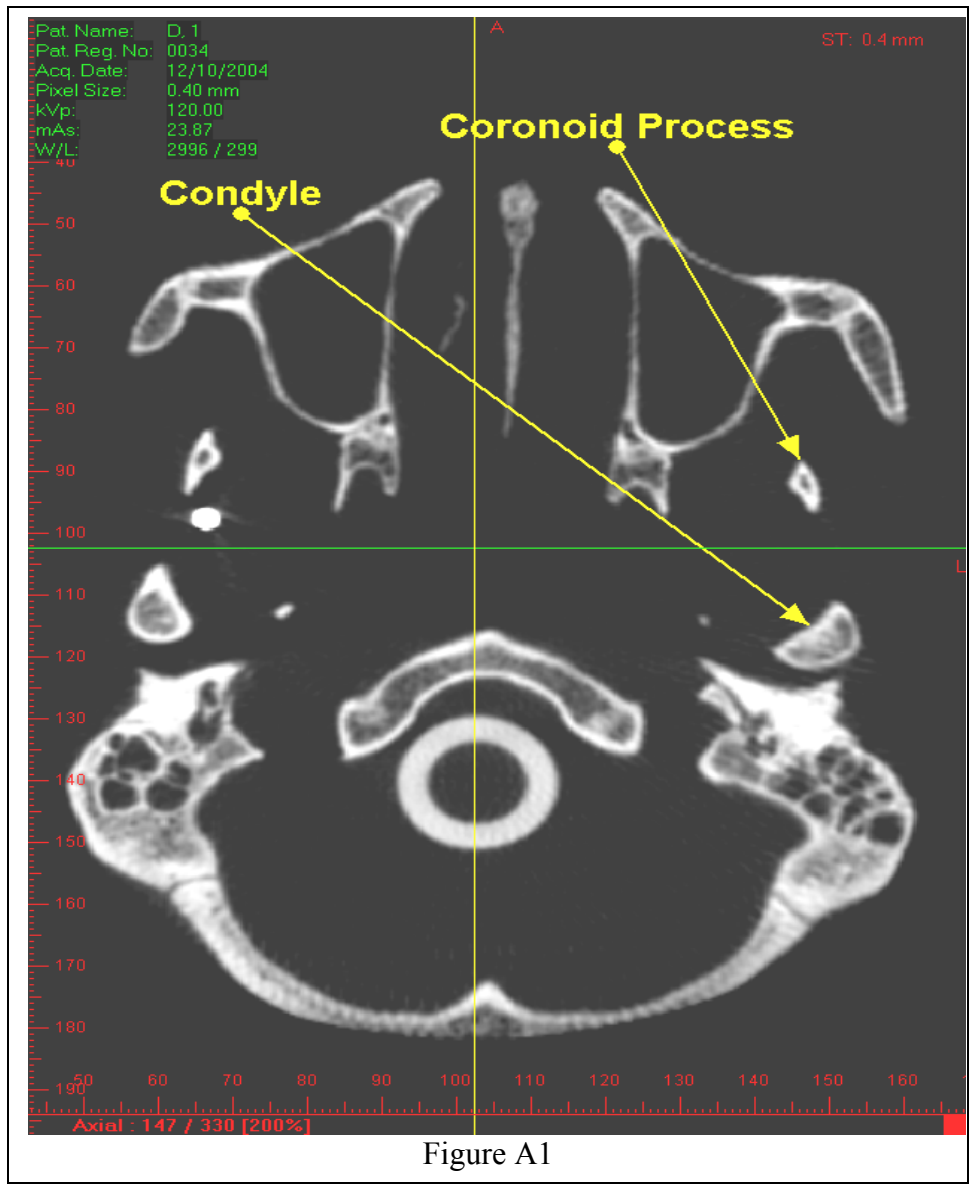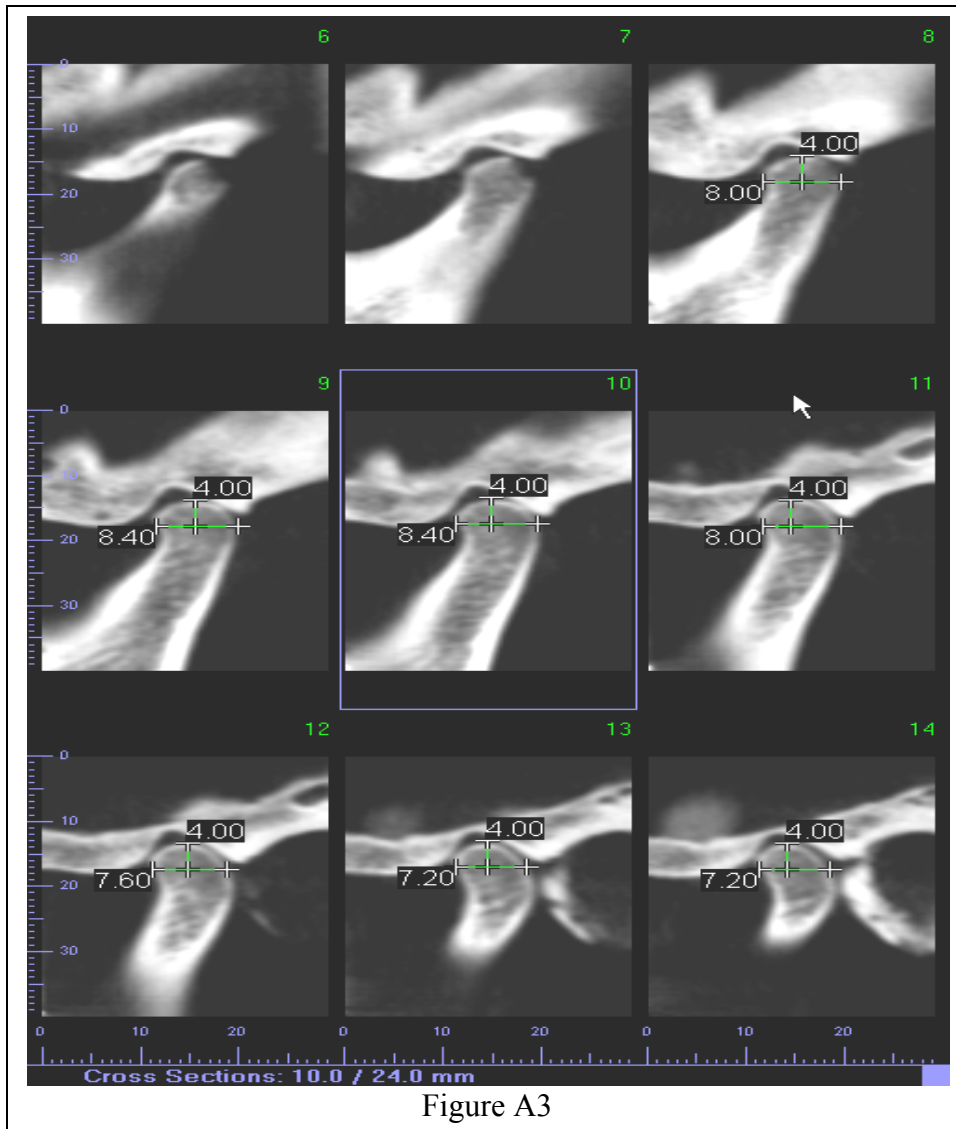
B. *Condylar Length*

1. Opened image with iCAT software.

2. Interpolate image.

3. Set resolution to 3000/300.

4. Maximized window.

5. Enlarged image to 200%

6. Scrolled through transverse cross-section until condyle and coronoid process were visible (Figure B1).

7. Selected TMJ tool and placed separately but bilaterally through condyle and coronoid on right and left sides. This was an anterior to posterior slice (Figure B2).

8. Selected the frontal cut images and enlarged the window.

9. Changed thickness of slice to 8.4mm.

10. Select measure tool and measure condyles in the greatest dimension from the medial to the lateral pole of each condyle. Record the largest measurement taken (Figure B3).
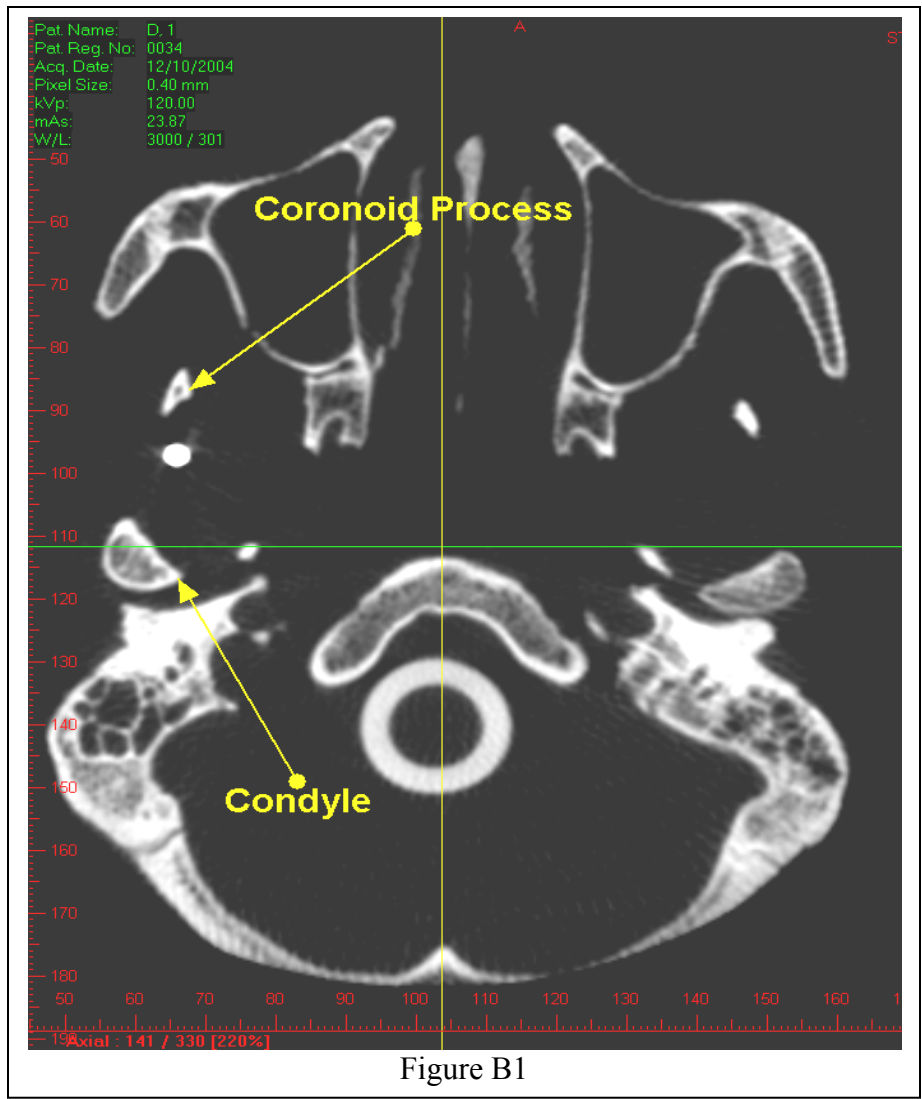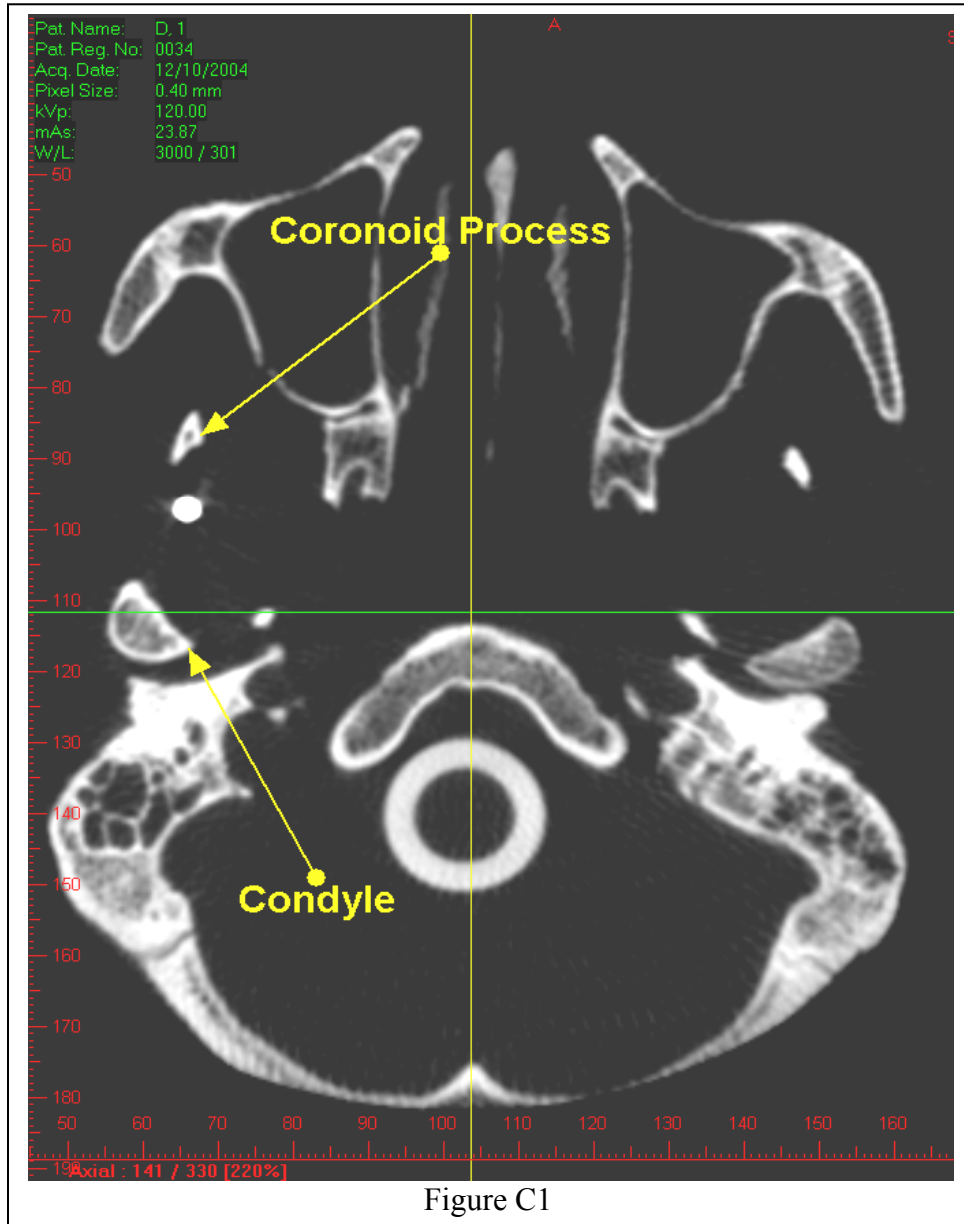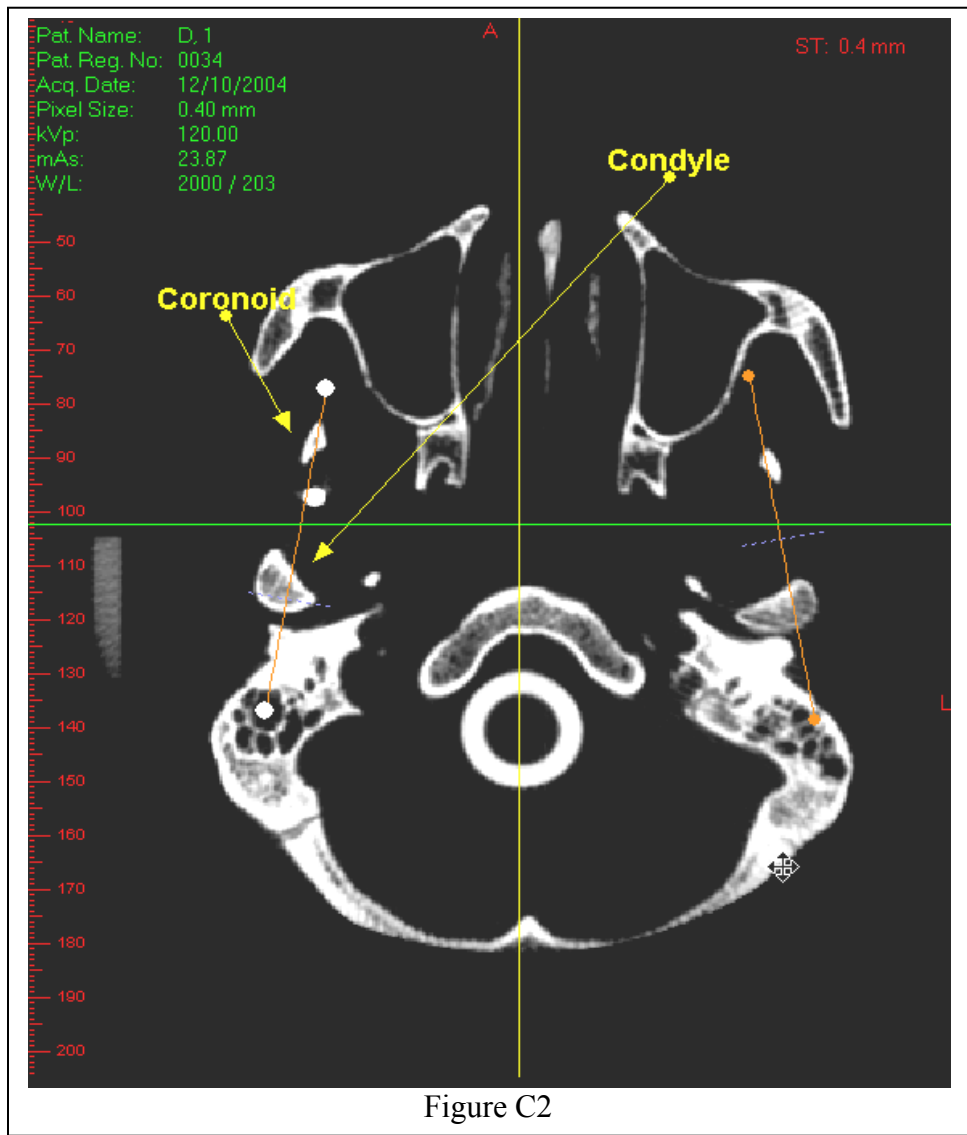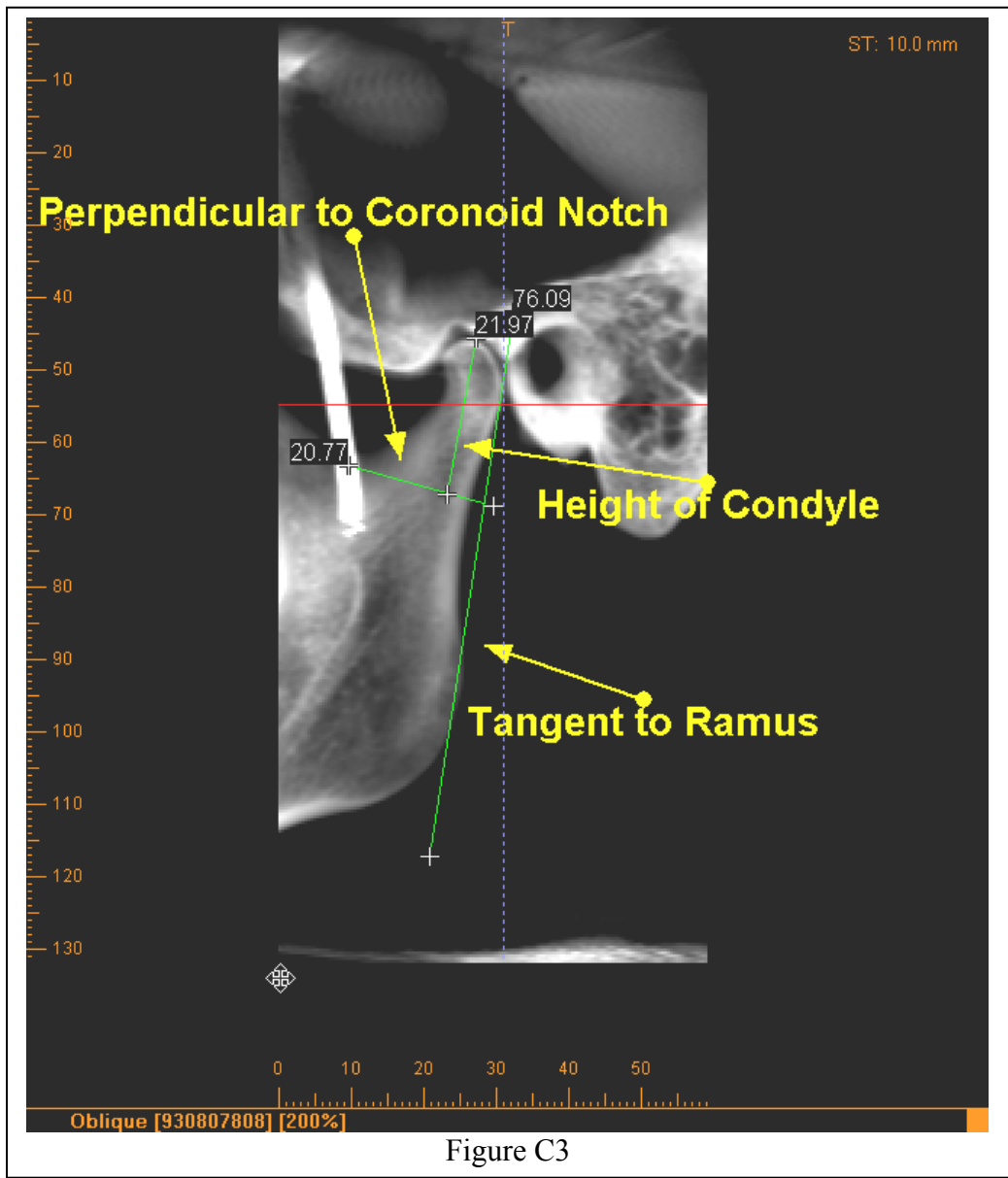
Figure B1

Figure B2

Figure B3

C. Condylar Height

1. Opened image with iCAT software.

2. Interpolated image.

3. Set resolution to 3000/300.

4. Maximized window.

5. Enlarged image to 200%.

6. Scrolled through transverse cross-section until condyle and coronoid process were visible (Figure C1).

7. Selected panoramic tool and placed separately but bilaterally through condyle and coronoid on right and left sides (Figure C2).

8. Selected sagittal image and enlarged to 200%.

9. Changed thickness of slice to 10.0mm.

10. Selected measure tool and drew line tangent to ramus (Figure C3).

11. Selected measure tool and drew line from inferior point of coronoid notch perpendicular to tangent line lateral to ramus (Figure C3).

12. Selected measure tool and measured most superior point of condyle along a plane that is parallel to the ramus and perpendicular to the line drawn from the coronoid notch (Figure C3).
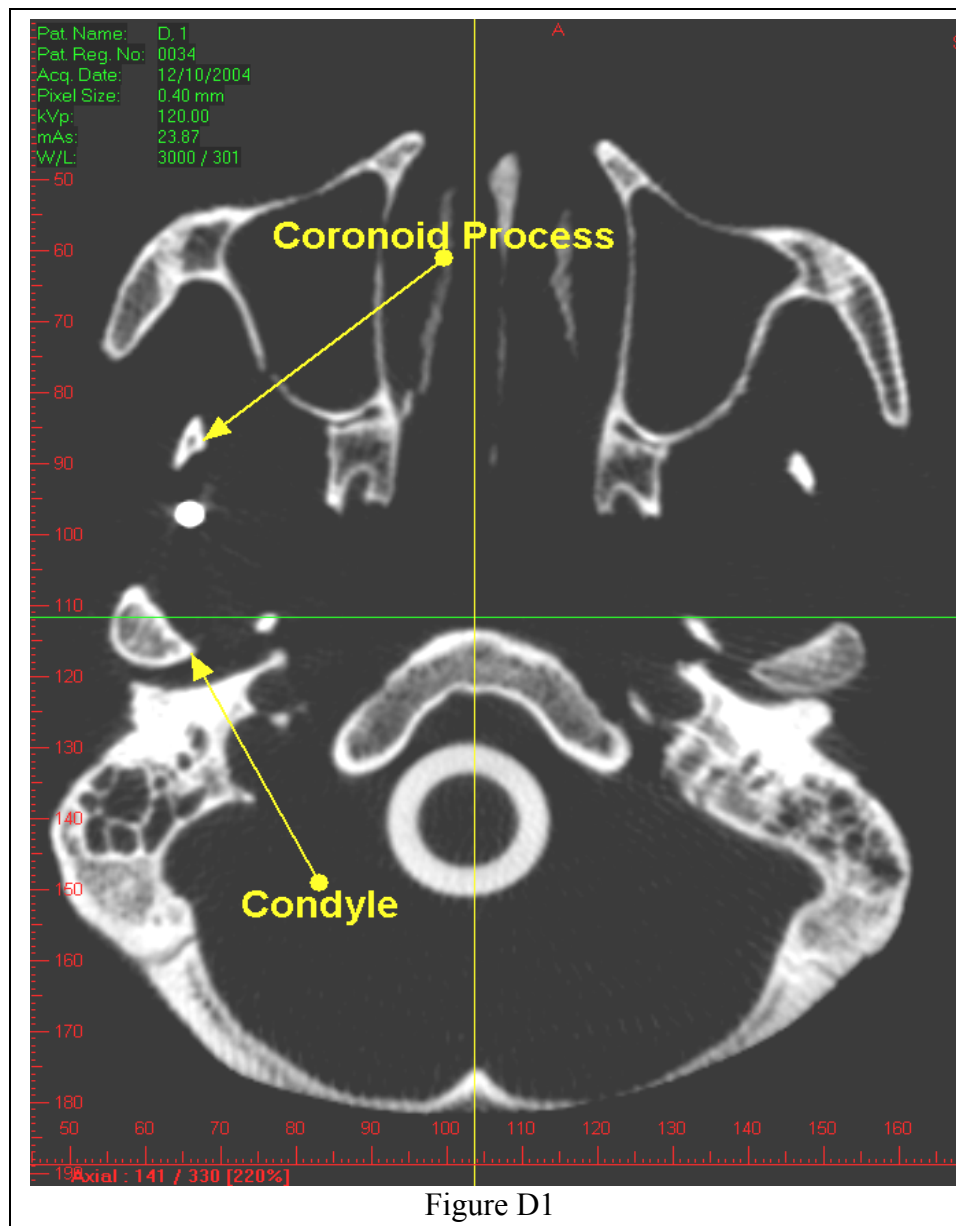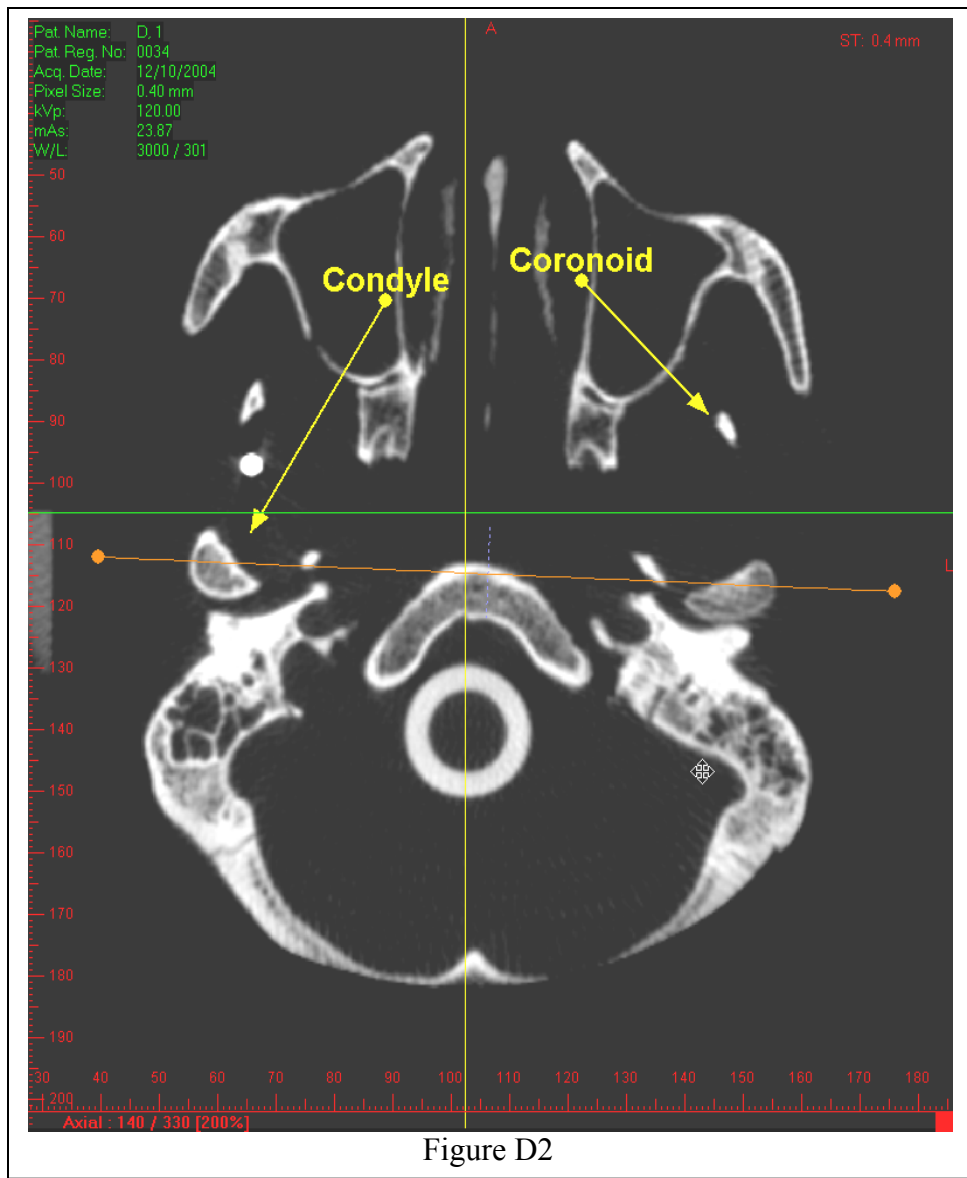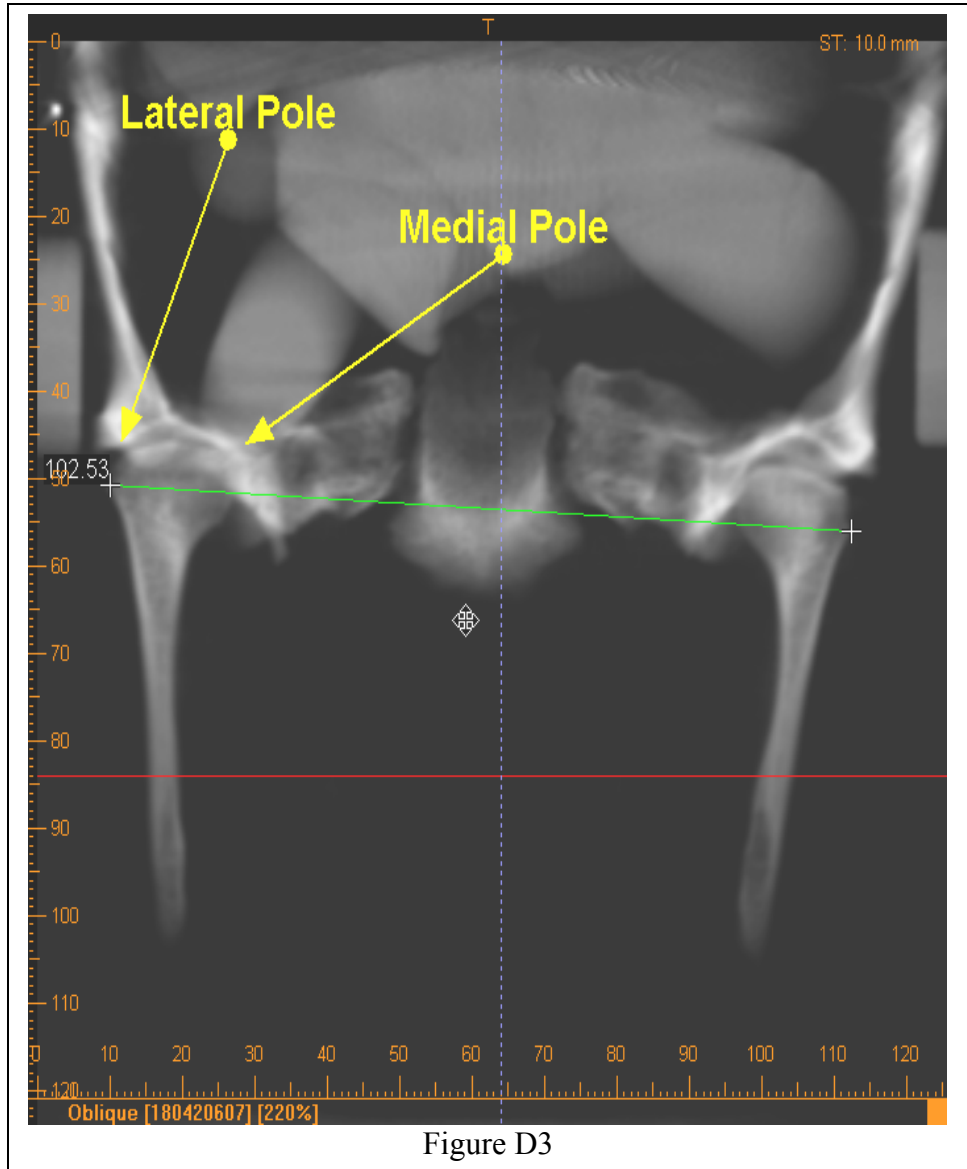
Figure C1

Figure C2

Figure C3

D. Lateral Length Between Condyles

1. Opened image with iCAT software.

2. Interpolated image.

3. Set resolution to 3000/300.

4. Enlarged image to 200%.

5. Maximized window.

6. Scrolled through transverse cross-section until condyle and coronoid process were visible (Figure D1).

7. Selected panoramic tool and made one cut that includes both right and left condyles (Figure D2).

8. Selected frontal cut image and enlarged to 200%.

9. Changed thickness of slice to 10.0mm.

10. Selected measure tool and measured from the most lateral aspect of right and left condyles. The greatest distance between lateral poles (Figure D3).
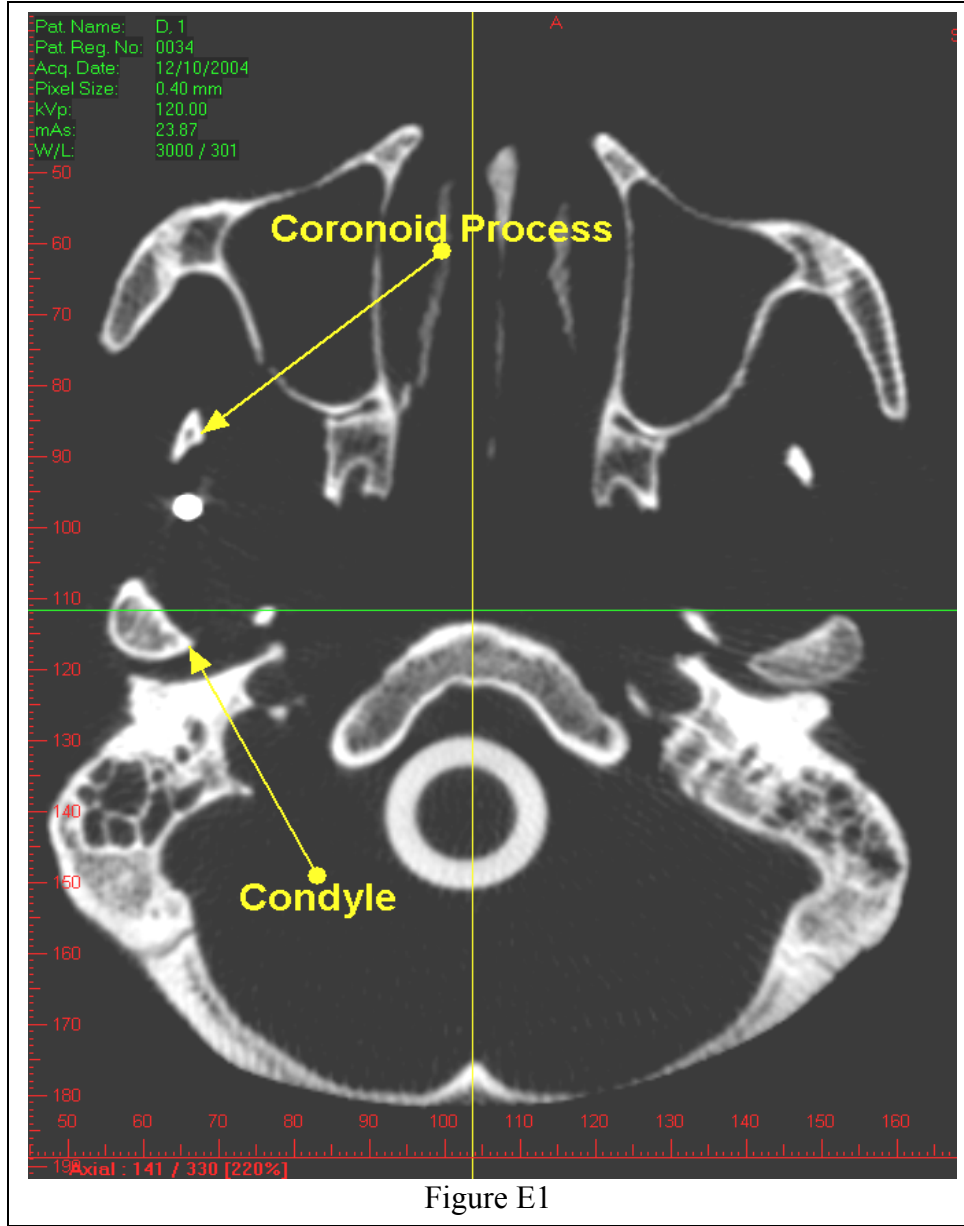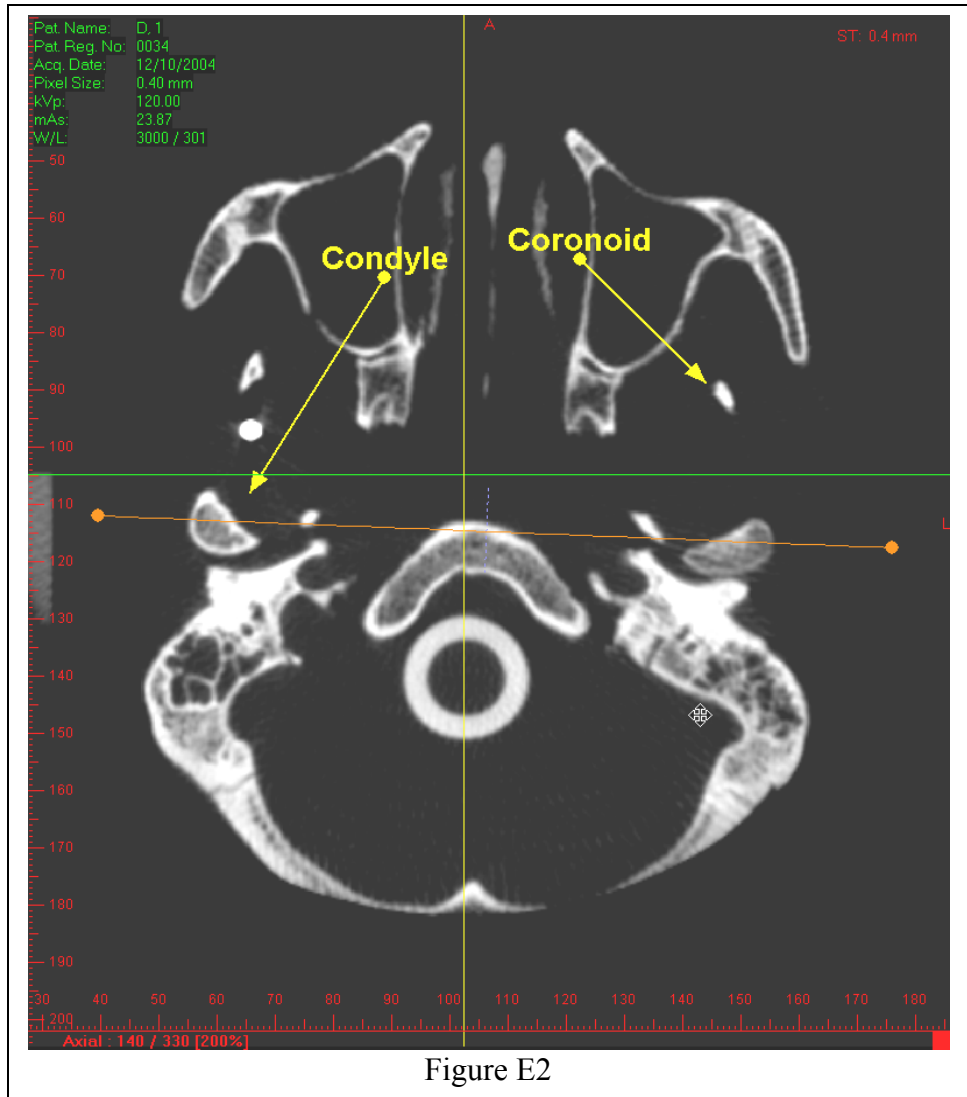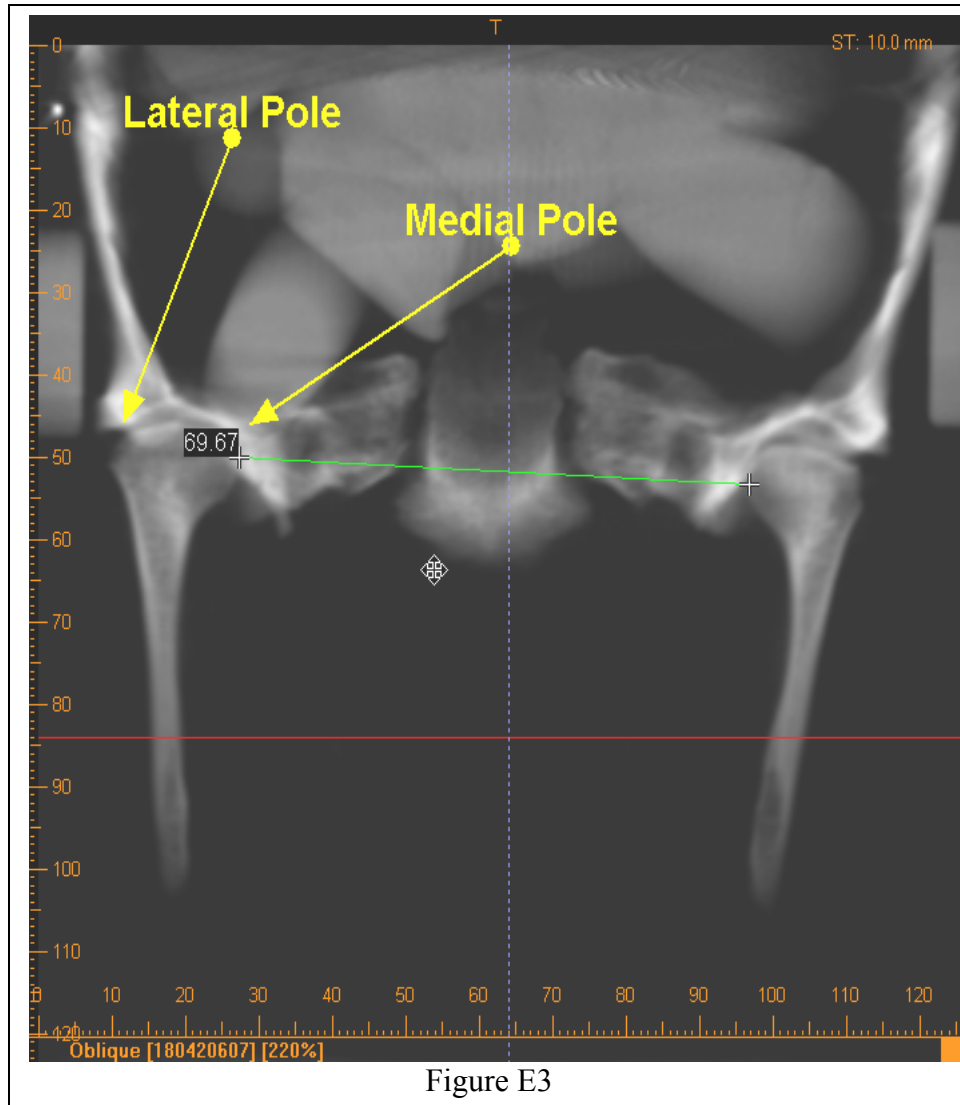
Figure D1

Figure D2

Figure D3

E. Medial Length Between Condyles

1. Opened image with iCAT software.

2. Interpolated image.

3. Set resolution to 3000/300.

4. Enlarged image to 200%.

5. Maximized window.

6. Scrolled through transverse cross-section until condyle and coronoid process were visible (Figure E1).

7. Selected panoramic tool and made one cut that includes both right and left condyles (Figure E2).

8. Selected frontal cut image and enlarged to 200%.

9. Changed thickness of slice to 10.0mm..

10. Selected measure tool and drew line from the most medial aspect of right and left condyles. The smallest distance between medial poles (Figure E3).

Figure E1

Figure E2

Figure E3

F. Molar Length (Distal 6's)

1. Opened image with iCAT software.

2. Interpolated image.

3. Set resolution to 3000/300.

4. Maximized window.

5. Enlarged transverse image to 200% (Figure F1).

6. Scrolled to point where mandibular dentition visible from 6 to 6 (Figure F2).

7. Selected measure tool and measured from right mandibular 6 distal contact to left

   mandibular 6 distal contact (Figure F3).

Figure F1

Figure F2

Figure F3
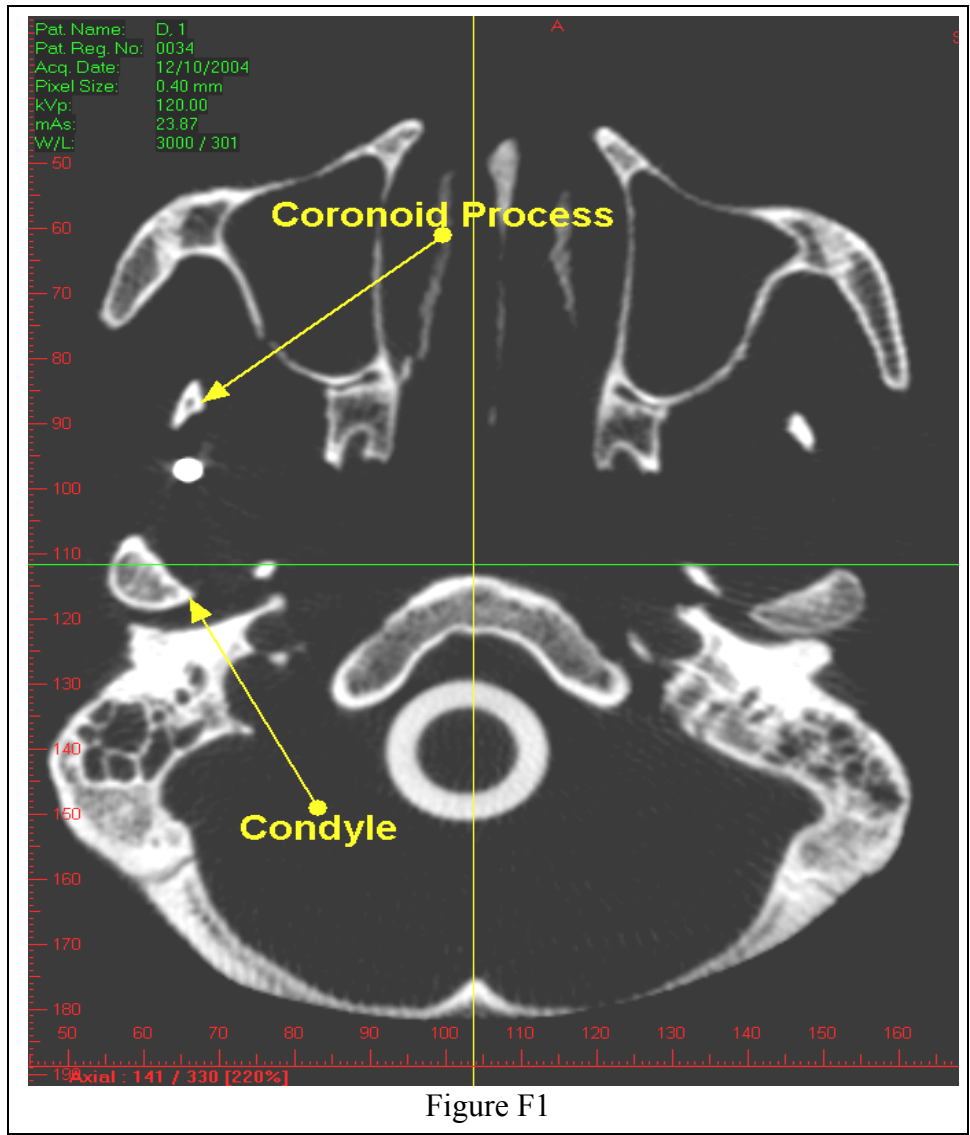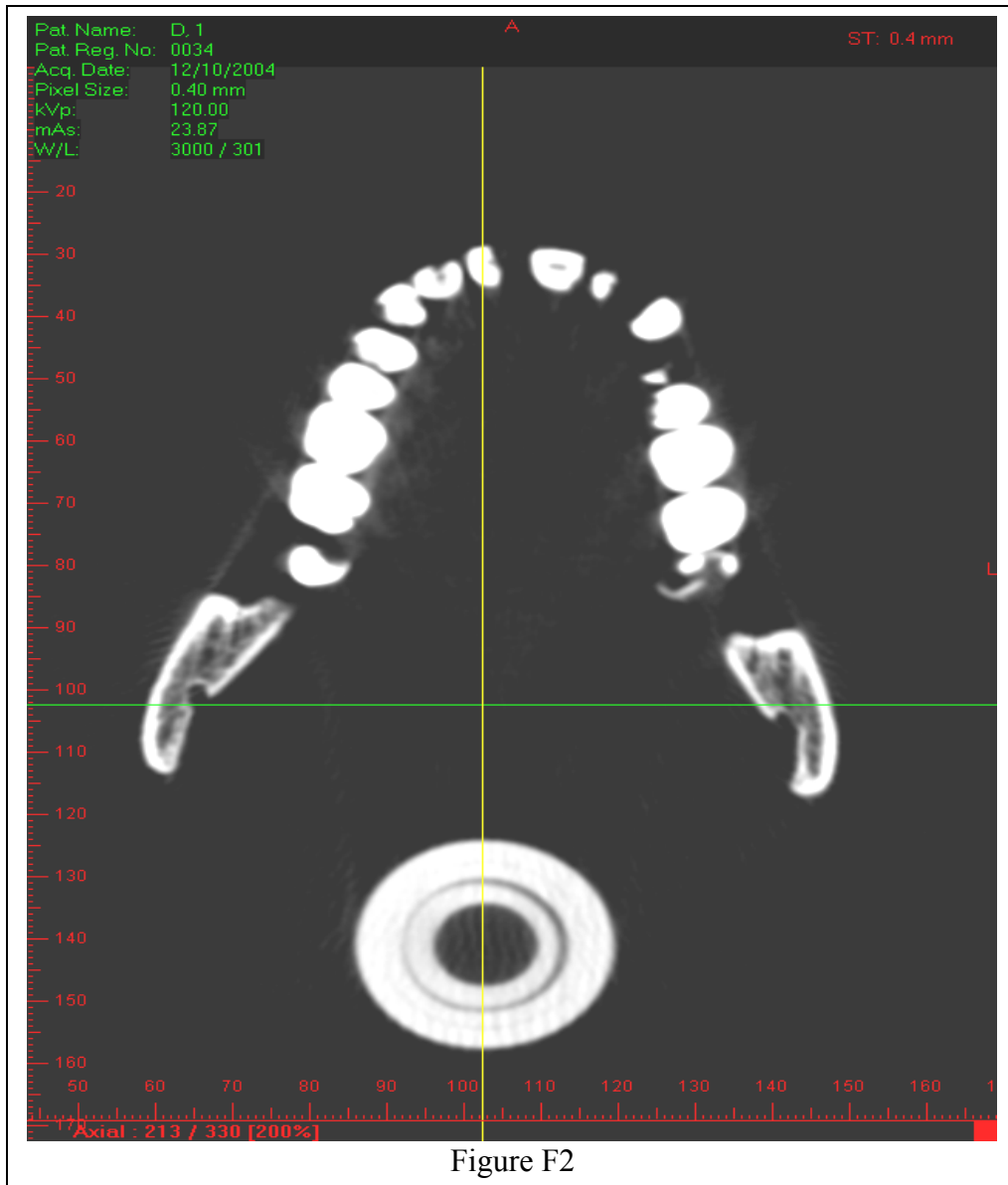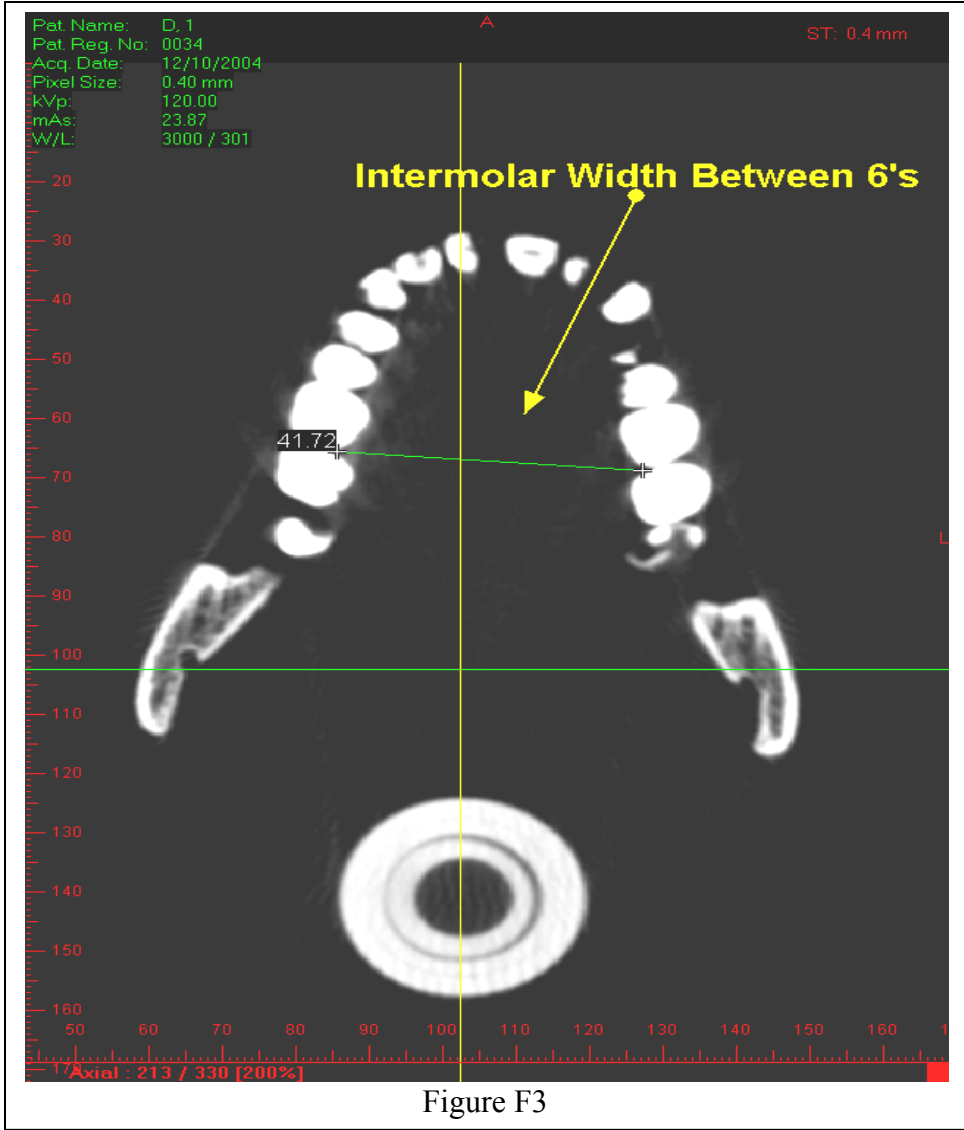
G. Pogonion to Condyle

1. Opened image with iCAT software.

2. Interpolated image.

3. Set resolution to 3000/300.

4. Enlarged image 200%.

5. Maximized window.

6. Scrolled through transverse cross-section until condyle and coronoid process were visible (Figure G1).

7. Selected panoramic tool and placed separately but bilaterally through condyle and pogonion on right and left sides.

8. Scrolled on through the transverse cross sections until pogonion was seen.

9. Adjusted panoramic cuts to make sure they went through pogonion (Figure G2).

10. Selected sagittal image and enlarged to 200%.

11. Changed thickness of slice to 12.4mm.

12. Selected measure tool and measured line from condylion to pogonion bilaterally (Figure G3).
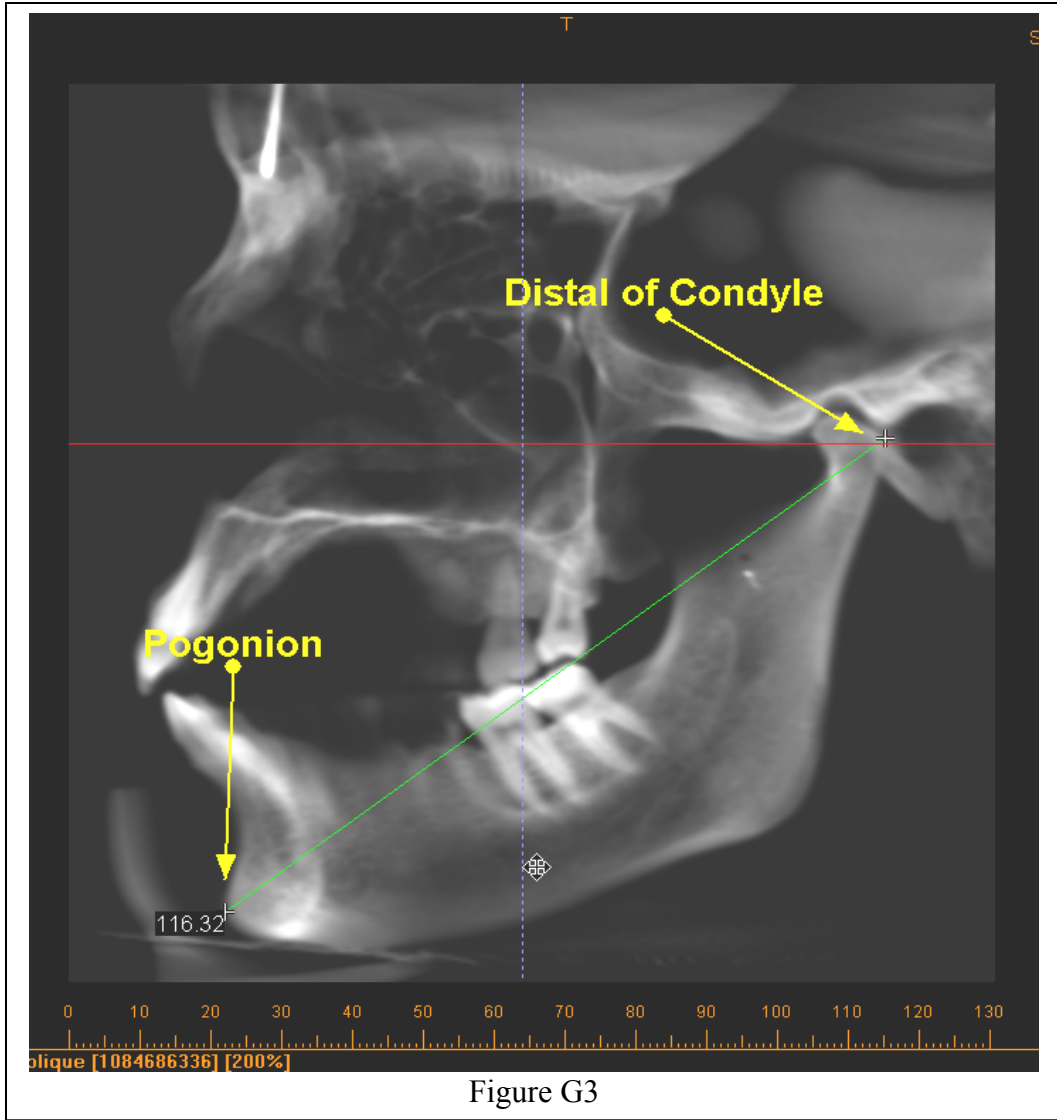
Figure G1

Figure G2

Figure G3

H. Pogonion to Distal 2nd Molar

1. Opened image with iCAT software.

2. Interpolated image.

3. Set resolution to 3000/300.

4. Enlarged image to 200%.

5. Maximized window.

6. Scrolled through transverse cross-section until condyle and coronoid process were visible (Figure H1).

7. Selected panoramic tool and placed separately but bilaterally through condyle and pogonion.

8. Scrolled through the transverse cross sections until pogonion was seen.

9. Adjusted panoramic cuts to make sure they went through pogonion (Figure H2).

10. Selected sagittal images and enlarged to 200%.

11. Changed thickness of slice to 20.4mm.

12. Selected measure tool and measured from distal of second molar to pogonion bilaterally (Figure H3).

Figure H1

Figure H2

Figure H3
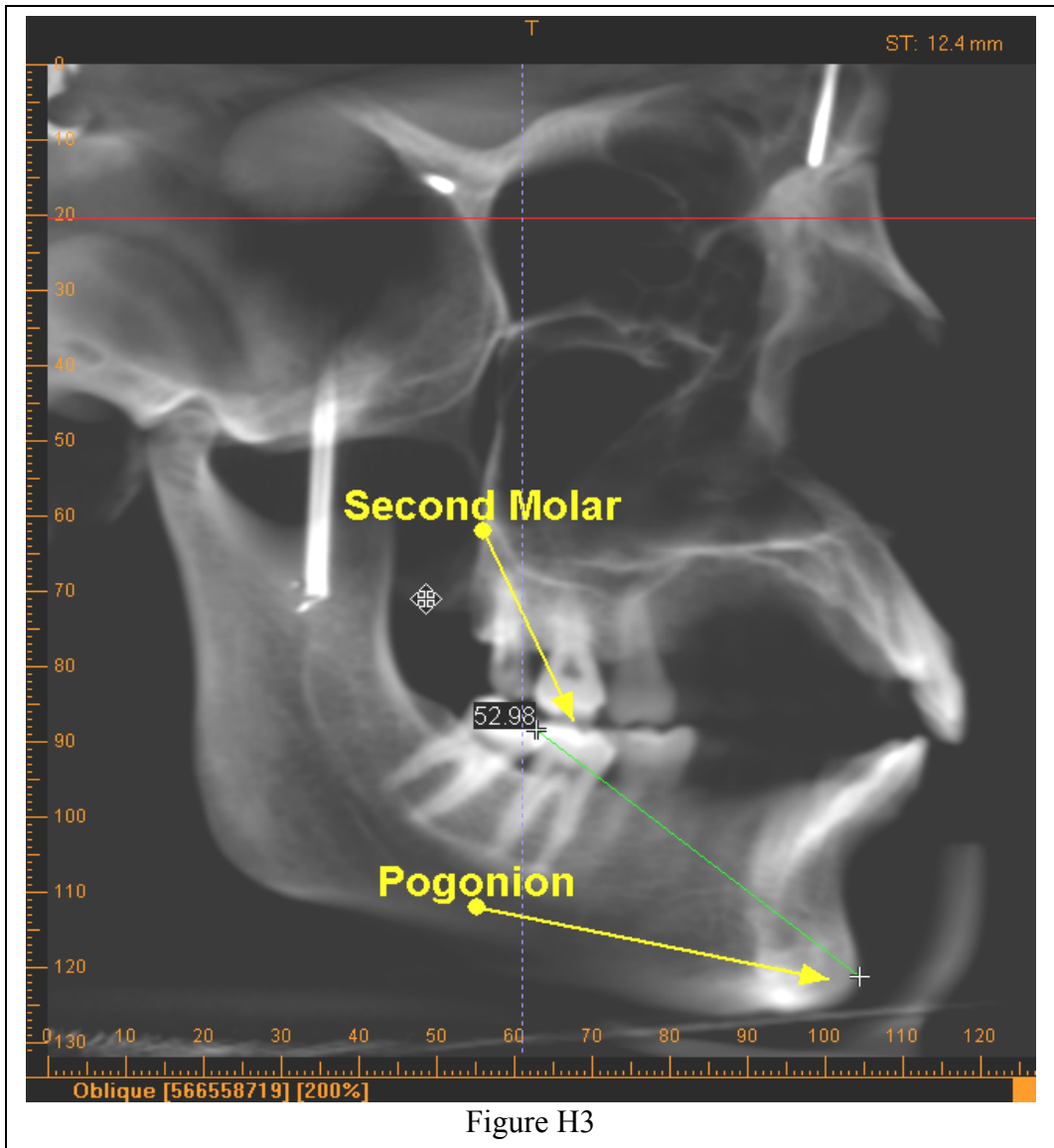
I. Lateral Pole to Gonion
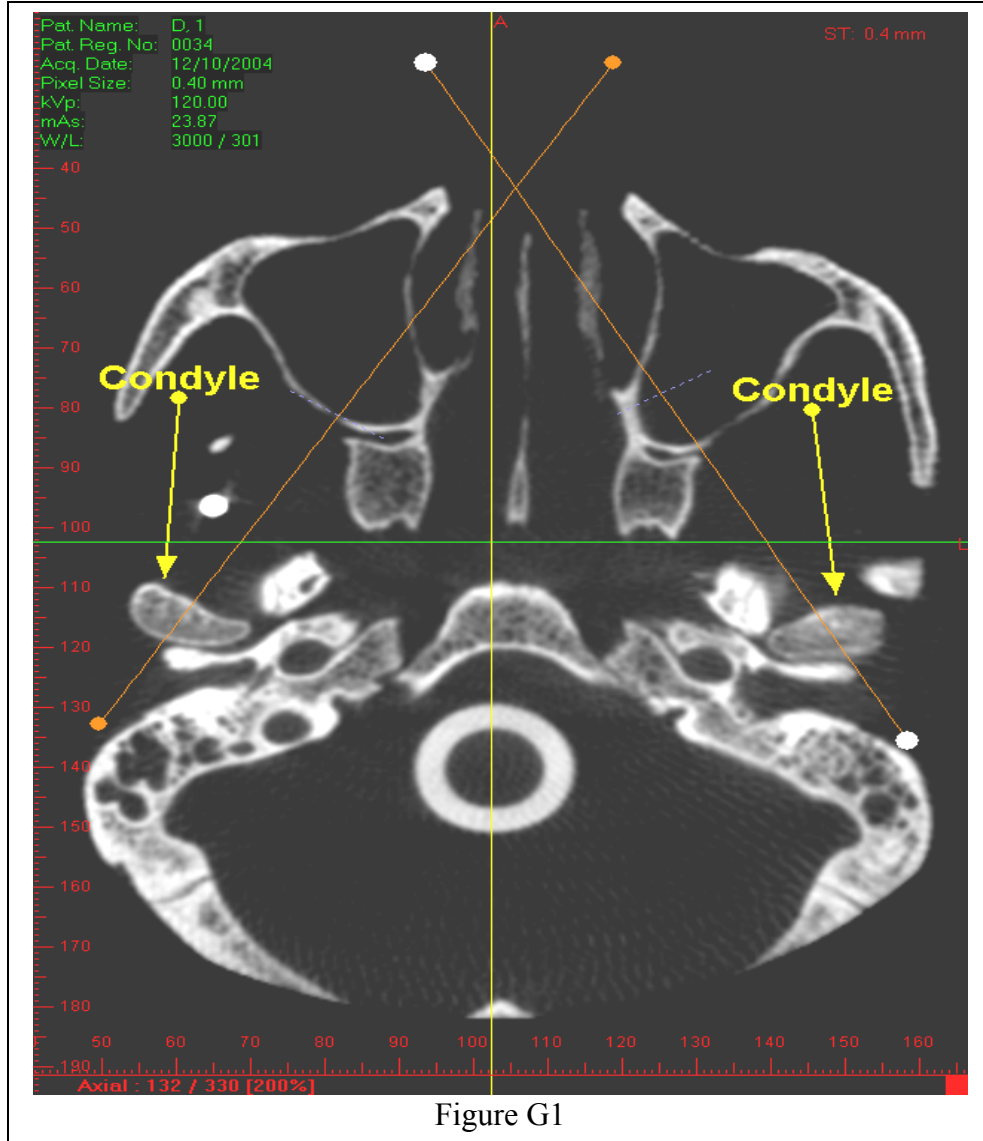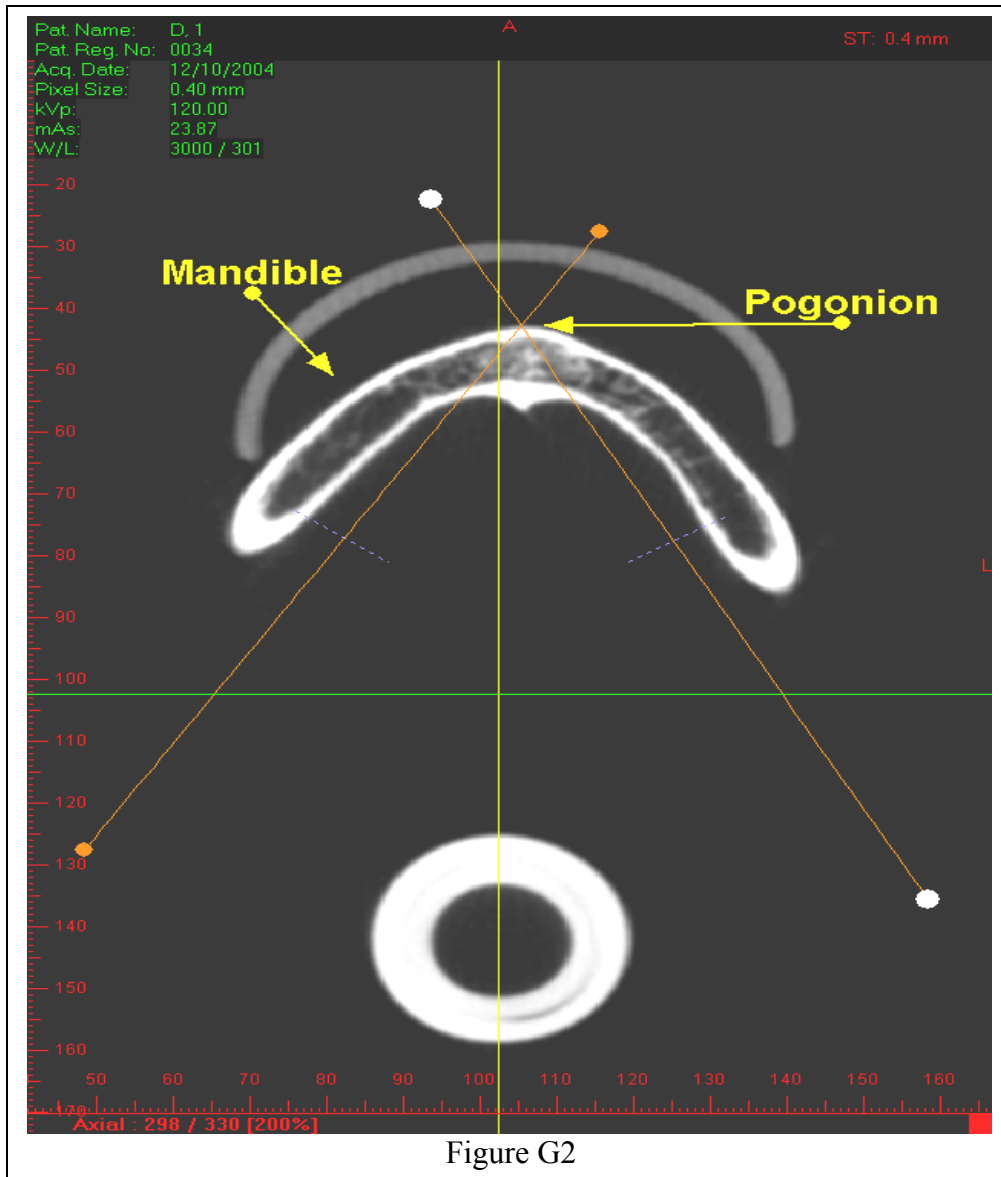
1. Opened image with iCAT software.

2. Interpolated image.

3. Set resolution to 3000/300.

4. Enlarged image 200%.

5. Maximized window.

6. Scrolled through transverse cross-section until condyle and coronoid process were visible (Figure I1).

7. Selected panoramic tool and made single cut just anterior to right and left condyles (Figure I2).

8. Selected image with frontal cut and enlarged to 200%.

9. Selected image thickness of 28.0mm.

10. Selected measure tool.

11. Measured from lateral pole of condyle to gonion bilaterally (Figure I3).
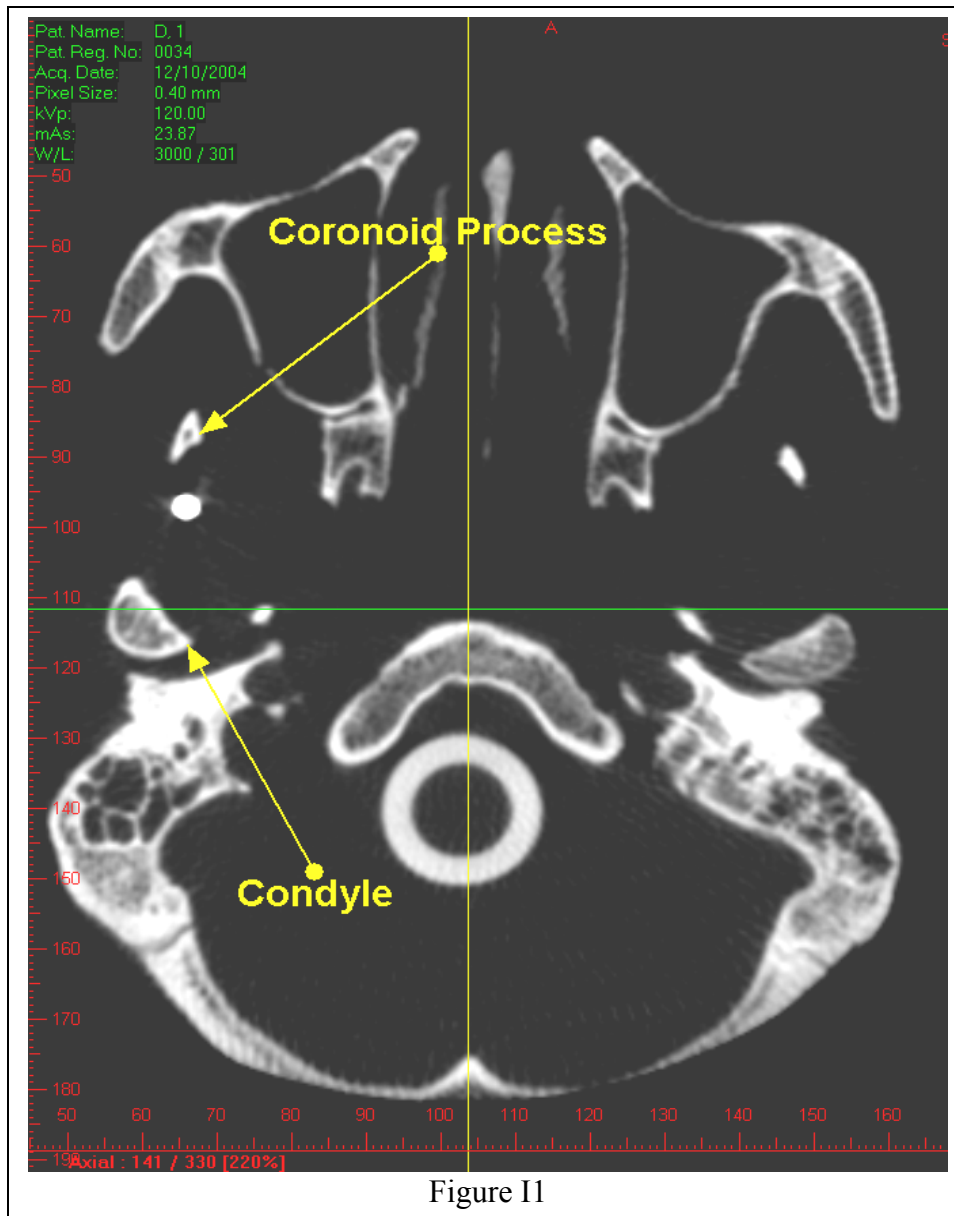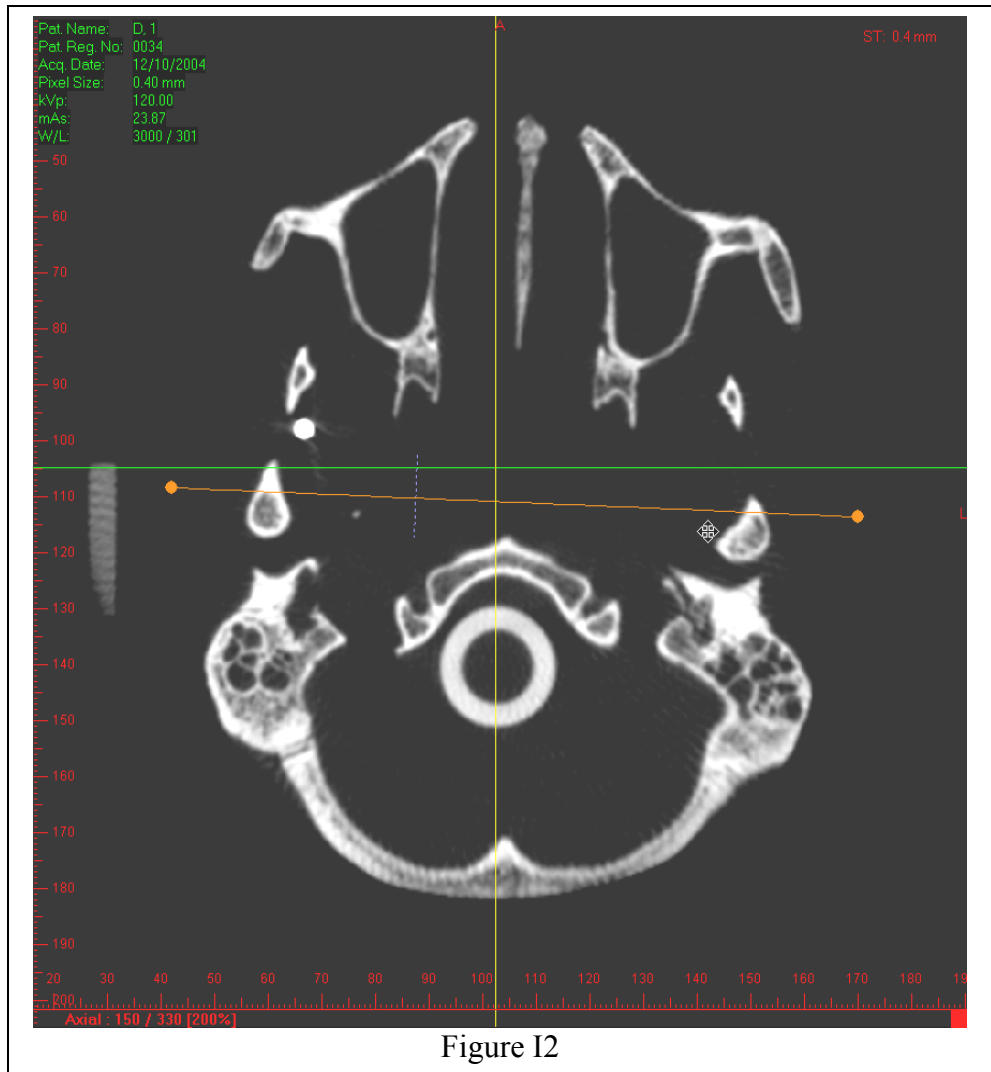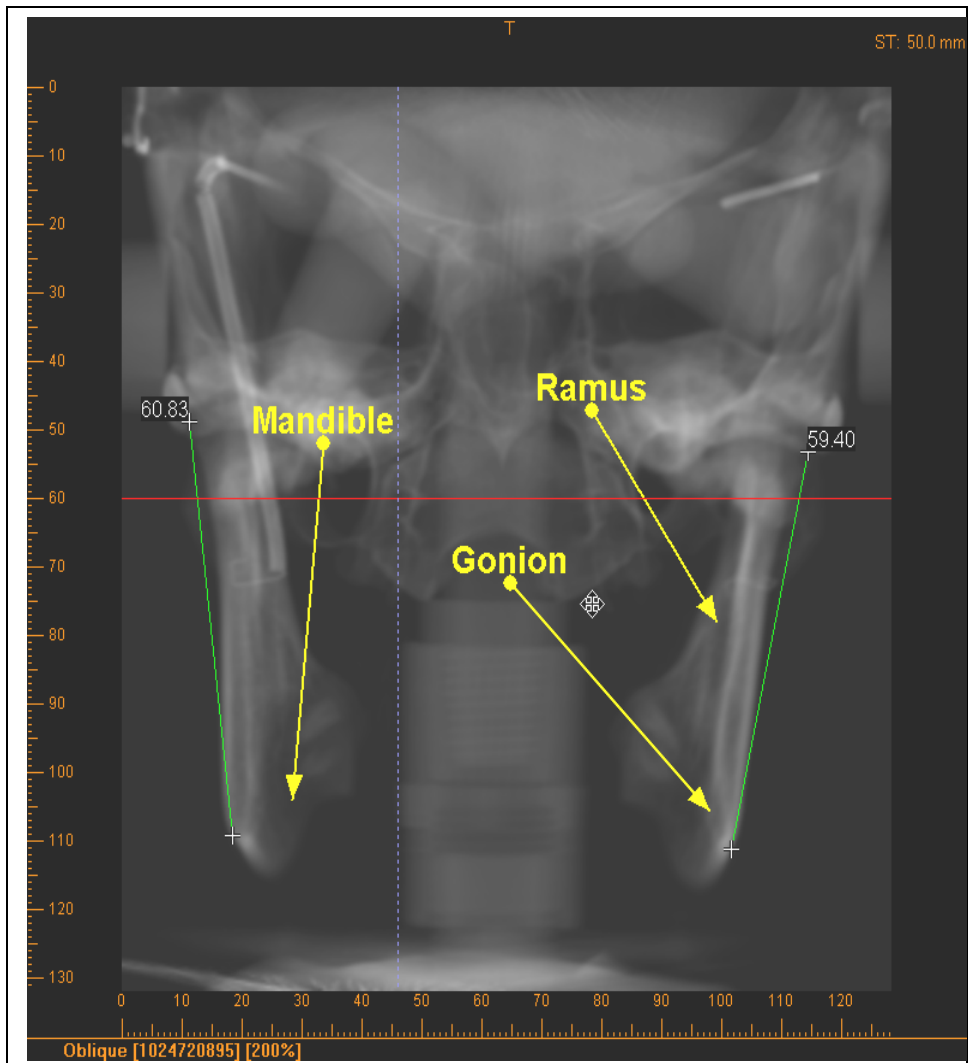
Figure I1

Figure I2
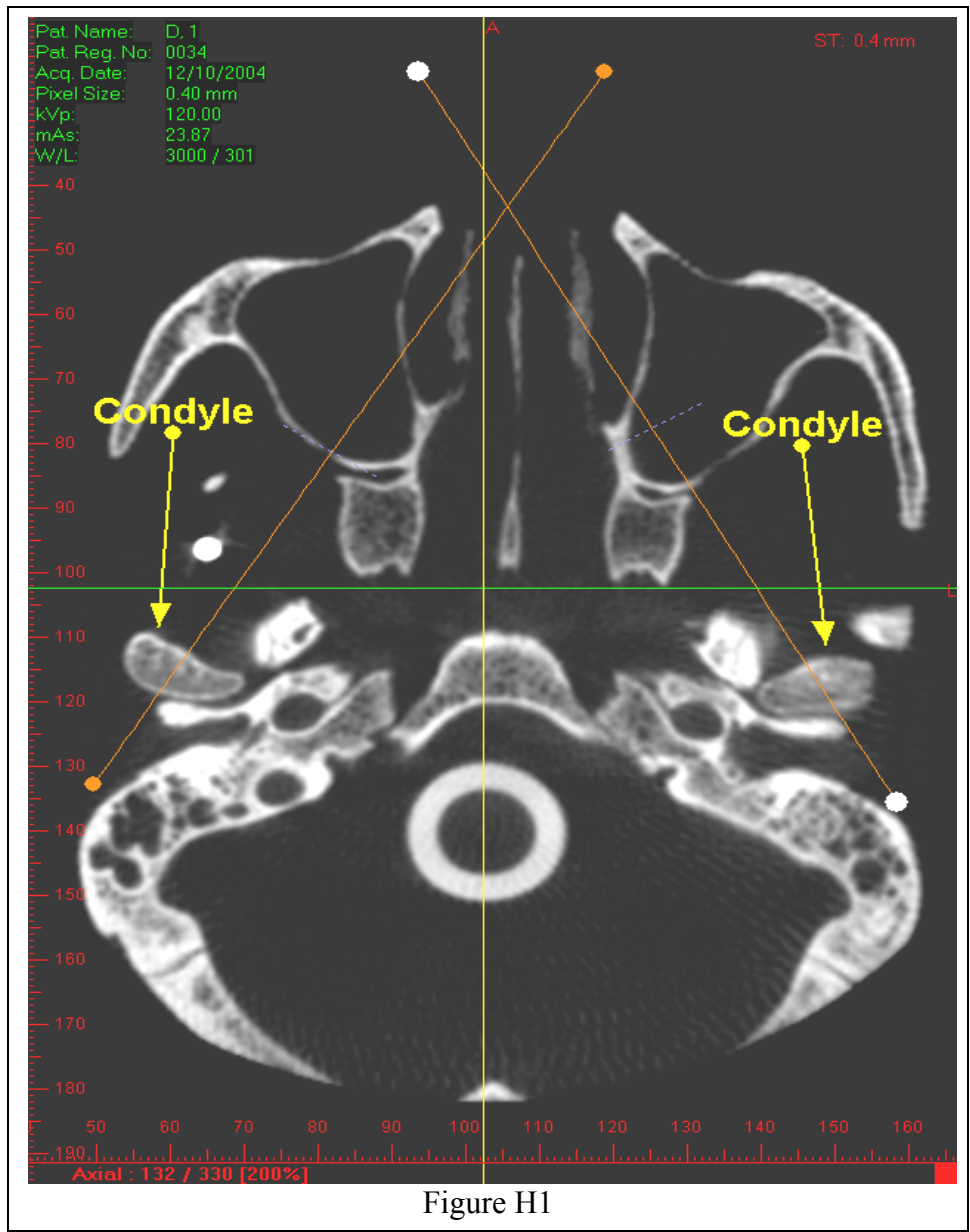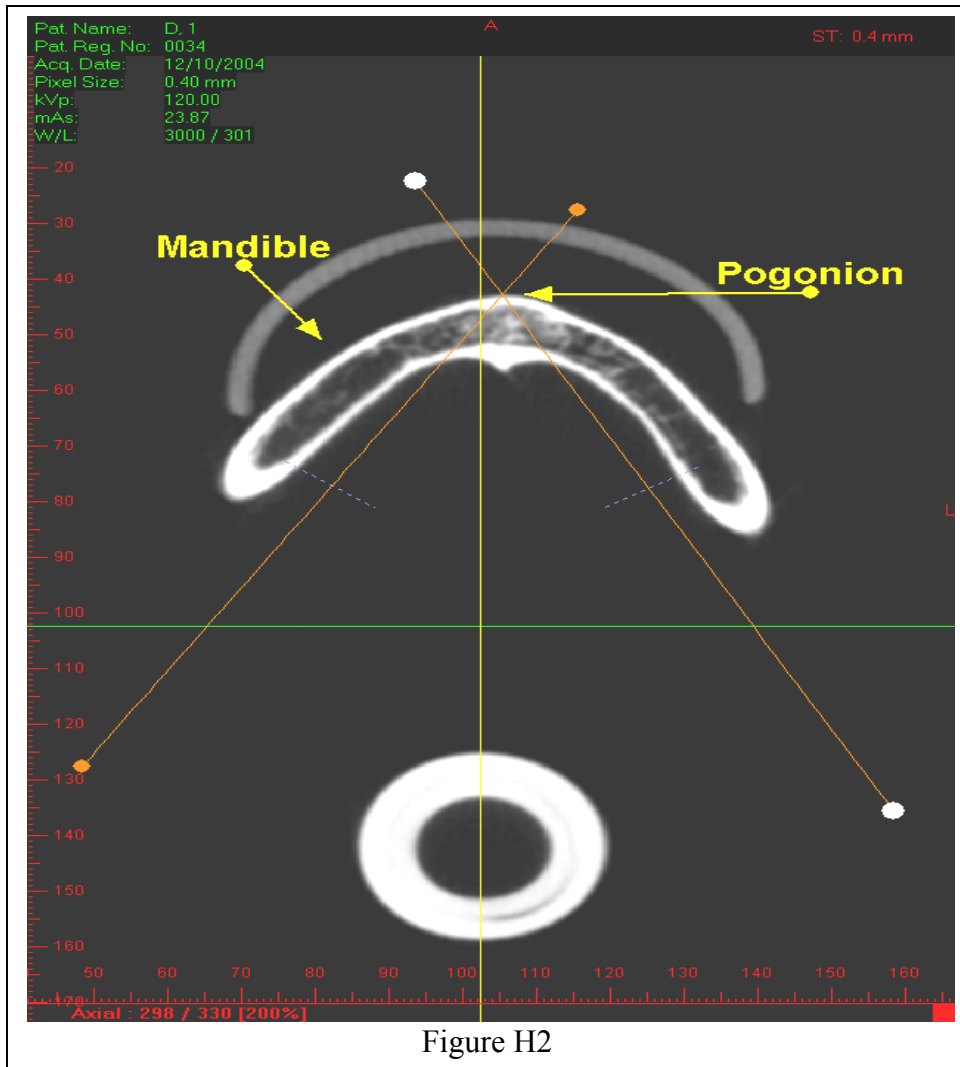
Figure I3

J. Gonion to Gonion

1. Opened image with iCAT software.

2. Interpolated image.

3. Set resolution to 3000/300.

4. Enlarged image 200%.

5. Maximized window.

6. Scrolled through transverse cross-section until condyle and coronoid process were visible (Figure J1).

7. Selected panoramic tool and made single cut through right and left condyles (Figure J2).

8. Selected image with frontal cut and enlarged to 200%.

9. Selected image thickness of 50mm.

10. Selected measure tool.

11. Measured from gonion to gonion bilaterally. Greatest width of mandible at angle of mandible (Figure J3).

Figure J1

Figure J2

Figure J3
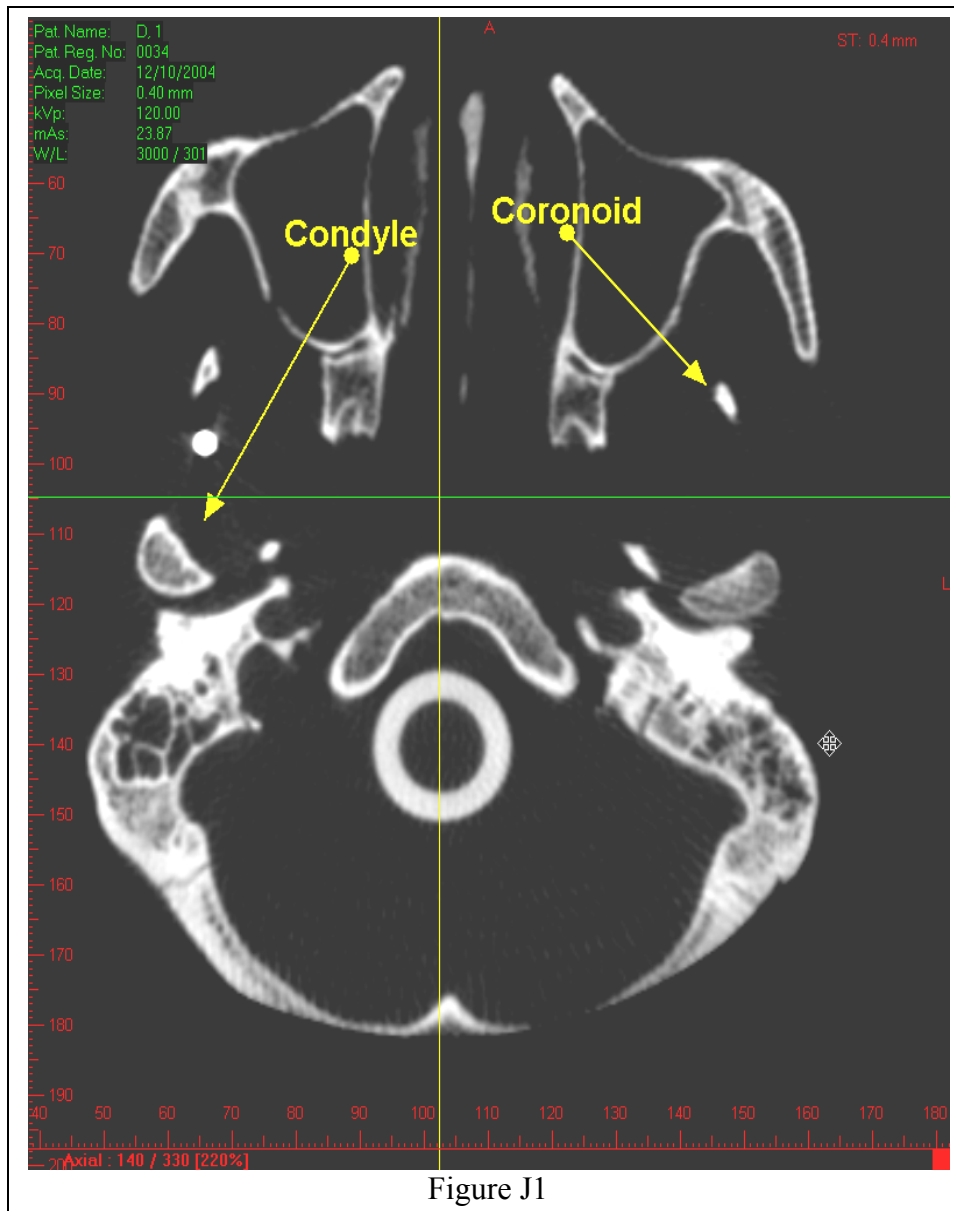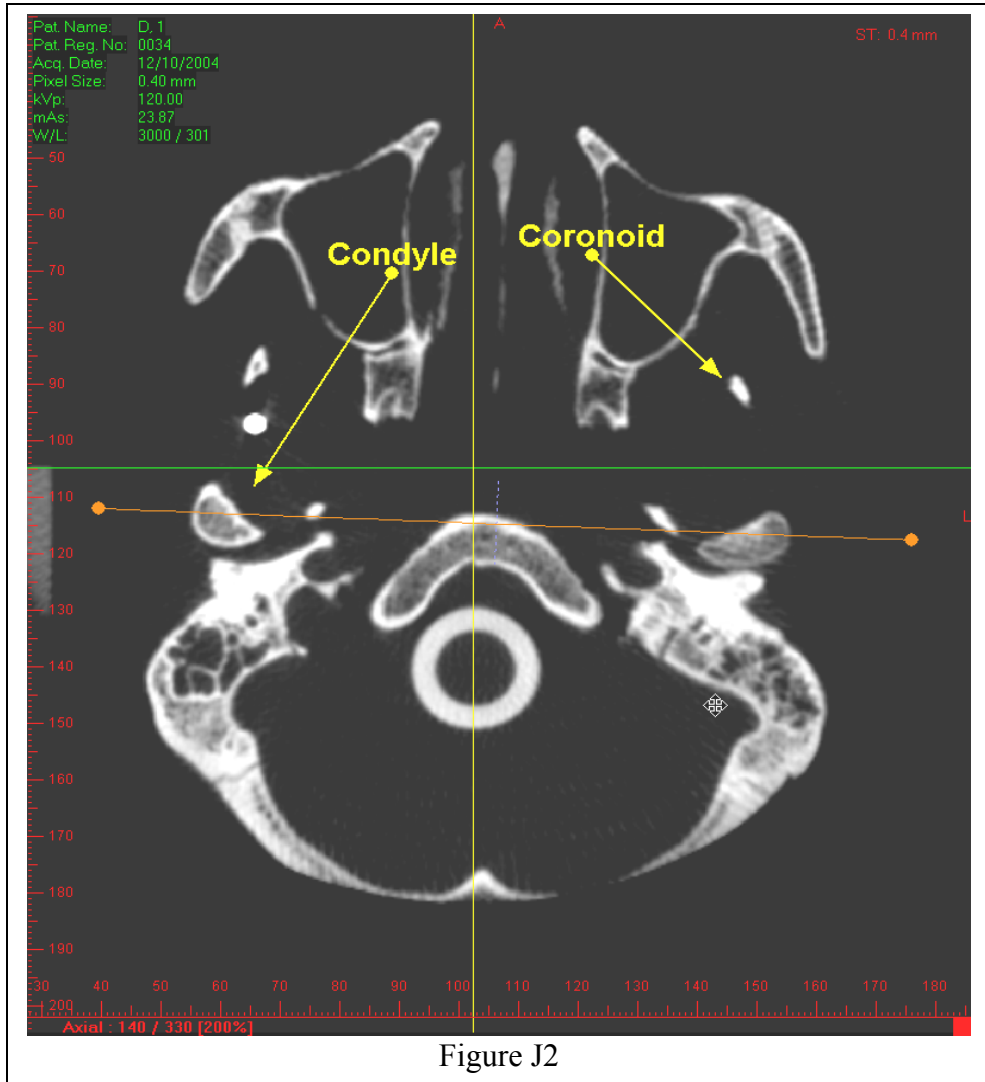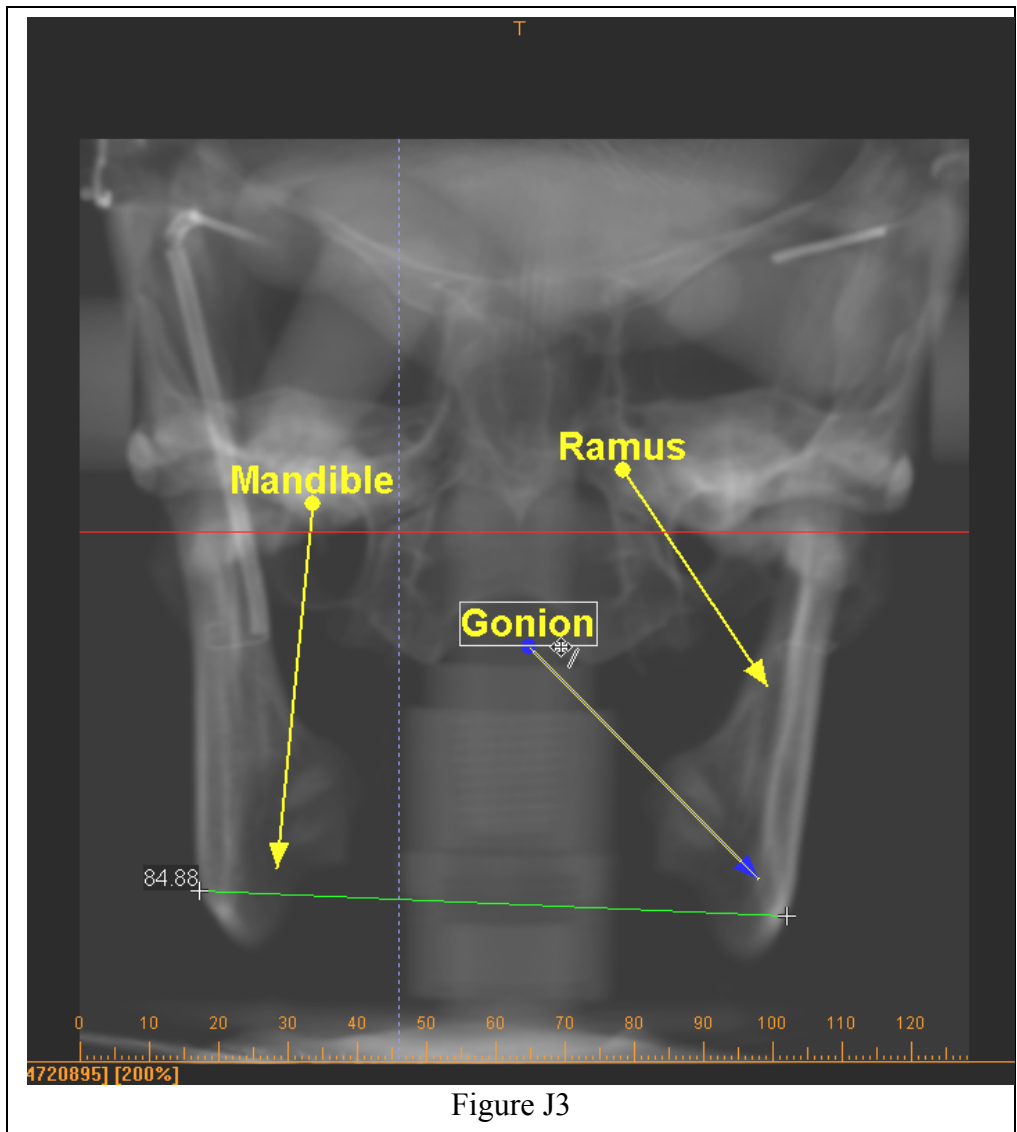
Reference Type: Journal Article
Record Number: 264
Author: Brooks, S. L.; Brand, J. W.; Gibbs, S. J.; Hollender, L.; Lurie, A. G.; Omnell, K. A.; Westesson, P. L.; White, S. C.
Year: 1997
Title: Imaging of the temporomandibular joint: a position paper of the American Academy of Oral and Maxillofacial Radiology
Journal: Oral Surg Oral Med Oral Pathol Oral Radiol Endod
Volume: 83
Issue: 5
Pages: 609-18
Date: May
Accession Number: 9159823
URL:
http://www.ncbi.nlm.nih.gov/entrez/query.fcgi?cmd=Retrieve&db=PubMed&dopt=Citation&list_uids=9159823
Author Address: University of Michigan, Ann Arbor, USA. slbrooks@umich.edu

Reference Type: Book
Record Number: 265
Author: Dixon, DC.
Year: 1995
Title: Radiographic diagnosis of temporomandibular disorders
Series Editor: PL., Sadowsky
Series Title: Seminars in Orthodontics
City: Philadelphia
Publisher: WB Saunders
Volume: 1 (4)
Number of Pages: 207-221

Reference Type: Journal Article
Record Number: 229
Author: Uematsu, H.; Ichida, T.; Masumi, S.; Morimoto, Y.; Tanaka, T.; Konoo, T.; Yamaguchi, K.
Year: 2002
Title: Diagnostic image analyses of activator treated temporomandibular joint in growth and maturing stages
Journal: Cranio
Volume: 20

Issue: 4
Pages: 254-63
Date: Oct
Accession Number: 12403183
URL:
http://www.ncbi.nlm.nih.gov/entrez/query.fcgi?cmd=Retrieve&db=PubMed&dopt=Citation&list_uids=12403183
Author Address: Department of Orthodontics, Kyushu Dental College, Kitakyushu, Japan. uematsu@kyu-dent.ac.jp

Reference Type: Journal Article
Record Number: 225
Author: Peltola, J. S.; Kononen, M.; Nystrom, M.
Year: 1995
Title: A follow-up study of radiographic findings in the mandibular condyles of orthodontically treated patients and associations with TMD
Journal: J Dent Res
Volume: 74
Issue: 9
Pages: 1571-6
Date: Sep
Accession Number: 7560418
URL:
http://www.ncbi.nlm.nih.gov/entrez/query.fcgi?cmd=Retrieve&db=PubMed&dopt=Citation&list_uids=7560418
Author Address: Department of Dental Radiology, University of Helsinki, Finland.

Reference Type: Journal Article
Record Number: 217
Author: Carlton, K. L.; Nanda, R. S.
Year: 2002
Title: Prospective study of posttreatment changes in the temporomandibular joint
Journal: Am J Orthod Dentofacial Orthop
Volume: 122
Issue: 5
Pages: 486-90
Date: Nov
Accession Number: 12439476
URL:
http://www.ncbi.nlm.nih.gov/entrez/query.fcgi?cmd=Retrieve&db=PubMed&dopt=Citation&list_uids=12439476
Author Address: Department of Orthodoontics, College of Dentistry, University of Oklahoma, Oklahoma City, 73190, USA. ram-nanda@ouhsc.edu

Reference Type: Journal Article
Record Number: 227

Author: Solberg, W. K.; Hansson, T. L.; Nordstrom, B.
Year: 1985
Title: The temporomandibular joint in young adults at autopsy: a morphologic classification and evaluation
Journal: J Oral Rehabil
Volume: 12
Issue: 4
Pages: 303-21
Date: Jul
Accession Number: 3862793
URL:
http://www.ncbi.nlm.nih.gov/entrez/query.fcgi?cmd=Retrieve&db=PubMed&dopt=Citation&list_uids=3862793

Reference Type: Journal Article
Record Number: 242
Author: Tsiklakis, K.; Syriopoulos, K.; Stamatakis, H. C.
Year: 2004
Title: Radiographic examination of the temporomandibular joint using cone beam computed tomography
Journal: Dentomaxillofac Radiol
Volume: 33
Issue: 3
Pages: 196-201
Date: May
Accession Number: 15371321
URL:
http://www.ncbi.nlm.nih.gov/entrez/query.fcgi?cmd=Retrieve&db=PubMed&dopt=Citation&list_uids=15371321
Author Address: Department of Oral Diagnosis and Oral Radiology, Dental School, University of Athens, 12 Perikleous Str., 154 51 N. Psychiko, Athens, Greece. ktsiklak@dent.uoa.gr

Reference Type: Journal Article
Record Number: 292
Author: Lipton, JA.; Raymond, AD.
Year: 1996
Title: National Institutes of Health Technology Assessment Conference on the Management of Temporomandibular Disorders, Bethesda, MD
Journal: Oral Surg Oral Med Oral Pathol Endod
Volume: 83
Pages: 49-183

Reference Type: Journal Article

Record Number: 300
Author: Mohl, N. D.
Year: 1993
Title: Reliability and validity of diagnostic modalities for temporomandibular disorders
Journal: Adv Dent Res
Volume: 7
Issue: 2
Pages: 113-9
Date: Aug
Accession Number: 8259998
URL:
http://www.ncbi.nlm.nih.gov/entrez/query.fcgi?cmd=Retrieve&db=PubMed&dopt=Citation&list_uids=8259998
Author Address: Department of Oral Medicine, State University of New York at Buffalo 14214.

Reference Type: Journal Article
Record Number: 308
Author: Rao, V. M.; Bacelar, M. T.
Year: 2004
Title: MR imaging of the temporomandibular joint
Journal: Neuroimaging Clin N Am
Volume: 14
Issue: 4
Pages: 761-75
Date: Nov
Accession Number: 15489151
URL:
http://www.ncbi.nlm.nih.gov/entrez/query.fcgi?cmd=Retrieve&db=PubMed&dopt=Citation&list_uids=15489151
Author Address: Department of Radiology, Thomas Jefferson University Hospital, 132 South 10th Street, 1072 Main Building, Philadelphia, PA 19107, USA.

Reference Type: Journal Article
Record Number: 306
Author: Gynther, G. W.; Tronje, G.; Holmlund, A. B.
Year: 1996
Title: Radiographic changes in the temporomandibular joint in patients with generalized osteoarthritis and rheumatoid arthritis
Journal: Oral Surg Oral Med Oral Pathol Oral Radiol Endod
Volume: 81
Issue: 5
Pages: 613-8
Date: May
Accession Number: 8734713

URL:
http://www.ncbi.nlm.nih.gov/entrez/query.fcgi?cmd=Retrieve&db=PubMed&dopt=Citation&list_uids=8734713
Author Address: Department of Oral and Maxillofacial Surgery, Huddinge Hospital, Karolinska Institutet, Sweden.

Reference Type: Journal Article
Record Number: 307
Author: Larheim, T. A.
Year: 1995
Title: Current trends in temporomandibular joint imaging
Journal: Oral Surg Oral Med Oral Pathol Oral Radiol Endod
Volume: 80
Issue: 5
Pages: 555-76
Date: Nov
Accession Number: 8556465
URL:
http://www.ncbi.nlm.nih.gov/entrez/query.fcgi?cmd=Retrieve&db=PubMed&dopt=Citation&list_uids=8556465
Author Address: Department of Oral Radiology, Faculty of Dentistry, University of Oslo, Norway.

Reference Type: Electronic Source
Record Number: 309
Author: American Board of Orthodontics
Year: 2001
Title: Guidelines for Quality Assessment of Orthodontic Care
Access Year: 2005
Access Date: January 22
URL:
http://www.americanboardortho.com/professionals/road_to_cert/common/info/info_2002.pdf

Reference Type: Journal Article
Record Number: 302
Author: Atchison, K. A.; Luke, L. S.; White, S. C.
Year: 1992
Title: An algorithm for ordering pretreatment orthodontic radiographs
Journal: Am J Orthod Dentofacial Orthop
Volume: 102
Issue: 1
Pages: 29-44
Date: Jul
Accession Number: 1307857

URL:
http://www.ncbi.nlm.nih.gov/entrez/query.fcgi?cmd=Retrieve&db=PubMed&dopt=Citation&list_uids=1307857
Author Address: School of Dentistry, University of California, Los Angeles.

Reference Type: Journal Article
Record Number: 278
Author: Luke, L. S.; Lee, P.; Atchison, K. A.; White, S. C.
Year: 1997
Title: Orthodontic residents' indications for use of the lateral TMJ tomogram and the posteroanterior cephalogram
Journal: J Dent Educ
Volume: 61
Issue: 1
Pages: 29-36
Date: Jan
Accession Number: 9024340
URL:
http://www.ncbi.nlm.nih.gov/entrez/query.fcgi?cmd=Retrieve&db=PubMed&dopt=Citation&list_uids=9024340
Author Address: Section of Pediatric Dentistry and Orthodontics, UCLA School of Dentistry 90095-1668, USA. larryl@dent.ucla.edu

Reference Type: Journal Article
Record Number: 310
Author: Moss, M. L.
Year: 1997
Title: The functional matrix hypothesis revisited. 1. The role of mechanotransduction
Journal: Am J Orthod Dentofacial Orthop
Volume: 112
Issue: 1
Pages: 8-11
Date: Jul
Accession Number: 9228835
URL:
http://www.ncbi.nlm.nih.gov/entrez/query.fcgi?cmd=Retrieve&db=PubMed&dopt=Citation&list_uids=9228835
Author Address: Department of Anatomy and Cell Biology, College of Physicians and Surgeons, Columbia University. moss@cucers1.civil.columbia.edu

Reference Type: Journal Article
Record Number: 254
Author: Moulin-Romsee, C.; Verdonck, A.; Schoenaers, J.; Carels, C.
Year: 2004
Title: Treatment of hemifacial microsomia in a growing child: the importance of co-operation between the orthodontist and the maxillofacial surgeon

Journal: J Orthod
Volume: 31
Issue: 3
Pages: 190-200
Date: Sep
Accession Number: 15489363
URL:
http://www.ncbi.nlm.nih.gov/entrez/query.fcgi?cmd=Retrieve&db=PubMed&dopt=Citation&list_uids=15489363
Author Address: Katholieke Universiteit Leuven, 3000 Leuven, Belgium.

Reference Type: Journal Article
Record Number: 255
Author: Wolford, L. M.; Mehra, P.; Reiche-Fischel, O.; Morales-Ryan, C. A.; Garcia-Morales, P.
Year: 2002
Title: Efficacy of high condylectomy for management of condylar hyperplasia
Journal: Am J Orthod Dentofacial Orthop
Volume: 121
Issue: 2
Pages: 136-50; discussion 150-1
Date: Feb
Accession Number: 11840126
URL:
http://www.ncbi.nlm.nih.gov/entrez/query.fcgi?cmd=Retrieve&db=PubMed&dopt=Citation&list_uids=11840126
Author Address: Oral and Maxillofacial Surgery, Baylor College of Dentistry, Texas A & M University System, Dallas, TX, USA. lwolford@swbell.net

Reference Type: Journal Article
Record Number: 257
Author: Pollack, B.
Year: 1988
Title: Cases of note: Michigan jury awards $850,000 in ortho case: a tempest in a teapot
Journal: J Mich Dent Assoc
Volume: 70
Issue: 11-12
Pages: 540-2
Date: Nov-Dec
Accession Number: 3271888
URL:
http://www.ncbi.nlm.nih.gov/entrez/query.fcgi?cmd=Retrieve&db=PubMed&dopt=Citation&list_uids=3271888

Reference Type: Book Section

Record Number: 256
Author: Seligman, DA; Okeson, JP
Year: 2001
Title: Orthodontics Occlusion and Temporomandibular Disorders
Editor: McNamara, JA; Brudon, WL
Book Title: Orthodontics and Dentofacial Orthopedics
City: Ann Arbor
Publisher: Needham Press
Pages: 519-543

Reference Type: Journal Article
Record Number: 259
Author: Fernandez Sanroman, J.; Gomez Gonzalez, J.M.; Alonso del Hoyo, J.
Year: 1997
Title: Relationship between condylar position, dentofacial deformity and temporomandibular joint dysfunction: an MRI and CT prospective study.
Journal: J Craniomaxillofac Surg
Volume: 26
Pages: 35-42

Reference Type: Journal Article
Record Number: 251
Author: Pancherz, H.; Ruf, S.; Thomalske-Faubert, C.
Year: 1999
Title: Mandibular articular disk position changes during Herbst treatment: a prospective longitudinal MRI study
Journal: Am J Orthod Dentofacial Orthop
Volume: 116
Issue: 2
Pages: 207-14
Date: Aug
Accession Number: 10434095
URL:
http://www.ncbi.nlm.nih.gov/entrez/query.fcgi?cmd=Retrieve&db=PubMed&dopt=Citation&list_uids=10434095
Author Address: Department of Orthodontics, University of Giessen, Germany.

Reference Type: Journal Article
Record Number: 258
Author: Pancherz, H.; Michailidou, C.
Year: 2004
Title: Temporomandibular joint growth changes in hyperdivergent and hypodivergent Herbst subjects. A long-term roentgenographic cephalometric study
Journal: Am J Orthod Dentofacial Orthop

Volume: 126
Issue: 2
Pages: 153-61; quiz 254-5
Date: Aug
Accession Number: 15316469
URL:
http://www.ncbi.nlm.nih.gov/entrez/query.fcgi?cmd=Retrieve&db=PubMed&dopt=Citation&list_uids=15316469
Author Address: Department of Orthodontics, University of Giessen, Giessen, Germany. hans.pancherz@dentist.med.uni-giessen.de

Reference Type: Journal Article
Record Number: 253
Author: Kitai, N.; Kreiborg, S.; Bakke, M.; Paulsen, H. U.; Moller, E.; Darvann, T. A.; Pedersen, H.; Takada, K.
Year: 2002
Title: Three-dimensional magnetic resonance image of the mandible and masticatory muscles in a case of juvenile chronic arthritis treated with the Herbst appliance
Journal: Angle Orthod
Volume: 72
Issue: 1
Pages: 81-7
Date: Feb
Accession Number: 11843278
URL:
http://www.ncbi.nlm.nih.gov/entrez/query.fcgi?cmd=Retrieve&db=PubMed&dopt=Citation&list_uids=11843278
Author Address: Department of Orthodontics and Dentofacial Orthopedics, Graduate School of Dentistry, Osaka University, Suita, Japan. nkitai@dent.osaka-u.ac.jp

Reference Type: Book Section
Record Number: 252
Author: Proffit, W.R.
Year: 1991
Title: Treatment planning: the search for wisdom.
Editor: Proffit WR, White RP Jr
Book Title: Surgical Orthodontic Treatment
City: St. Louis
Publisher: Mosby-Year Book
Pages: 158-159

Reference Type: Journal Article
Record Number: 294
Author: Westesson, P. L.

Title: Current concepts of temporomandibular joint imaging. Proceedings 10th Int Congre Dento-Maxillo-Fac Radiologists
Journal: Int Assoc Dentomaxillofacial Radiology
Volume: 194
Pages: 4-21

Reference Type: Journal Article
Record Number: 293
Author: Katzberg, R W
Year: 1989
Title: State of the art: Temporomandibular joint imaging.
Journal: Ann Roy Aust Coll Dent Surg
Volume: 10
Pages: 32-52

Reference Type: Journal Article
Record Number: 232
Author: Blackwood HJ
Year: 1963
Title: Arthritis of the mandibular joint
Journal: Br Dent J
Volume: 115
Pages: 317-326

Reference Type: Journal Article
Record Number: 224
Author: Ong, T. K.; Franklin, C. D.
Year: 1996
Title: A clinical and histopathological study of osteoarthrosis of the temporomandibular joint
Journal: Br J Oral Maxillofac Surg
Volume: 34
Issue: 2
Pages: 186-92
Date: Apr
Accession Number: 8861296
URL:
http://www.ncbi.nlm.nih.gov/entrez/query.fcgi?cmd=Retrieve&db=PubMed&dopt=Citation&list_uids=8861296
Author Address: Maxillo-Facial Unit, Newcastle General Hospital, Newcastle upon Tyne, UK.

Reference Type: Journal Article

Record Number: 219
Author: Dahlstrom, L.; Lindvall, A. M.
Year: 1996
Title: Assessment of temporomandibular joint disease by panoramic radiography: reliability and validity in relation to tomography
Journal: Dentomaxillofac Radiol
Volume: 25
Issue: 4
Pages: 197-201
Date: Sep
Accession Number: 9084273
URL:
http://www.ncbi.nlm.nih.gov/entrez/query.fcgi?cmd=Retrieve&db=PubMed&dopt=Citation&list_uids=9084273
Author Address: Orofacial Pain Clinic, Molndal Hospital, Sweden.

Reference Type: Book
Record Number: 231
Author: Hollender, L. G.
Year: 1994
Title: Controversies in Oral and Maxillofacial Surgery
Series Editor: Worthington P, Evan JR
City: Philadelphia
Publisher: WB Saunders
Number of Pages: 1-12

Reference Type: Journal Article
Record Number: 220
Author: Kjellberg, H.; Ekestubbe, A.; Kiliaridis, S.; Thilander, B.
Year: 1994
Title: Condylar height on panoramic radiographs. A methodologic study with a clinical application
Journal: Acta Odontol Scand
Volume: 52
Issue: 1
Pages: 43-50
Date: Feb
Accession Number: 8184679
URL:
http://www.ncbi.nlm.nih.gov/entrez/query.fcgi?cmd=Retrieve&db=PubMed&dopt=Citation&list_uids=8184679
Author Address: Department of Orthodontics, Faculty of Odontology, University of Goteborg, Sweden.

Reference Type: Journal Article

Record Number: 226
Author: Ruf, S.; Pancherz, H.
Year: 1995
Title: Is orthopantomography reliable for TMJ diagnosis? An experimental study on a dry skull
Journal: J Orofac Pain
Volume: 9
Issue: 4
Pages: 365-74
Date: Fall
Accession Number: 8995908
URL:
http://www.ncbi.nlm.nih.gov/entrez/query.fcgi?cmd=Retrieve&db=PubMed&dopt=Citation&list_uids=8995908
Author Address: Department of Orthodontics, Justus-Liebig University, Giessen, Germany.

Reference Type: Journal Article
Record Number: 295
Author: Hlawitschka, M; Eckelt, U
Year: 2002
Title: Assessment of patients treated for intracapsular fractures of the mandibular condyle by closed techniques
Journal: J Oral Maxillofac Surg
Volume: 60
Pages: 784-791

Reference Type: Journal Article
Record Number: 297
Author: Paulsen, H. U.
Year: 1997
Title: Morphological changes of the TMJ condyles of 100 patients treated with the Herbst appliance in the period of puberty to adulthood: a long-term radiographic study
Journal: Eur J Orthod
Volume: 19
Issue: 6
Pages: 657-68
Date: Dec
Accession Number: 9458599
URL:
http://www.ncbi.nlm.nih.gov/entrez/query.fcgi?cmd=Retrieve&db=PubMed&dopt=Citation&list_uids=9458599
Author Address: Department of Orthodontics, Copenhagen Municipal Dental Health Service, Denmark.

Reference Type: Journal Article
Record Number: 298
Author: McCormick, S. U.; Grayson, B. H.; McCarthy, J. G.; Staffenberg, D.
Year: 1995
Title: Effect of mandibular distraction on the temporomandibular joint: Part 2, Clinical study
Journal: J Craniofac Surg
Volume: 6
Issue: 5
Pages: 364-7
Date: Sep
Accession Number: 9020715
URL:
http://www.ncbi.nlm.nih.gov/entrez/query.fcgi?cmd=Retrieve&db=PubMed&dopt=Citation&list_uids=9020715
Author Address: Department of Otolaryngology, New York Eye and Ear Infirmary, New York University Medical Center, NY 10016, USA.

Reference Type: Journal Article
Record Number: 211
Author: Hatcher, D. C.; Aboudara, C. L.
Year: 2004
Title: Diagnosis goes digital
Journal: Am J Orthod Dentofacial Orthop
Volume: 125
Issue: 4
Pages: 512-5
Date: Apr
Accession Number: 15067269
URL:
http://www.ncbi.nlm.nih.gov/entrez/query.fcgi?cmd=Retrieve&db=PubMed&dopt=Citation&list_uids=15067269
Author Address: Diagnostic Digital Imaging, 1 Scripps Drive, Suite 101, Sacramento, CA 95825, USA. david@ddicentral.com

Reference Type: Journal Article
Record Number: 286
Author: Robb, RA.
Year: 1982
Title: Dynamic Spatial Reconstructor: An X-ray Video Fluoroscopic CT scanner for dynamic volume imaging of moving organs.
Journal: IEEE Trans Med Imaging
Volume: MI-1
Issue: 1
Pages: 22-23

Reference Type: Conference Proceedings
Record Number: 287
Author: Fahrig, R.
Year of Conference: 1998
Title: Computed rotational angiography: system performance assessment using in vitro and in vivo models
Conference Name: SPIE Conference on Medical Imaging
Conference Location: San Diego, CA

Reference Type: Journal Article
Record Number: 268
Author: Fahrig, R.; Fox, A. J.; Lownie, S.; Holdsworth, D. W.
Year: 1997
Title: Use of a C-arm system to generate true three-dimensional computed rotational angiograms: preliminary in vitro and in vivo results
Journal: AJNR Am J Neuroradiol
Volume: 18
Issue: 8
Pages: 1507-14
Date: Sep
Accession Number: 9296192
URL:
http://www.ncbi.nlm.nih.gov/entrez/query.fcgi?cmd=Retrieve&db=PubMed&dopt=Citation&list_uids=9296192
Author Address: Department of Medical Biophysics, University of Western Ontario, London, Canada.

Reference Type: Journal Article
Record Number: 269
Author: Wiesent, K.; Barth, K.; Navab, N.; Durlak, P.; Brunner, T.; Schuetz, O.; Seissler, W.
Year: 2000
Title: Enhanced 3-D-reconstruction algorithm for C-arm systems suitable for interventional procedures
Journal: IEEE Trans Med Imaging
Volume: 19
Issue: 5
Pages: 391-403
Date: May
Accession Number: 11021683
URL:
http://www.ncbi.nlm.nih.gov/entrez/query.fcgi?cmd=Retrieve&db=PubMed&dopt=Citation&list_uids=11021683

Author Address: Medical Engineering Group, Siemens AG, Erlangen/Forchheim, Germany. Karl.Wiesent@med.siemens.de

Reference Type: Journal Article
Record Number: 270
Author: Saint-Felix, D.; Trousset, Y.; Picard, C.; Ponchut, C.; Romeas, R.; Rougee, A.
Year: 1994
Title: In vivo evaluation of a new system for 3D computerized angiography
Journal: Phys Med Biol
Volume: 39
Issue: 3
Pages: 583-95
Date: Mar
Accession Number: 15551600
URL:
http://www.ncbi.nlm.nih.gov/entrez/query.fcgi?cmd=Retrieve&db=PubMed&dopt=Citation&list_uids=15551600
Author Address: General Electric Medical Systems Europe, 283 rue de la Miniere, 78530 Buc, France.

Reference Type: Journal Article
Record Number: 271
Author: Ning, R.; Chen, B.; Yu, R.; Conover, D.; Tang, X.; Ning, Y.
Year: 2000
Title: Flat panel detector-based cone-beam volume CT angiography imaging: system evaluation
Journal: IEEE Trans Med Imaging
Volume: 19
Issue: 9
Pages: 949-63
Date: Sep
Accession Number: 11127608
URL:
http://www.ncbi.nlm.nih.gov/entrez/query.fcgi?cmd=Retrieve&db=PubMed&dopt=Citation&list_uids=11127608
Author Address: Department of Radiology and Electrical and Computer Engineering, University of Rochester, NY 14642, USA. ruola@einstein.rad.rochester.edu

Reference Type: Conference Proceedings
Record Number: 289
Author: Ning, R.
Year of Conference: 2000
Title: Real time flat panel detector-based volume tomographic angiography imaging: detector evaluation.
Conference Name: SPIE Conference on Medical Imaging
Conference Location: San Diego, CA

Reference Type: Thesis
Record Number: 288
Author: Wang, X.
Year: 1997
Title: Volume Tomographic Angiography
University: University of Rochester

Reference Type: Journal Article
Record Number: 272
Author: Schueler, B. A.; Sen, A.; Hsiung, H. H.; Latchaw, R. E.; Hu, X.
Year: 1997
Title: Three-dimensional vascular reconstruction with a clinical x-ray angiography system
Journal: Acad Radiol
Volume: 4
Issue: 10
Pages: 693-9
Date: Oct
Accession Number: 9344292
URL:
http://www.ncbi.nlm.nih.gov/entrez/query.fcgi?cmd=Retrieve&db=PubMed&dopt=Citation&list_uids=9344292
Author Address: Department of Diagnostic Radiology, Mayo Clinic, Rochester, MN 55905, USA.

Reference Type: Journal Article
Record Number: 290
Author: Kawata, Y.; Niki, N.; Kumazaki, T.
Year: 1996
Title: Measurement of blood vessel characteristics for disease detection based on cone beam CT images.
Journal: IEEE Trans Med Imaging
Volume: 43
Issue: 6
Pages: 3348-3354

Reference Type: Journal Article
Record Number: 274
Author: Jaffray, D. A.; Siewerdsen, J. H.
Year: 2000
Title: Cone-beam computed tomography with a flat-panel imager: initial performance characterization

Journal: Med Phys
Volume: 27
Issue: 6
Pages: 1311-23
Date: Jun
Accession Number: 10902561
URL:
http://www.ncbi.nlm.nih.gov/entrez/query.fcgi?cmd=Retrieve&db=PubMed&dopt=Citation&list_uids=10902561
Author Address: Department of Radiation Oncology, William Beaumont Hospital, Royal Oak, Michigan 48073, USA. djaffray@beaumont.edu

Reference Type: Journal Article
Record Number: 275
Author: Siewerdsen, J. H.; Jaffray, D. A.
Year: 2001
Title: Cone-beam computed tomography with a flat-panel imager: magnitude and effects of x-ray scatter
Journal: Med Phys
Volume: 28
Issue: 2
Pages: 220-31
Date: Feb
Accession Number: 11243347
URL:
http://www.ncbi.nlm.nih.gov/entrez/query.fcgi?cmd=Retrieve&db=PubMed&dopt=Citation&list_uids=11243347
Author Address: Department of Radiation Oncology, William Beaumont Hospital, Royal Oak, Michigan 48073, USA. jsiewerd@beaumont.edu

Reference Type: Journal Article
Record Number: 273
Author: Siewerdsen, J. H.; Jaffray, D. A.
Year: 1999
Title: Cone-beam computed tomography with a flat-panel imager: effects of image lag
Journal: Med Phys
Volume: 26
Issue: 12
Pages: 2635-47
Date: Dec
Accession Number: 10619249
URL:
http://www.ncbi.nlm.nih.gov/entrez/query.fcgi?cmd=Retrieve&db=PubMed&dopt=Citation&list_uids=10619249
Author Address: Department of Radiation Oncology, William Beaumont Hospital, Royal Oak, Michigan 48073, USA. jsiewerd@beaumont.edu

Reference Type: Journal Article
Record Number: 299
Author: Cho, P S; Johnson, R H; Griffin, T W
Year: 1995
Title: Cone-beam CT for radiotherapy applications
Journal: Phys Med Biol
Volume: 40
Pages: 1863-1883

Reference Type: Conference Proceedings
Record Number: 291
Author: Ning, R.; Chen, B.
Year of Conference: 2001
Title: Cone beam volume CT mammographic imaging: feasibility study.
Conference Name: Proceedings of SPIE-The International Society for Optical Engineering

Reference Type: Electronic Source
Record Number: 215
Author: Winter, A
Year: 2000
Title: Newtom 9000 Accuracy
URL: http://www.endomail.com/articles/aw01newtom.html

Reference Type: Journal Article
Record Number: 212
Author: Mozzo, P.; Procacci, C.; Tacconi, A.; Martini, P. T.; Andreis, I. A.
Year: 1998
Title: A new volumetric CT machine for dental imaging based on the cone-beam technique: preliminary results
Journal: Eur Radiol
Volume: 8
Issue: 9
Pages: 1558-64
Accession Number: 9866761
URL:
http://www.ncbi.nlm.nih.gov/entrez/query.fcgi?cmd=Retrieve&db=PubMed&dopt=Citation&list_uids=9866761
Author Address: Department of Medical Physics, University Hospital, Verona, Italy.

Reference Type: Electronic Source
Record Number: 282

Author: Dus, I.

Title: The Next "Revolution" American Association of Dental Maxillofacial Radiographic Technicians

Access Year: 2004

Access Date: November 30

URL: http://www.aadmrt.com/static.aspx?content=current/Dus_fall03

Reference Type: Journal Article

Record Number: 279

Author: Vannier, M. W.

Year: 2003

Title: Craniofacial computed tomography scanning: technology, applications and future trends

Journal: Orthod Craniofac Res

Volume: 6 Suppl 1

Pages: 23-30; discussion 179-82

Accession Number: 14606531

URL: http://www.ncbi.nlm.nih.gov/entrez/query.fcgi?cmd=Retrieve&db=PubMed&dopt=Citation&list_uids=14606531

Author Address: Department of Radiology, University of Iowa, Iowa City, IA 52242, USA. michael-vannier@uiowa.edu

Reference Type: Journal Article

Record Number: 280

Author: Mah, J.; Hatcher, D.

Year: 2003

Title: Current status and future needs in craniofacial imaging

Journal: Orthod Craniofac Res

Volume: 6 Suppl 1

Pages: 10-6; discussion 179-82

Accession Number: 14606529

URL: http://www.ncbi.nlm.nih.gov/entrez/query.fcgi?cmd=Retrieve&db=PubMed&dopt=Citation&list_uids=14606529

Author Address: Craniofacial Virtual Reality Laboratory, School of Dentistry, University of Southern California, Los Angeles, CA 90089-0641, USA. jamesmah@usc.edu

Reference Type: Journal Article

Record Number: 283

Author: Adams, GL.; Hatcher, DC.; Miller, AJ.

Year: 2002

Title: Comparison between traditional two-dimensional cephalometry and a three-dimensional approach.

Journal: American Journal of Orthodontics and Dentofacial Orthopedics
Volume: 22
Issue: 1
Pages: 117
Date: July

Reference Type: Journal Article
Record Number: 233
Author: Christiansen, E. L.; Thompson, J. R.; Kopp, S.
Year: 1986
Title: Intra- and inter-observer variability and accuracy in the determination of linear and angular measurements in computed tomography. An in vitro and in situ study of human mandibles
Journal: Acta Odontol Scand
Volume: 44
Issue: 4
Pages: 221-9
Date: Aug
Accession Number: 3465194
URL:
http://www.ncbi.nlm.nih.gov/entrez/query.fcgi?cmd=Retrieve&db=PubMed&dopt=Citation&list_uids=3465194

Reference Type: Journal Article
Record Number: 234
Author: Waitzman, AA.; Posnick, JC.; Armstrong, DC.; Pron, GE.
Year: 1992
Title: Craniofacial skeletal measurements based on computed tomography: Part I. Accuracy and reproducibility
Journal: Cleft Palate Craniofac J
Volume: 29
Issue: 2
Pages: 112-7
Date: Mar
Accession Number: 1571344
URL:
http://www.ncbi.nlm.nih.gov/entrez/query.fcgi?cmd=Retrieve&db=PubMed&dopt=Citation&list_uids=1571344
Author Address: Division of Plastic Surgery, Hospital for Sick Children, Toronto, Ontario, Canada.

Reference Type: Journal Article
Record Number: 247
Author: Ahlqvist, J.; Bryndahl, F.; Eckerdal, O.; Isberg, A.

Year: 1998
Title: Sources of radiographic distortion in conventional and computed tomography of the temporal bone
Journal: Dentomaxillofac Radiol
Volume: 27
Issue: 6
Pages: 351-7
Date: Nov
Accession Number: 10895634
URL:
http://www.ncbi.nlm.nih.gov/entrez/query.fcgi?cmd=Retrieve&db=PubMed&dopt=Citation&list_uids=10895634
Author Address: Department of Oral and Maxillofacial Radiology, Umea University, Sweden.

Reference Type: Journal Article
Record Number: 245
Author: Ahlqvist, J. B.; Isberg, A. M.
Year: 1999
Title: Validity of computed tomography in imaging thin walls of the temporal bone
Journal: Dentomaxillofac Radiol
Volume: 28
Issue: 1
Pages: 13-9
Date: Jan
Accession Number: 10202473
URL:
http://www.ncbi.nlm.nih.gov/entrez/query.fcgi?cmd=Retrieve&db=PubMed&dopt=Citation&list_uids=10202473
Author Address: Department of Oral and Maxillofacial Radiology, Umea University, Sweden.

Reference Type: Journal Article
Record Number: 235
Author: Naitoh, M.; Katsumata, A.; Nohara, E.; Ohsaki, C.; Ariji, E.
Year: 2004
Title: Measurement accuracy of reconstructed 2-D images obtained by multi-slice helical computed tomography
Journal: Clin Oral Implants Res
Volume: 15
Issue: 5
Pages: 570-4
Date: Oct
Accession Number: 15355399

URL:
http://www.ncbi.nlm.nih.gov/entrez/query.fcgi?cmd=Retrieve&db=PubMed&dopt=Citation&list_uids=15355399
Author Address: Department of Oral and Maxillofacial Radiology, School of Dentistry, Aichi-Gakuin University, Japan. mune@dpc.aichi-gakuin.ac.jp

Reference Type: Journal Article
Record Number: 246
Author: Lo, L. J.; Lin, W. Y.; Wong, H. F.; Lu, K. T.; Chen, Y. R.
Year: 2000
Title: Quantitative measurement on three-dimensional computed tomography: an experimental validation using phantom objects
Journal: Changgeng Yi Xue Za Zhi
Volume: 23
Issue: 6
Pages: 354-9
Date: Jun
Accession Number: 10958038
URL:
http://www.ncbi.nlm.nih.gov/entrez/query.fcgi?cmd=Retrieve&db=PubMed&dopt=Citation&list_uids=10958038
Author Address: Department of Plastic and Reconstructive Surgery, Chang Gung Memorial Hospital, Taipei, R.O.C. lunjoulo@ms1.hinet.net

Reference Type: Journal Article
Record Number: 236
Author: Cavalcanti, M. G.; Rocha, S. S.; Vannier, M. W.
Year: 2004
Title: Craniofacial measurements based on 3D-CT volume rendering: implications for clinical applications
Journal: Dentomaxillofac Radiol
Volume: 33
Issue: 3
Pages: 170-6
Date: May
Accession Number: 15371317
URL:
http://www.ncbi.nlm.nih.gov/entrez/query.fcgi?cmd=Retrieve&db=PubMed&dopt=Citation&list_uids=15371317
Author Address: Department of Radiology, College of Dentistry, University of Sao Paulo,Sao Paulo, Brazil. mgpcaval@usp.br

Reference Type: Journal Article
Record Number: 249
Author: Kobayashi, K.; Shimoda, S.; Nakagawa, Y.; Yamamoto, A.
Year: 2004

Title: Accuracy in measurement of distance using limited cone-beam computerized tomography
Journal: Int J Oral Maxillofac Implants
Volume: 19
Issue: 2
Pages: 228-31
Date: Mar-Apr
Accession Number: 15101594
URL:
http://www.ncbi.nlm.nih.gov/entrez/query.fcgi?cmd=Retrieve&db=PubMed&dopt=Citation&list_uids=15101594
Author Address: Department of Oral Radiology, Tsurumi University School of Dental Medicine, Yokohama, Japan.

Reference Type: Electronic Source
Record Number: 285
Author: Lascala, CA.
Year: 2004
Title: Accuracy of Linear Measurements Obtained by Cone Beam Computerized Tomography. Poster Presentation #1952.
Access Year: 2004
Access Date: December 13
URL: http://iadr.confex.com/iadr/2004Hawaii/techprogram/abstract_45634.

Reference Type: Personal Communication
Record Number: 281
Author: Concepts, TMJ
Year: 2004
Recipient: Scarfe, William
City: Ventura
Date: November 17

Reference Type: Journal Article
Record Number: 228
Author: Stheeman, S. E.; van 't Hof, M. A.; Mileman, P. A.; van der Stelt, P. F.
Year: 1995
Title: Use of the Delphi technique to develop standards for quality assessment in diagnostic radiology
Journal: Community Dent Health
Volume: 12
Issue: 4
Pages: 194-9
Date: Dec
Accession Number: 8536080

URL:
http://www.ncbi.nlm.nih.gov/entrez/query.fcgi?cmd=Retrieve&db=PubMed&dopt=Citation&list_uids=8536080
Author Address: Department of Oral Radiology, Academic Centre for Dentistry Amsterdam, The Netherlands.

Reference Type: Journal Article
Record Number: 210
Author: Ludlow, JB.; Davies-Ludlow, LE.; Brooks, SL.
Year: 2003
Title: Dosimetry of two extraoral direct digital imaging devices: NewTom cone beam CT and Orthophos Plus DS panoramic unit
Journal: Dentomaxillofac Radiol
Volume: 32
Issue: 4
Pages: 229-34
Date: Jul
Accession Number: 13679353
URL:
http://www.ncbi.nlm.nih.gov/entrez/query.fcgi?cmd=Retrieve&db=PubMed&dopt=Citation&list_uids=13679353
Author Address: Department of Diagnostic Sciences and General Dentistry, University of North Carolina School of Dentistry, Chapel Hill, North Carolina 27599, USA. jbl@email.unc.edu

Reference Type: Journal Article
Record Number: 313
Author: Chidiac, J. J.; Shofer, F. S.; Al-Kutoub, A.; Laster, L. L.; Ghafari, J.
Year: 2002
Title: Comparison of CT scanograms and cephalometric radiographs in craniofacial imaging
Journal: Orthod Craniofac Res
Volume: 5
Issue: 2
Pages: 104-13
Date: May
Accession Number: 12086325
URL:
http://www.ncbi.nlm.nih.gov/entrez/query.fcgi?cmd=Retrieve&db=PubMed&dopt=Citation&list_uids=12086325
Author Address: Department of Prosthodontics, School of Dentistry, Lebanese University, Beirut.

Reference Type: Journal Article
Record Number: 311
Author: Leon, S. D.

Year: 2004
Title: The use of panoramic radiography for evaluating temporomandibular disorders
Journal: Gen Dent
Volume: 52
Issue: 4
Pages: 339-41
Date: Jul-Aug
Accession Number: 15366301
URL:
http://www.ncbi.nlm.nih.gov/entrez/query.fcgi?cmd=Retrieve&db=PubMed&dopt=Citation&list_uids=15366301

Reference Type: Journal Article
Record Number: 237
Author: Cavalcanti, M. G.; Vannier, M. W.
Year: 1998
Title: Quantitative analysis of spiral computed tomography for craniofacial clinical applications
Journal: Dentomaxillofac Radiol
Volume: 27
Issue: 6
Pages: 344-50
Date: Nov
Accession Number: 10895633
URL:
http://www.ncbi.nlm.nih.gov/entrez/query.fcgi?cmd=Retrieve&db=PubMed&dopt=Citation&list_uids=10895633
Author Address: Department of Radiology, Faculty of Odontology, University of Sao Paulo, Brazil.